NAVAL POSTGRADUATE SCHOOL
MONTEREY, CALIFORNIA

THESIS

EFFECTS OF GEOMETRIC AND MATERIAL IMPERFECTIONS ON THE DYNAMIC RESPONSE OF CYLINDRICAL SHELLS SUBJECTED TO UNDERWATER EXPLOSION

by

Robert E. Kaufman

June 1995

Thesis Advisor: **Young S. Shin**

Approved for public release; distribution is unlimited.

REPORT DOCUMENTATION PAGE

Form Approved OMB No. 0704-0188

1. AGENCY USE ONLY *(Leave blank)*	2. REPORT DATE June 1995	3. REPORT TYPE AND DATES COVERED Engineer's Thesis

4. TITLE AND SUBTITLE EFFECTS OF GEOMETRIC AND MATERIAL IMPERFECTIONS ON THE DYNAMIC RESPONSE OF CYLINDRICAL SHELLS SUBJECTED TO UNDERWATER EXPLOSION

5. FUNDING NUMBERS

6. AUTHOR(S) Robert E. Kaufman

7. PERFORMING ORGANIZATION NAME(S) AND ADDRESS(ES)
Naval Postgraduate School
Monterey CA 93943-5000

8. PERFORMING ORGANIZATION REPORT NUMBER

9. SPONSORING/MONITORING AGENCY NAME(S) AND ADDRESS(ES)

10. SPONSORING/MONITORING AGENCY REPORT NUMBER

11. SUPPLEMENTARY NOTES The views expressed in this thesis are those of the author and do not reflect the official policy or position of the Department of Defense or the U.S. Government.

12a. DISTRIBUTION/AVAILABILITY STATEMENT
Approved for public release; distribution is unlimited.

12b. DISTRIBUTION CODE

13. ABSTRACT *(maximum 200 words)*

* The effects of initial geometric and material property imperfections on the non-linear dynamic response of cylindrical shells subjected to an underwater explosion was investigated. Finite element and boundary element programs were used to perform the analysis of the dynamic response of these shells. The geometric and material modal imperfections were introduced into the finite element models. The dynamic response and deformation of the cylinder were then compared for each of the eight modal imperfection cases to the dynamic response of a perfect cylindrical model. The modal imperfection distribution of the combined geometric and material imperfections are then introduced into an aluminum model and compared to experimental results obtained from underwater explosion testing. This analysis shows that a more accurate prediction of the damage and dynamic response is achieved by introducing these imperfection distributions into the numerical analysis .

14. SUBJECT TERMS Underwater Shock, Geometric and Material Imperfections			15. NUMBER OF PAGES 115
			16. PRICE CODE
17. SECURITY CLASSIFICATION OF REPORT Unclassified	18. SECURITY CLASSIFICATION OF THIS PAGE Unclassified	19. SECURITY CLASSIFICATION OF ABSTRACT Unclassified	20. LIMITATION OF ABSTRACT UL

NSN 7540-01-280-5500

Standard Form 298 (Rev. 2-89)
Prescribed by ANSI Std. 239-18 298-102

Approved for public release; distribution is unlimited.

EFFECTS OF GEOMETRIC AND MATERIAL IMPERFECTIONS ON THE DYNAMIC RESPONSE OF CYLINDRICAL SHELLS SUBJECTED TO UNDERWATER EXPLOSION

Robert E. Kaufman
Lieutenant, United States Navy
B.S.M.E., University of Florida, 1985

Submitted in partial fulfillment
of the requirements for the degree of

MASTER OF SCIENCE IN MECHANICAL ENGINEERING
and
MECHANICAL ENGINEER
from the
NAVAL POSTGRADUATE SCHOOL
June 1995

Author: Robert E. Kaufman

Approved by: Young S. Shin, Advisor

Young W. Kwon, Second Reader

Matthew D. Kelleher, Chairman
Department of Mechanical Engineering

ABSTRACT

The effects of initial geometric and material property imperfections on the non-linear dynamic response of cylindrical shells subjected to an underwater explosion was investigated. Finite element and boundary element programs were used to perform the analysis of the dynamic response of these shells. The geometric and material modal imperfections were introduced into the finite element models. The dynamic response and deformation of the cylinder were then compared for each of the eight modal imperfection cases to the dynamic response of a perfect cylindrical model. The modal imperfection distribution of the combined geometric and material imperfections are then introduced into an aluminum model and compared to experimental results obtained from underwater explosion testing. This analysis shows that a more accurate prediction of the damage and dynamic response is achieved by introducing these imperfection distributions into the numerical analysis.

TABLE OF CONTENTS

ACKNOWLEDGEMENTS

I would like to express my deep gratitude and appreciation to Dr. Young S. Shin and Dr. Young W. Kwon for their continued support, guidance and encouragement throughout this research. I would like to thank LT Jim Chisum, LT Tom Brasek, and LT Lou Chiong for providing their experience and expertise in underwater shock modeling. I am also grateful to Dr. John DeRuntz for the time and effort he provided to me over the course of this research. I gratefully acknowledge the Defense Nuclear Agency for their continued support of the underwater shock research program at the Naval Postgraduate School.

Many others not mentioned by name provided welcome assistance. To you, please forgive the omission. I thank you all.

Finally, I would like to dedicate this work to my wife, Kathleen and children, Carolyn, Chelsea, and Caleb who endured two and half years of separation while I pursed this academic goal. Their love, support, and encouragement made it all possible.

I. INTRODUCTION

The objective of this thesis is to investigate the effects of initial geometric and material property imperfections on the dynamic response of cylindrical shells subjected to an underwater explosion. The use of cylindrical shells in the design of modern structures has grown at an exponential rate since the end of World War I. The demand for these structures will continue to increase in the future due to their excellent weight critical mechanical properties. These properties help optimize the structural designs used in many modern weight sensitive technologies such as in the aerospace and defense related industries. The primary problem with many cylindrical shell structures has been the discrepancy between the magnitudes of analytically predicted and experimentally obtained buckling loads. These buckling loads can commonly vary by 50 percent. An explanation for these variations is the influence of boundary conditions, effects of pre-buckling due to edge constraints, or the effects of initial imperfections. Initial imperfections have been recognized as the major source in these inaccuracies.

Imperfections can be generalized into three types; shell geometry, material properties and loading distribution. The first type is shell geometry which has two components, radial and axial imperfections. Radial and axial imperfections are the small deviations in the radial and axial directions generated by manufacturing or fabrication processes. Manufacturing processes, like forging and turning, can introduce longitudinal curvatures and axial variation in shell thickness. Research in radial imperfections has been previously investigated by Kirkpatrick (1989) and Hooker (1993). The material property is the second type of imperfection. These are caused by slight variations in the density, modulus of elasticity, tangential hardening modulus or yield strength over the surface of the material. Material testing apparatus can also attribute to slight variations in these material properties. The various fabrication processes can also produce porosity or effect the surface finish. All of theses factors affect the material properties and hence the structural dynamic response. Loading distributions are the final type of imperfection. The loading distribution is a function of the explosive type, pulse geometry and contact area on impact.

The USA/DYNA3D computer codes were used to provide the numerical analysis for the shell responses. VEC/DYNA3D (Hallquist and Stillman 1990) was developed at Lawrence Livermore National Laboratory and is an explicit three-dimensional finite element program that has been effectively used in analyzing large deformation dynamic response of mechanical structures. The equations of motion are integrated in time by using a central difference method. The Underwater Shock Analysis, USA (DeRuntz 1989) is a boundary element code that is based on the Doubly Asymptotic Approximation (DAA). This allows for the accurate and efficient numerical analysis of the complex fluid-structure interaction of the underwater shock phenomena. The linkage between the two codes was developed in the early 1990's and has provided acceptable results of dynamic responses of cylindrical shells.

The finite element model for the VEC/DYNA3D program uses LS-INGRID (Hallquist and Stillman 1985), a pre-processor that provides flexibility in modeling of geometric shapes. The model for the dynamic analysis of the cylindrical shell utilizes a three-dimensional ring stiffened finite cylindrical model provided in Figure 1. The model uses

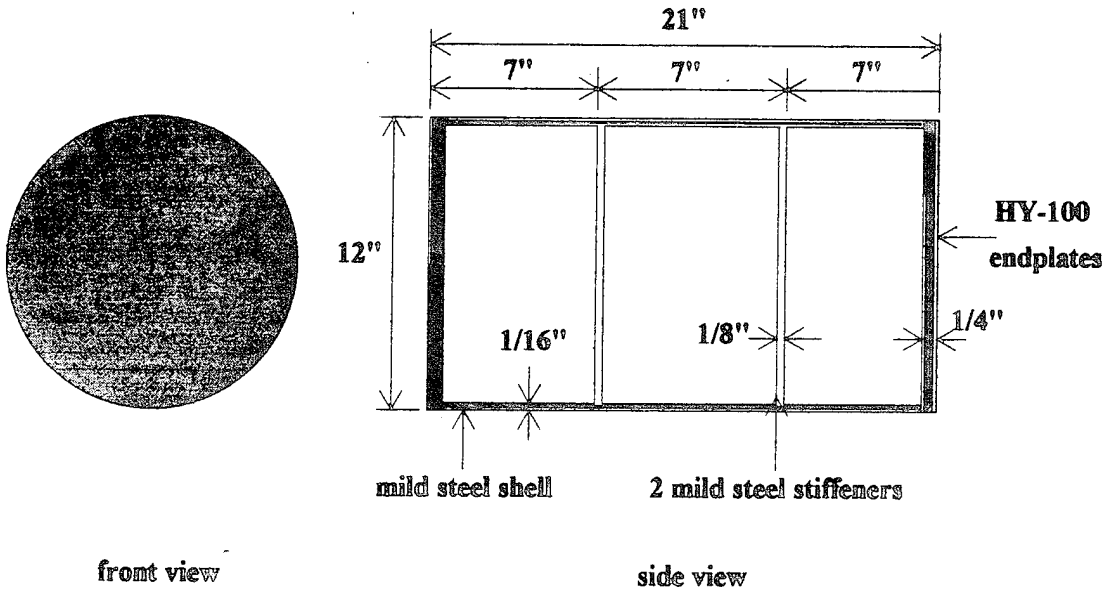

Figure 1. Dimensions of the INGRID Model

the Belytschko-Lin-Tsay 4 node shell element due to its computational efficiency in the DYNA3D program. The post-processor is provided by LS-TAURUS (Hallquist and Stillman 1990). It provides graphical output in the form of contour, fringe plots and time histories for a wide variety of output parameters such as stress, strain, displacements, velocities and accelerations.

In the remaining of this thesis the modal imperfection distribution for the initial geometric and material imperfections is discussed. An algorithm is generated and explained for radial, axial, material and combined cases. These modal imperfections are then introduced into the finite element mesh algorithm. Each of eight separate modal imperfection models is analyzed and compared to the dynamic response of a perfect model. A parametric study of axial and material property variations is performed to analyze their contributions to the total dynamic response. Then an optimized selection of the geometric and material modal imperfections is compared to experimentally obtained results from an underwater explosion.

II. IMPERFECTIONS

Initial Imperfections have slight variations in the assumed structural shape and have been recognized as a major source of inaccuracy in the predications of dynamic buckling of cylindrical shells. Imperfections can be categorized as either shell geometry, material property or loading distribution. The aerospace industry driven by weight critical, low margin of safety axially compressed cylinders has been investigating the effects of these imperfections in aluminum since the early 1960's . Several studies including Arbocz (1982) have been investigating the effects of general imperfections on the buckling of cylindrical shells. Arbocz has published an imperfection data bank that he notes should help improve design criteria for buckling of thin shells. This data bank complies results of imperfection sensitivity analysis for various materials. The imperfection sensitivity analysis physically measures the slight variations in the radial and axial directions. These are ultimately the most precise way to determine the imperfections in a cylindrical shell but cannot always be accomplished because of cost and schedule constraints.

A more cost effective solution to this cylindrical shell buckling problem is to integrate a more realistic initial imperfection into the analytical analysis. In finite element modeling the initial imperfections can be introduced into the finite element mesh algorithm. Each initial imperfection or a summation of modal imperfections will have a different modal imperfection distribution.

A. GEOMETRIC IMPERFECTIONS

The first category of imperfection is shell geometry. As stated above this will significantly contribute to both radial and axial imperfections. These radial and axial imperfections can be introduced into the mesh generator algorithm by modifying the geometric location of the particular node points in the finite element model.

For radial imperfections the numerical expression used was determined by Kirkpatrick (1989). He found that the dynamic response of a cylindrical structure subject to a blast loading more closely agreed to experimental data by introducing the initial modal

imperfections in the cylindrical structure. He used a summation of modal imperfections expressed as the cosine series in Eq. (1).

$$\delta R(\theta) = \sum_{n=1} A_n * \cos(n\theta + \phi_n) \quad (1)$$

where δR is the radial imperfection, θ is the angular position, N is the maximum modal contribution in the radial direction, A_n is the modal amplitude. and ϕ_n is a random modal phase shift. The random modal phase shift has been determined reasonably in many shells without welded seams. An empirical form for the modal amplitude is expressed as shown in Eq. (2).

$$A_n = \frac{X}{n^r} \quad (2)$$

where A_n is the modal amplitude of the n^{th} modal imperfection, n is the mode number and X and r are coefficients used to fit the data for the shells of a given construction. Kirkpatrick accurately modeled the modal amplitude in Eq. (3) and Eq. (4) as a percentage of the shell thickness for mode numbers less than six and greater than seven.

$$A_n = 0.05*h \qquad n \leq 6 \quad (3)$$

$$A_n = \frac{2*h}{n^2} \qquad n > 7 \quad (4)$$

The second type of geometric imperfection to be investigated are axial imperfections. Axial imperfections according to Kirkpatrick were neglected in his research due to the small

variations along the axial direction as compared to the radial. This thesis models the axial imperfections with a similar model as the radial imperfection. The axial imperfection uses the same summation of modal imperfection expressed as the cosine series Eq. (5) but as a function of axial distance. In accordance to Kirkpatricks, small variations along the axial directions a reduced axial modal amplitude in Eq. (6) and Eq. (7) has been used.

$$\delta A(y) = \sum_{m=1} A_m * \cos(m * 2 * \pi * y + \Phi_m) \qquad (5)$$

$$A_m = \frac{1}{4} * (0.05 * h) \qquad m \leq 6 \qquad (6)$$

$$A_m = \frac{1}{4} * \frac{2 * h}{n^2} \qquad m > 7 \qquad (7)$$

Where δA is the axial imperfection, y is the axial position, M is the maximum modal contribution in the axial direction, A_m is the modal amplitude and ϕ_m is a random modal phase shift.

1. Three-Dimensional Mesh Plots

Manufacturing, machining, or fabrication processes can contribute to shell geometry imperfections. To incorporate these processes into the imperfection algorithm, Arbocz (1982) conducted imperfection sensitivity analysis of various fabricated cylinders and recorded their radial and axial variations. This data provides a three-dimensional plots of circumferential angle, axial distance versus radial imperfection. The mesh plots have characteristic imperfection distribution that can be associated with a type of fabrication process. Three-dimensional mesh plots clearly show periodic oscillations in radial and

axial directions. These magnitudes and geometric shapes of these plots are a function of modal amplitude and random phase shift. These three-dimensional mesh plots in this thesis are created by the initial modal imperfection introduced into the mesh algorithm.

2. Initial Modal Imperfection

Previous research by Hooker (1993) implemented a sixth modal and a summation of the first ten modal imperfections in the radial direction. His data showed that the final deformation or damage pattern is a function of the introduced initial modal imperfection. He also concluded that the use of another modal imperfection would have only changed the shape of the final deformation and not the final results. The summation of the first ten modal imperfection is a reasonable assumption because of what Arbocz (1982) determined. He stated that imperfections have characteristic distributions that include decreasing modal amplitudes with increasing mode number. This indicates that the lower modal imperfections dominate the deformation patterns.

An axial view of the initial sixth modal imperfection pattern with a modal amplitude of 0.05*h scaled by a factor of 100 is shown in Figure 2. The sixth modal imperfection clearly shows a symmetric six crest and trough pattern. As explained by Hooker the mode 6 imperfection was initially chosen for its ease of identifying its distinctive geometric pattern. The sixth modal imperfection with random phase shift also scaled by a factor of 100 is shown in Figure 3. It has the similar pattern but rotated by a random phase angle. With the summation of each of the first ten mode shapes the random phase provides a significantly different deformation pattern than the non- random case. This in turn will create a different dynamic response and final deformation pattern.

The final deformation pattern can be readily observed from the deformation plot. The dynamic response can be directly determined from analysis of the hoop and axial strain data. Lindberg (1987) states that circumferential (hoop) strain or specifically as its related to compressive hoop stress is the major cause of buckling in cylindrical shells. He further defines buckling as the resultant of the growth of initial imperfection in the structure in response to the applied load.

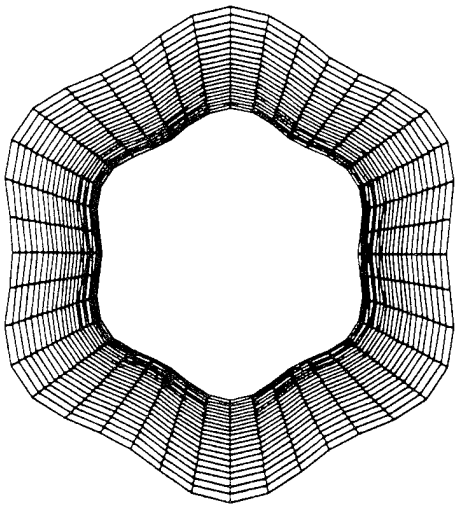

Figure 2. Initial Mode 6 Imperfection A_6=0.05*h, scaled up 100X

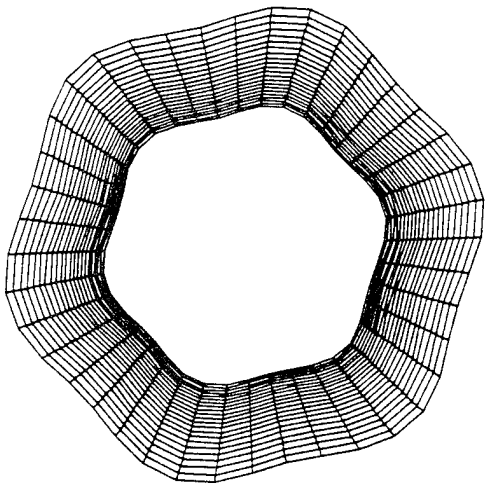

Figure 3. Initial Mode 6 Imperfection With Random Phase Shift A_6=0.05*h, scaled up 100X

B. MATERIAL IMPERFECTIONS

The second category of imperfection is material variation. In the USA/DYNA3D code the material properties that are adjustable are density, Poisson's ratio, yield strength, tangential hardening modulus, and modulus of elasticity. The modulus of elasticity was selected for initial investigation. The reasoning was that the modulus of elasticity would affect the mechanical properties more in the elastic region of the response than the other parameters. The material property variation was accomplished by generating a random modulus between plus and minus 5 percent of its tabulated value. This was then inserted into the mesh algorithm at each element of the mesh.

A subsequent material property analysis repeated this procedure for density, yield strength, and tangential hardening. Each factor was analyzed independently and then in combination. The Poisson's ratio was not analyzed due to the exceptionally small changes in numerical values. A three dimensional mesh plot was not produced of material modal imperfection because there where no coordinate changes associated with the finite element mesh algorithm.

C. LOADING DISTRIBUTIONS

The final source of imperfections is loading distributions. At this time the loading distribution phenomena is not well understood. In this report the effects of loading distributions are neglected because the shock wave created by the underwater explosion is modeled as a plane wave by the USA/DYNA3D code.

III. THREE DIMENSIONAL MODEL

The following is the initial three-dimensional model used to generate a radial and axial imperfection distribution using the combined boundary element and finite element program USA/DYNA3D. A three-dimensional ring stiffened finite cylindrical model is shown in Figure 4. Its dimensions as shown previously are 21 inches in length, six inch radius with two 1/8 inch thick stiffeners equally spaced seven inches apart along the axial direction. This three-dimensional finite cylindrical model has 40 elements around the circumference, and 22 elements in the axial direction with an element length of 0.96 inches. The radius-to-thickness ratio for thin-walled cylinder approximation is 24. The shell and stiffener material are modeled as mild steel, a kinematic/isotropic elastic-plastic material. The shell thickness is 0.06 inches. The endplate material is 1/4 inch HY-100 steel. The material properties used for the numerical models are provided in Table 1.

		Mild Steel	HY-100
Density	(lbm/ft^3)	490.0	490.0
Poisson's Ratio		0.3	0.3
Yield Strength	(ksi)	32.0	108.0
Young's Modulus	(psi)	$2.9x10^7$	$2.9x10^7$
Tangential Hardening Modulus	(psi)	$5.1x10^4$	$5.02x10^4$

Table 1. Material Properties

A. PERFECT CYLINDER MODEL

The perfect cylinder model is the original model developed by the LS-INGRID preprocessor. The input files are provided in Appendix A. It was subjected to an underwater

shock wave modeled as a plane wave with a peak amplitude of 2175 psi and a decay constant of 0.3625 msec. This approximation (Shin and Geers 1988) uses a exponential pressure relationship and is only good for pressure greater than about 1/3 of the peak value . This peak pressure pulse is generated from a 60 lbs charge of HBX-1 at a 10 foot depth and a standoff distance of 30 feet. The attack geometry is provided in Figure 5. The pressure profile, Figure 6 and cavitation curve Figure 7, for an HBX-1 explosive are provided for reference. For these particular parameters the cavitation curve shows that the target is on the boundary of the lower cavitation curve and hence could be subjected to bulk cavitation effects. The 10 foot underwater depth is also less than the gas bubble radius of 15.8 feet. This allows the gas bubble to vent to the surface and not migrate toward the target. If the gas bubble were not to vent to the surface a significant release of energy (47% of the explosive energy) would result in formible second pulse striking the target. These two factors could possibly provide a source for numerical error to the predicted dynamic response if compared to experimental data.

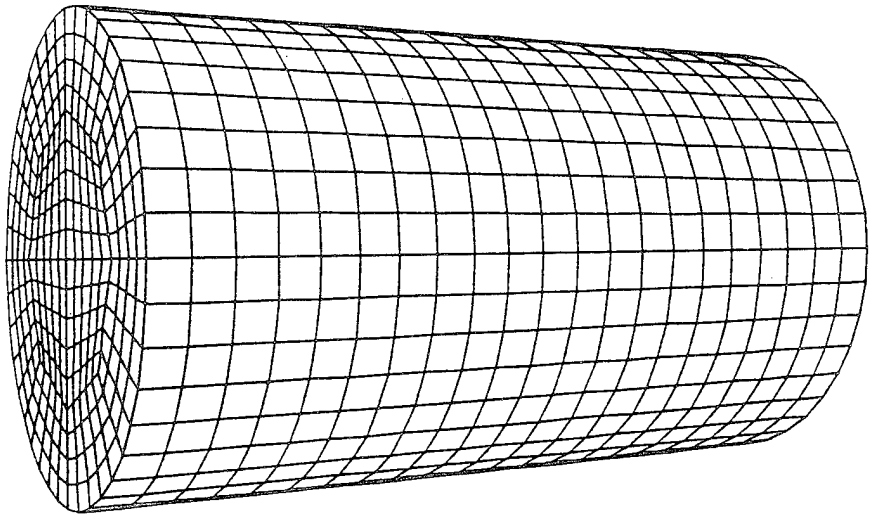

Figure 4. Three Dimensional Ring Stiffened Cylindrical Model

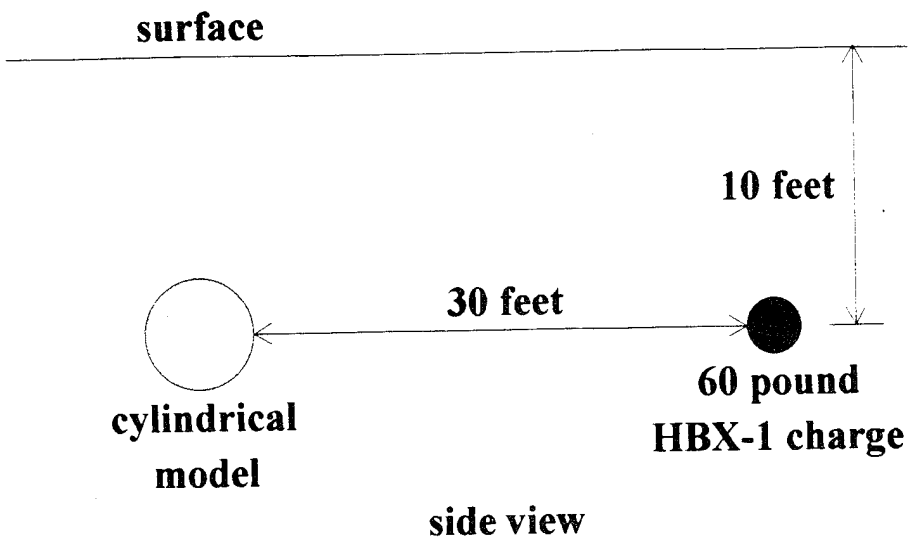

Figure 5. Attack Geometry

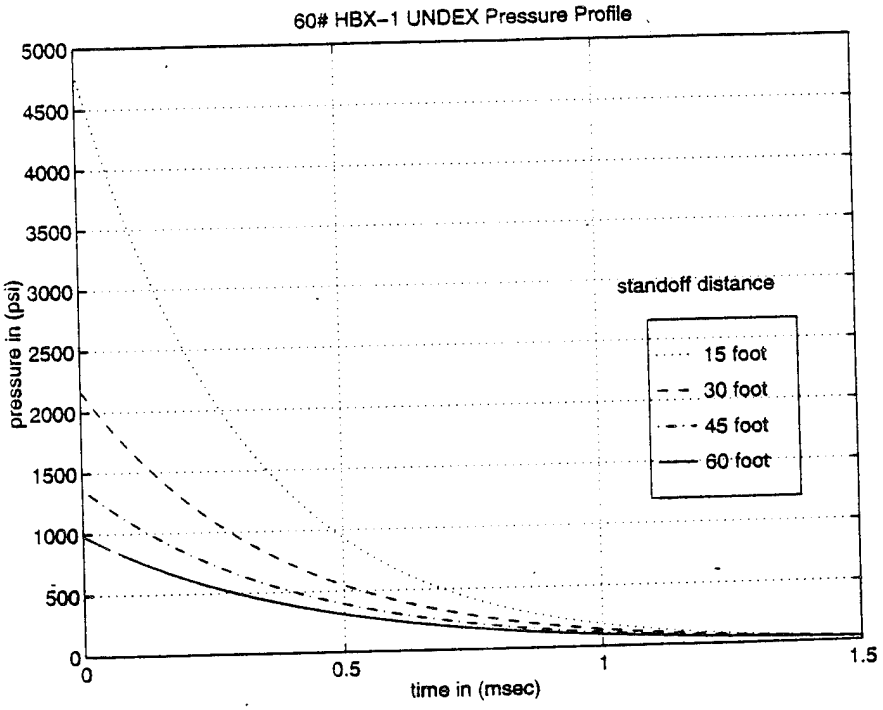

Figure 6. Pressure Profile for HBX-1 60 Pound Charge

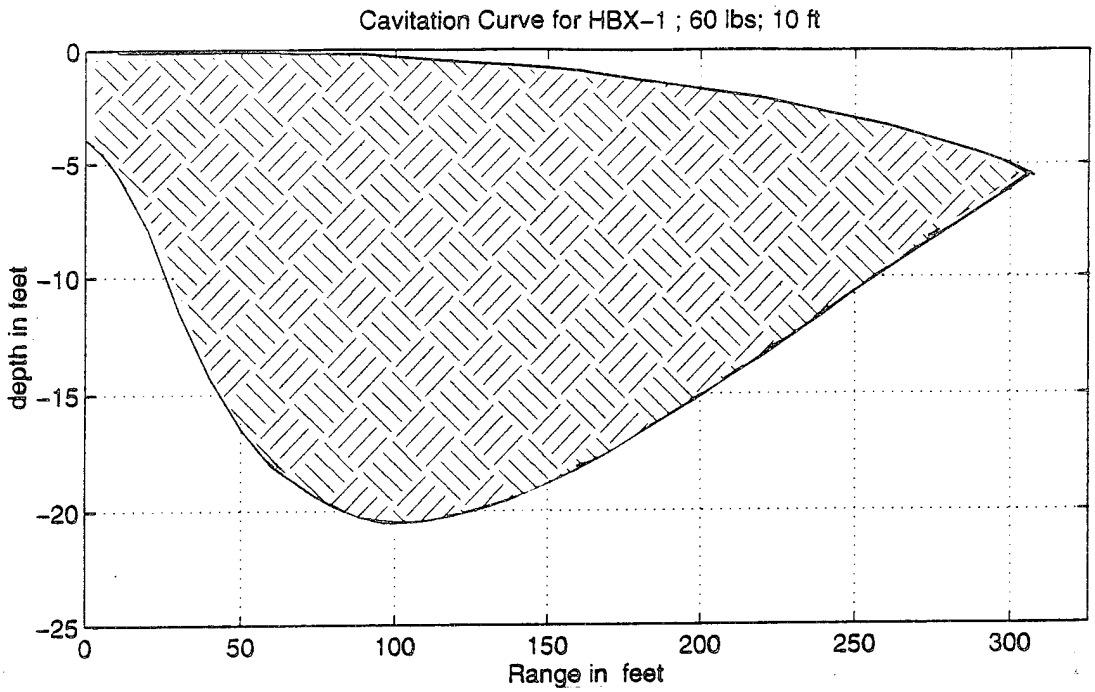

Figure 7. Cavitation Curve: HBX-1 60 Pound Charge, 10 Foot Depth

1. Perfect Model Full (PMF)

The Perfect Model Full is the original model which has 1360 wet elements and 1442 nodes. It has no modal imperfections introduced into its mesh algorithm and subsequently its modal imperfection distribution plot would be a flat plane.

The deformation analysis was conducted using axial and longitudinal deformation plots, von Mises stress contour and effective plastic strain plots. Axial and hoop strain time histories are provided for selected points of interest. Tabulated data for maximum von Mises and effective plastic strain are provided in Tables 2 and 3 in Appendix D.

The axial deformation plots, Figure 8 shows the time progression of the shock induced pulse for four time frames; 0.0384, 0.4896, 0.9881, and 1.9888 msec. This axial view has the endplates and stiffeners removed for enhanced visual recognition. There is an appearance of light radial deformation and some slight crumpling or wrinkling at a few peaks with an increase in time. The longitudinal deformation plots, Figure 9 for the same times shows the deformation as the shock progresses through the cylinder. The explosive charge is positioned perpendicular to the longitudinal axis. During the early time period after impact the deformation looks symmetric and has a general appearance to that of an accordion with a slight pinching near the two stiffeners and end plates. The deformation also appears to have little dependence on the radial angle of impact with the exception of the backside of the cylinder which has a couple small dishes between the stiffeners. The shell deformation near the stiffeners and end plates provide the most distinguishing feature as far as amplitude of the peaks or pinching that forms the accordion appearance.

The effective plastic strain contour plot, Figure 10 clearly shows the greater strains at the two ends front centerline. This coincides with Fox (1992) determination that the most severe deformation would occur at the locations near the end and backside of the cylinder. This results in the greater plastic strains at the ends and backside centerline possibly due to two phenomena. The first is the large inertia forces applied to the cylindrical shell created by the mass of the end plates. Second, the thickness of the end plates are significantly stiffer and they lack flexibility causing the thinner/weaker shell material to deform in the response to the applied force.

The longitudinal and circumferential (hoop) strain time histories at the front of the cylinder midpoint centerline will be compared with specific imperfect distributions in later sections.

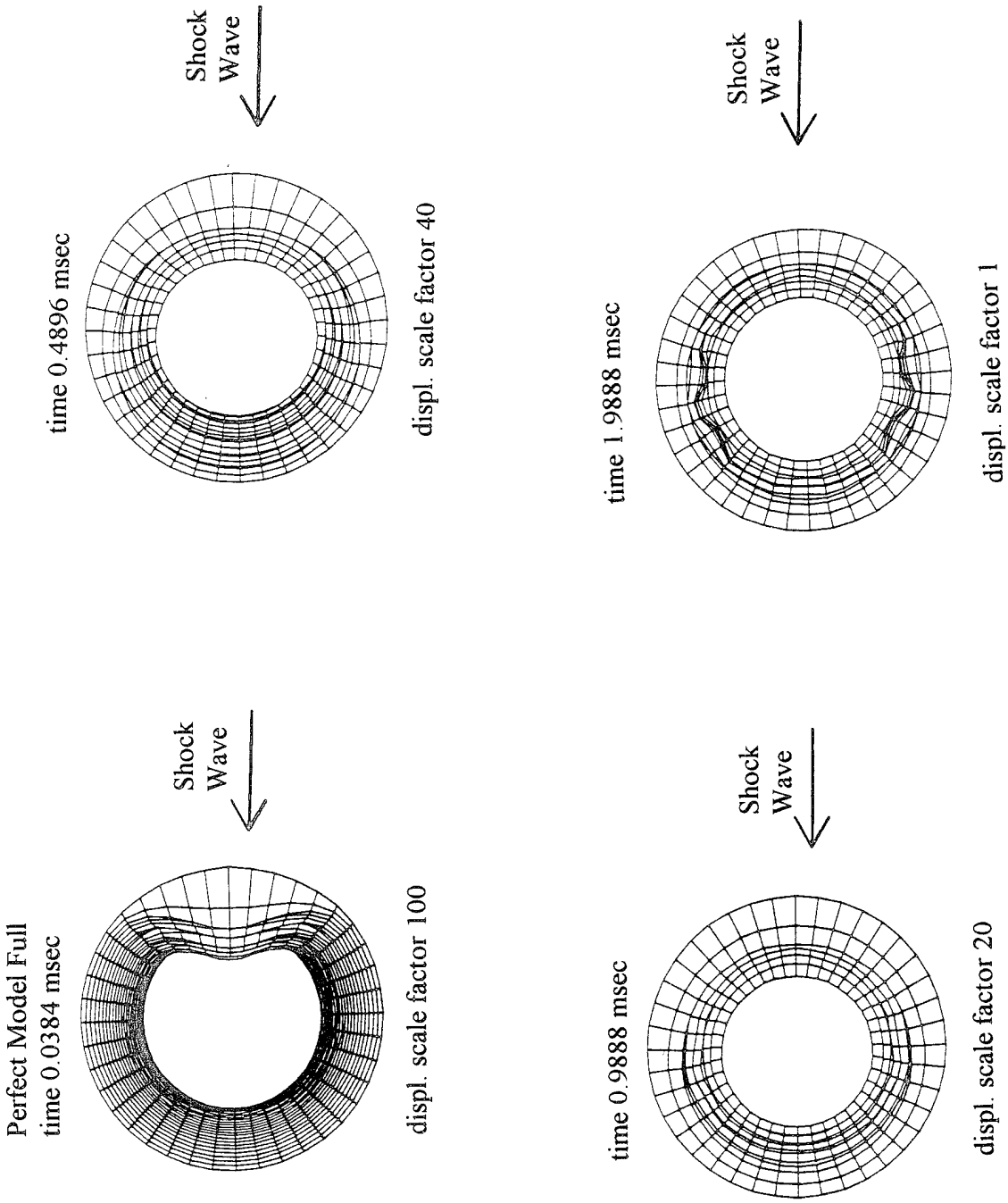

Figure 8. Perfect Model: Axial Deformation plots for 0.0384, 0.4896, 0.9881 and 1.9881 msec

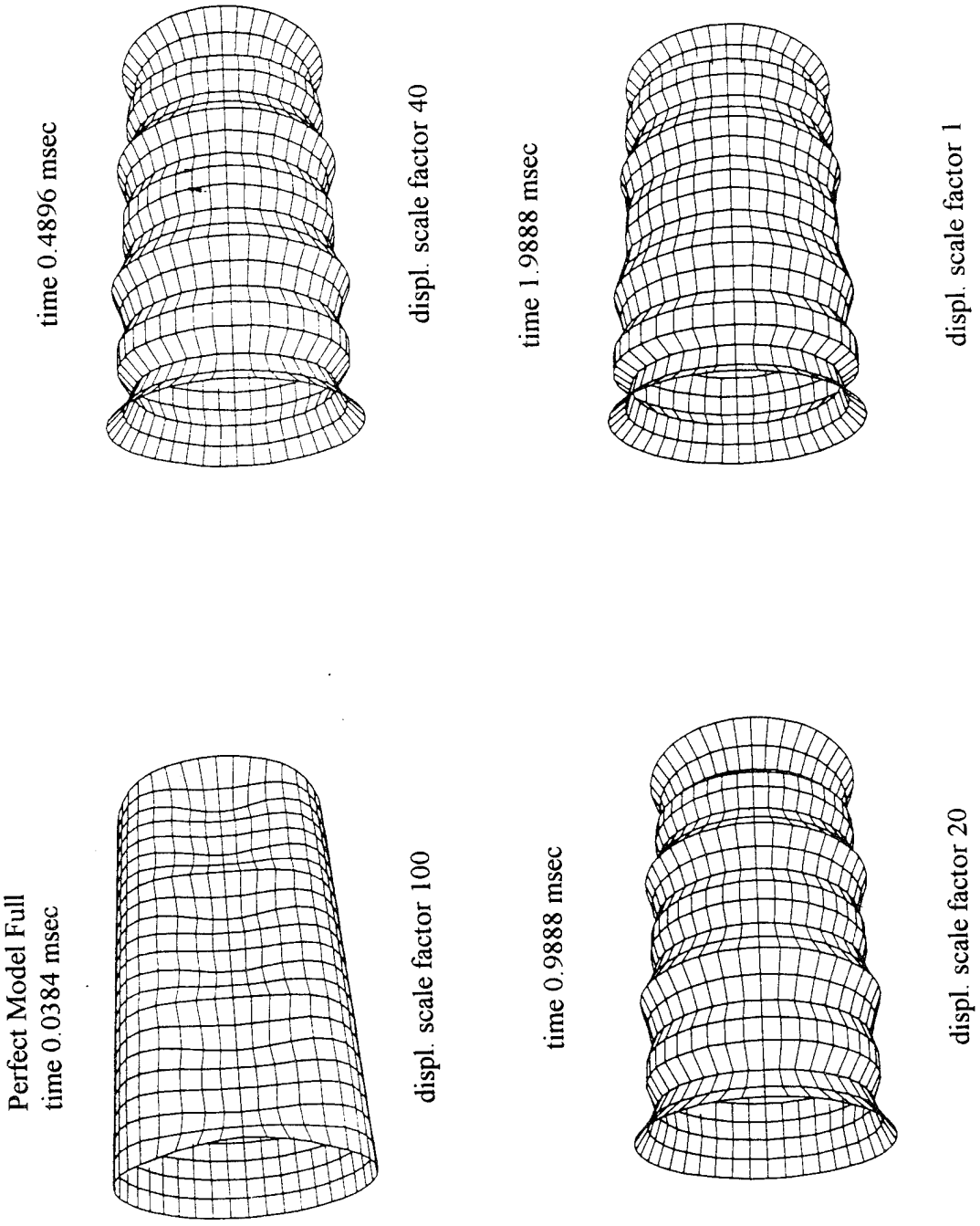

Figure 9. Perfect Model: Longitudinal Deformation plots for 0.0384, 0.4896, 0.9881 and 1.9881 msec

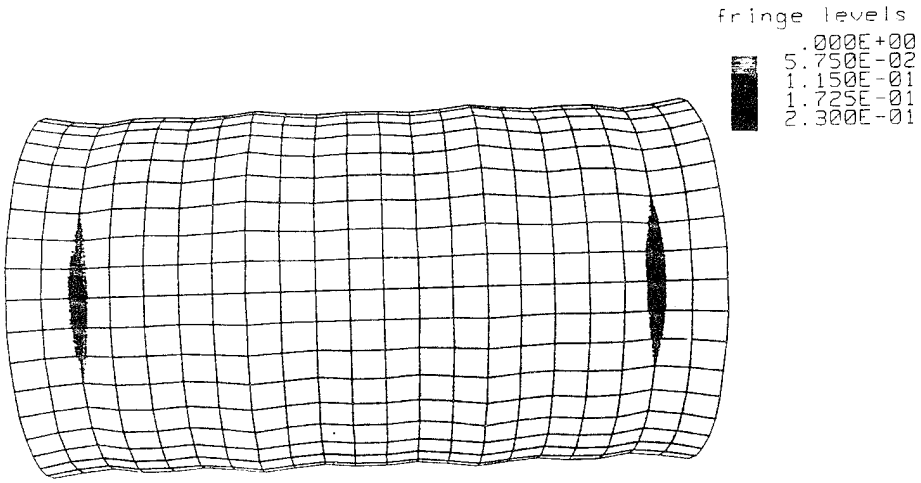

Figure 10. Perfect Model: Effective Plastic Strain frontside, Contour Plot for 0.4896 msec

B. IMPERFECT CYLINDER MODEL

The imperfect cylinder model was generated in the same manner as the perfect model with the exception of the introduction of modal imperfections into the mesh algorithm. The actual imperfection distribution that is introduced compared to the perfect model varies between zero and 0.3 percent of the radius to the that particular element. This thesis analyzes a combination of geometric and material modal imperfections. The eight different modal imperfection models analyzed by this thesis are:

1. Radial Imperfections (Rimp)
2. Axial Imperfections (Aimp)
3. Radial and Axial Imperfections (Imp)
4. Radial Imperfections with Random Phase Shift (Rimpp)
5. Axial Imperfections with Random Phase Shift (Aimpp)
6. Radial and Axial Imperfections with Random Phase Shift (Impp)
7. Material Imperfections (Mtl5)
8. Material, Radial and Axial Imperfections with Random Phase Shift (Mtlimpp)

Each of these models was subjected to the same underwater shock wave as the perfect model. These models use the radial, axial, and imperfection sensitivity analysis as outlined in the Imperfection section to introduce the modal imperfection distribution. These calculations are performed by a fortran program for geometric imperfections provided in Appendix B.

The geometric imperfection fortran program requires the input of the number of nodes on the surface of the cylinder. It then reads the DYNA3D input file ingrido and calculates a specific radius for each of the inputed nodes from their global X, Y and Z positions. For the random phase case a different random number generator was used for both radial and axial models to determine random phase angle. Then the summation of the cosine series for each modal imperfection was performed. For material imperfections a similar fortran program with a random number generator was used and is provided in Appendix C. In this program

each element has an associated material that is modified according to the random number generator. A summary of interesting axial and longitudinal deformation plots will be provided in the summary of results section.

1. Radial Imperfections (Rimp)

The radial imperfection model was the first model to be analyzed. It has only the radial imperfection introduced into the mesh algorithm and is essentially the same model used by Hooker (1993). The initial modal imperfection distribution introduced into the cylinder and the resultant three-dimensional mesh or carpet plot are provided in Figure 11. The top plot is an axial view of the cylinder with a modal imperfection amplitude magnified by a factor of 50. The bottom plot is the three-dimensional mesh or carpet plot and its modal imperfection amplitude is magnified by a factor of 100. The periodic oscillations are readily observed in the circumferential direction in the mesh plot.

Deformation analysis was conducted using axial and longitudinal deformation plots, von Mises stress contour and effective plastic strain plots. Axial and hoop strain time histories are provided for selected points of interest.

The axial deformation plot, Figure 12 shows a time progression from 0.0384, 0.4896, 0.9881, and 1.9888 msec. There appears an increase in the periodic crumpling with what seems to be ten peaks around the circumference of the cylinder. The ten peaks are probably the resultant of the summation of the first ten modal imperfections. There are two relatively sharp peaks symmetric on either side of the axis of charge between 1 and 2 msec. These two peaks look remarkably similar to the original deformation pattern. The sharpness of the peaks could signified that the plastic deformation for the mesh size is too large and probably can not be accurately determined. The longitudinal deformation plot, Figure 13 shows for the same times the deformation as the shock induced pulse progresses through the cylinder. The early time looks similar to pinching and accordion of the perfect model but visual difference are more readily apparent by 0.5 msec. These differences are the appearance of a frontside twin ridge dishing effect between the stiffeners and a greater magnitude of deformation than for the perfect case. Significant dishing, crumpling and

buckling are readily observable by 1 msec. This is probably the onset of failure.

A comparison of the maximum von Mises stresses between Rimp and model perfect show about 2 percent greater difference for radial imperfection within the first msec after impact. The tabulated data for maximum von Mises stresses are provided in Table 2 in Appendix D.

The effective plastic strain contour plot also shows a similar appearance to the model perfect. These plastic strains are also located on the frontside of the cylinder at the far ends and backside centerline. As noted before this is probably due to the deformation created by the effect that Fox (1992) described during the dynamic response of the cylinder. A comparison of the effective plastic strain between Rimp and model perfect shows about 11 percent greater difference for radial imperfection within the first msec after impact. The effective plastic strain data is provided in Table 3 in Appendix D.

The circumferential and longitudinal strain time histories at the front of the cylinder midpoint centerline, element 370 are compared to the perfect model in Figure 14. The hoop and axial strains are greater for the Radial imperfection case than for the perfect case in both plots.

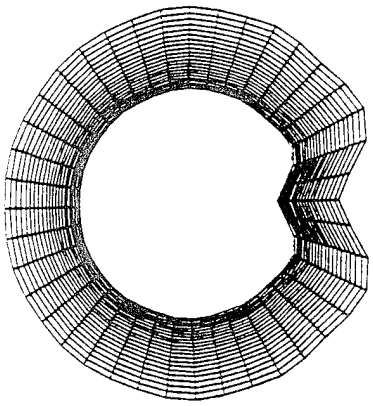

(a) Initial Modal Imperfection distribution, axial view, scaled up 50X

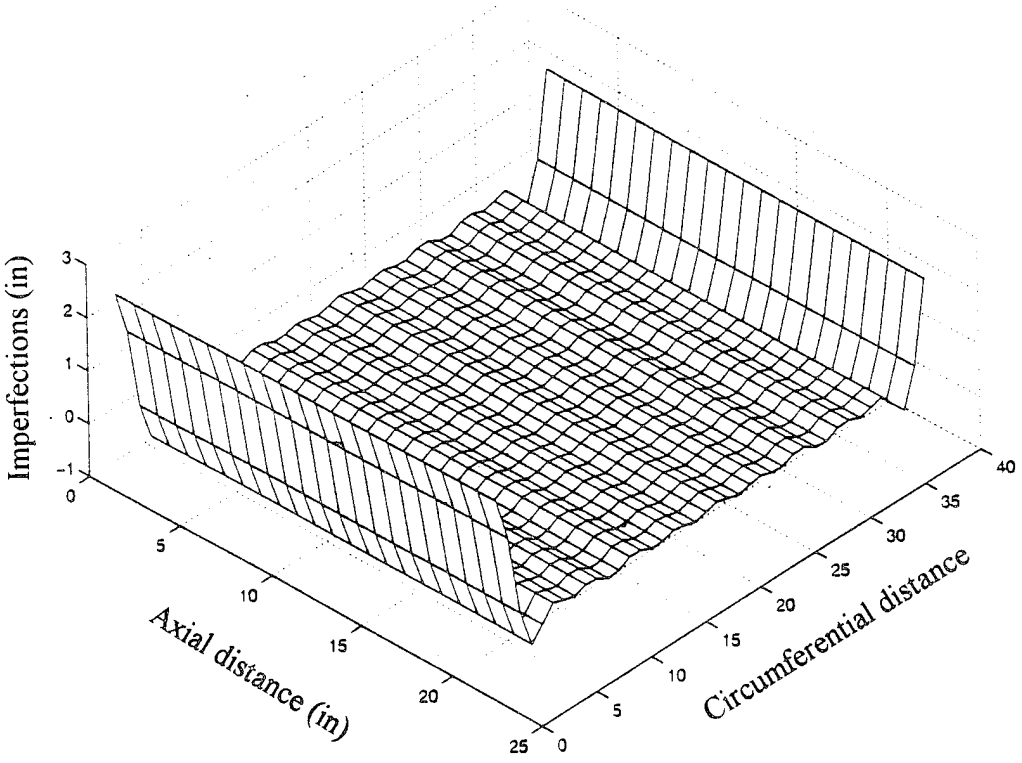

(b) Three Dimensional Mesh Plot of Cylindrical Surface, scaled up 100X

Figure 11. Radial Imperfection Distribution (Rimp): (a) Initial Modal Imperfection distribution, axial view (b) Three Dimensional Mesh Plot of Cylindrical Surface

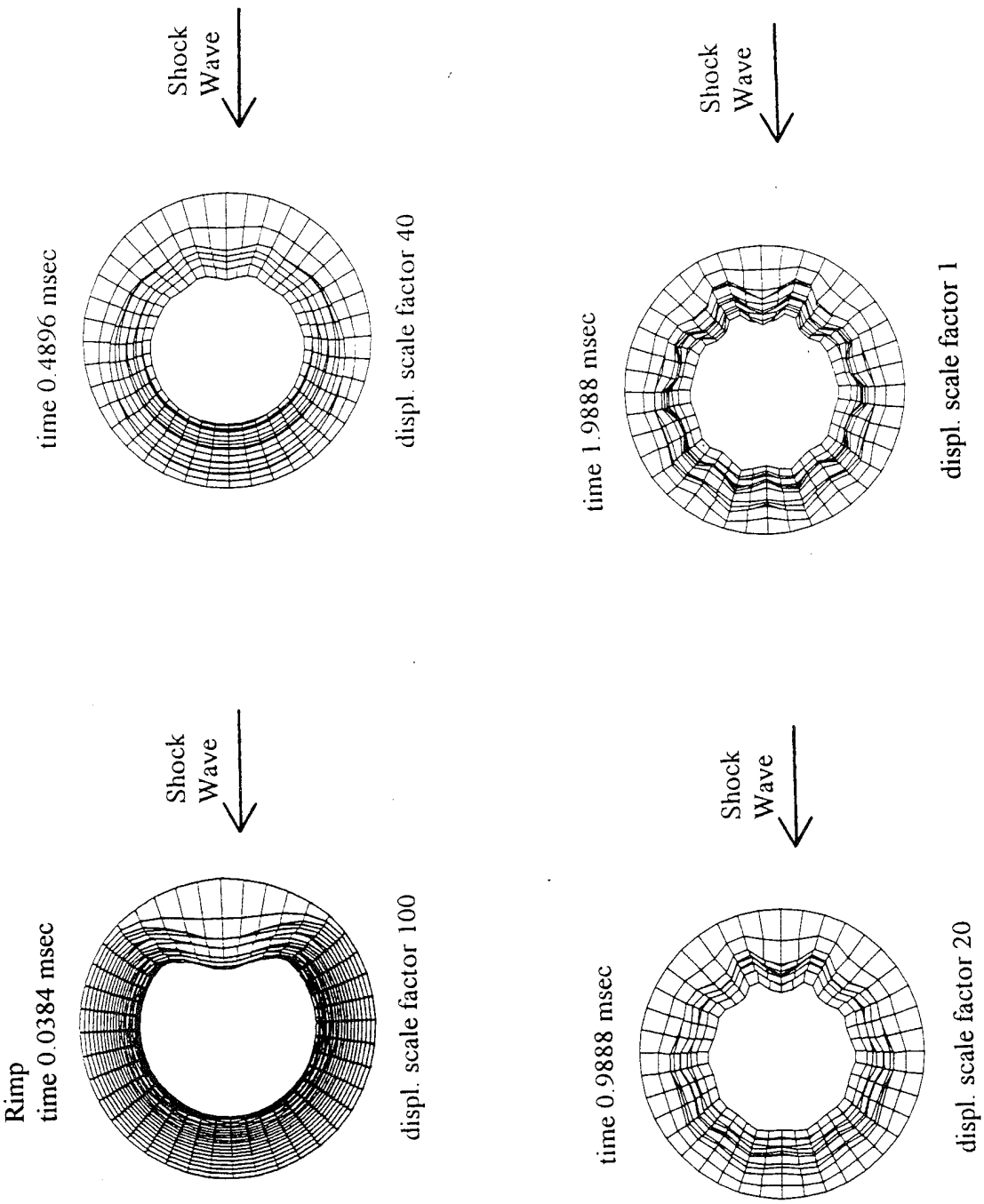

Figure 12. Radial Imperfections: Axial Deformation plots for 0.0384, 0.4896, 0.9888, and 1.9888 msec

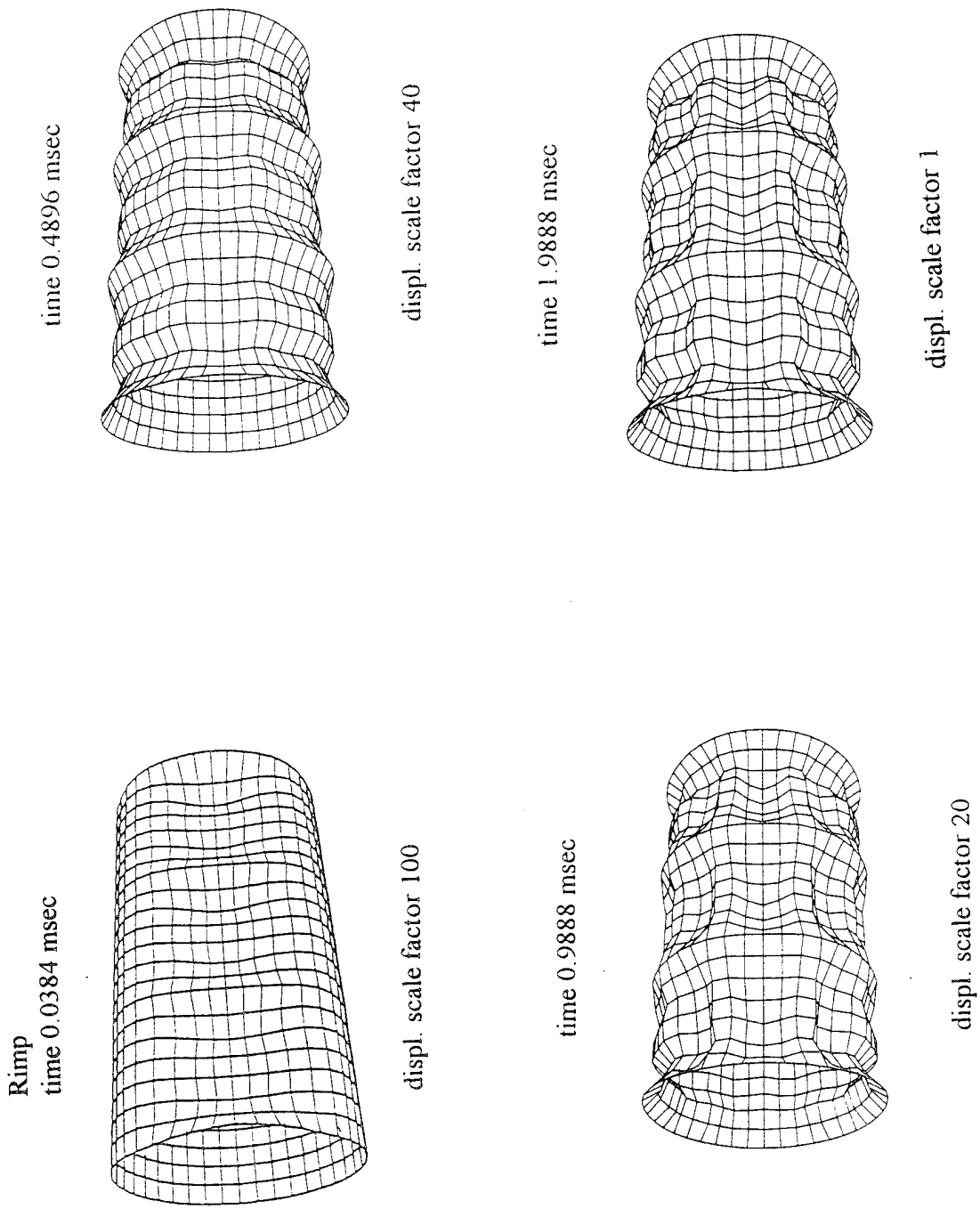

Figure 13. Radial Imperfections: Longitudinal Deformation plots for 0.0384, 0.4896, 0.9888 and 1.9888 msec

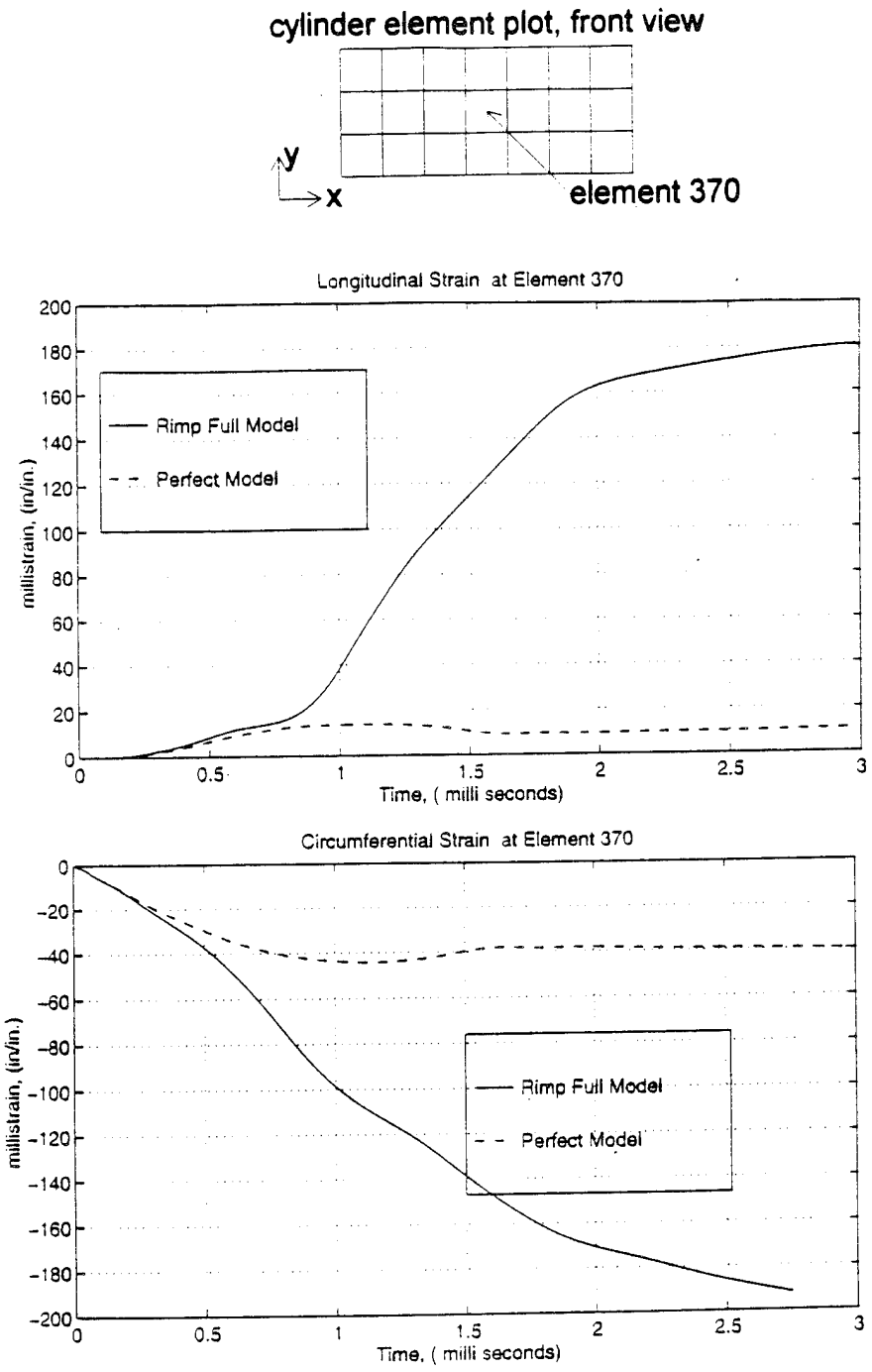

Figure 14. Radial Imperfections: Circumferential and Longitudinal Strain at front of Cylinder Midpoint Centerline

2. Axial Imperfections (Aimp)

The axial imperfection model was the second model to be analyzed. It has only the axial imperfection introduced into the mesh algorithm. The initial modal imperfection distribution introduced into the cylinder is a function of axial direction and is at a reduced, 1/4 the modal amplitude of the radial case. The three-dimensional mesh plot scaled by a factor of 100 and initial axial modal distribution scaled by a factor of 200 are provided in Figure 15. The bottom three-dimensional carpet plot has distinguishing ripples running along the axial direction. As can be seen in the top longitudinal view of the deformation plot these ripples were cause by a very slight oscillation along the axial direction.

Deformation analysis was conducted using axial and longitudinal deformation plots, von Mises stress contour and effective plastic strain plots. Axial and hoop strain time histories are provided for selected points of interest.

The axial deformation plot in Figure 16 shows a time progression from 0.0384, 0.4896, 0.9881, and 1.9888 msec. These plots have a strong resemblance to the model perfect case. They have the same light radial deformation and some slight crumpling at a few peaks with increasing time. The longitudinal deformation plot is shown in Figure 17. This deformation plot shows the shock induced pulse progresses through the cylinder as a function of time. The plot looks similar to the perfect model. The accordion appearance is the most distinguishable feature present.

The difference in maximum von Mises stresses and the effective plastic strain contour plots through the first 3 msec are essentially negligible. The data for the maximum von Mises and effective plastic strain is provided in Table 2 and Table 3 in Appendix D.

The circumferential and longitudinal strain time histories at the front of the cylinder midpoint centerline are shown in Figure 18. The two graphs clearly show the negligible difference through the first msec and no more than one percent difference for the following two msec.

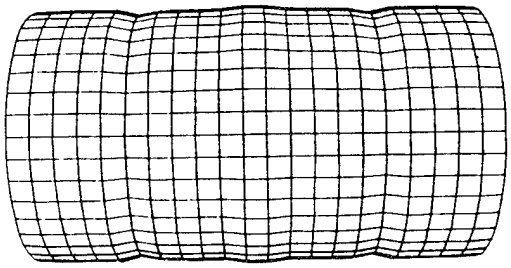

(a) Initial Modal Imperfection distribution, longitudinal view, scaled up 200X

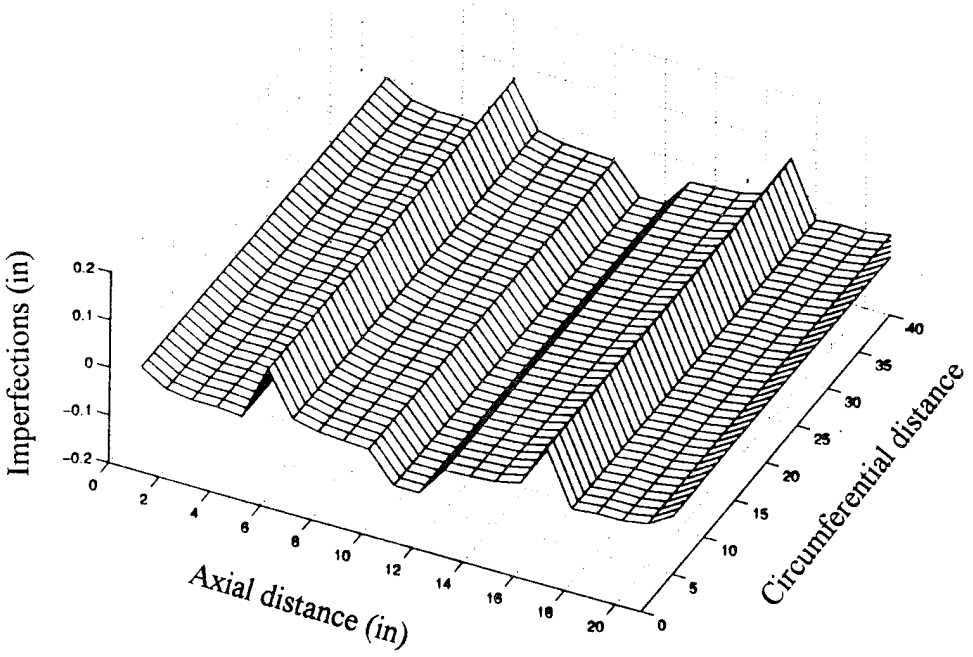

(b) Three Dimensional Mesh Plot of Cylindrical Surface, scaled up 100X

Figure 15. Axial Imperfection Distribution (Aimp): (a) Initial Modal Imperfection distribution, longitudinal view (b) Three Dimensional Mesh Plot of Cylindrical Surface

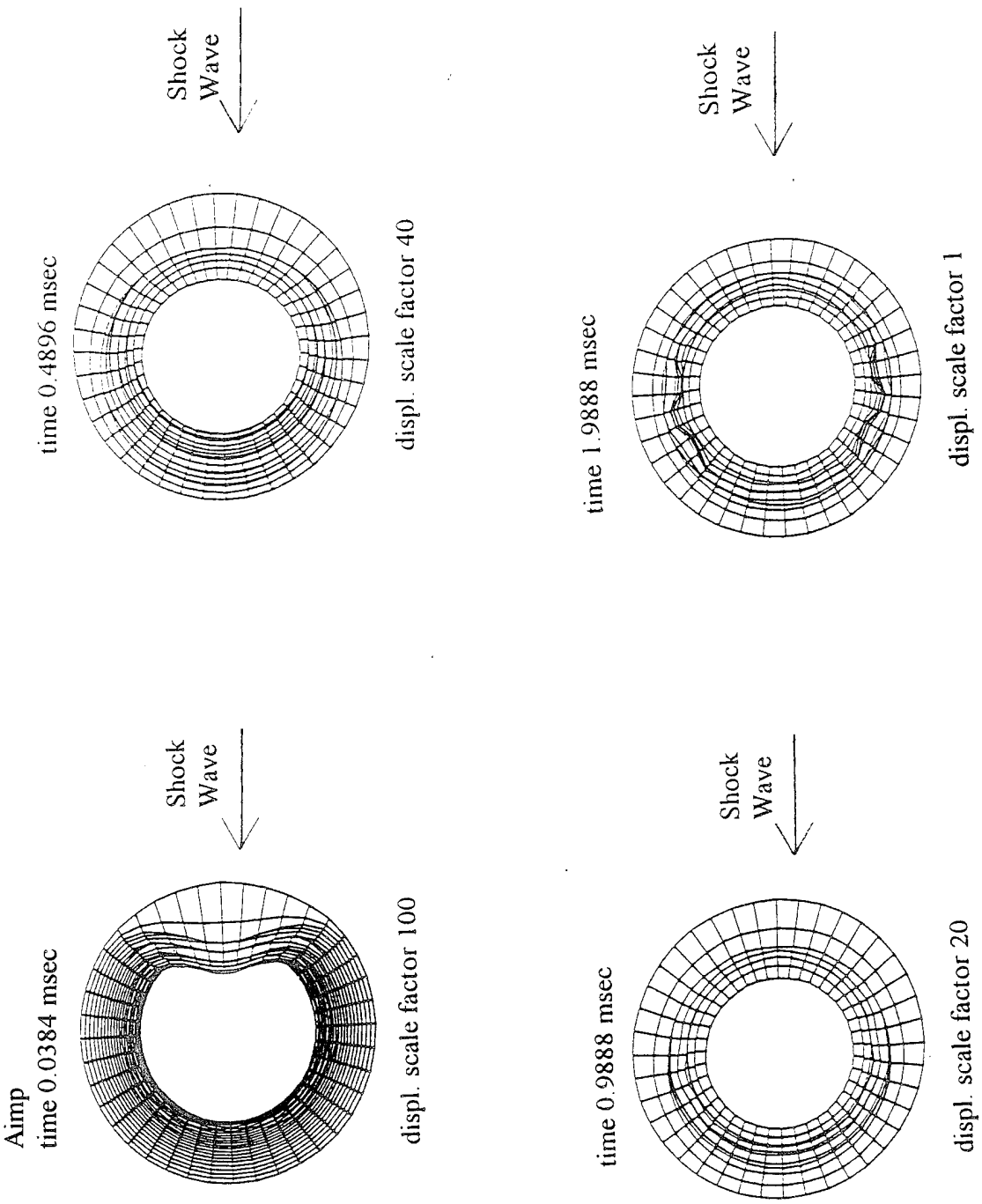

Figure 16. Axial Imperfections: Axial Deformation plots for 0.0384 0.4896, 0.9888, and 1.9888 msec

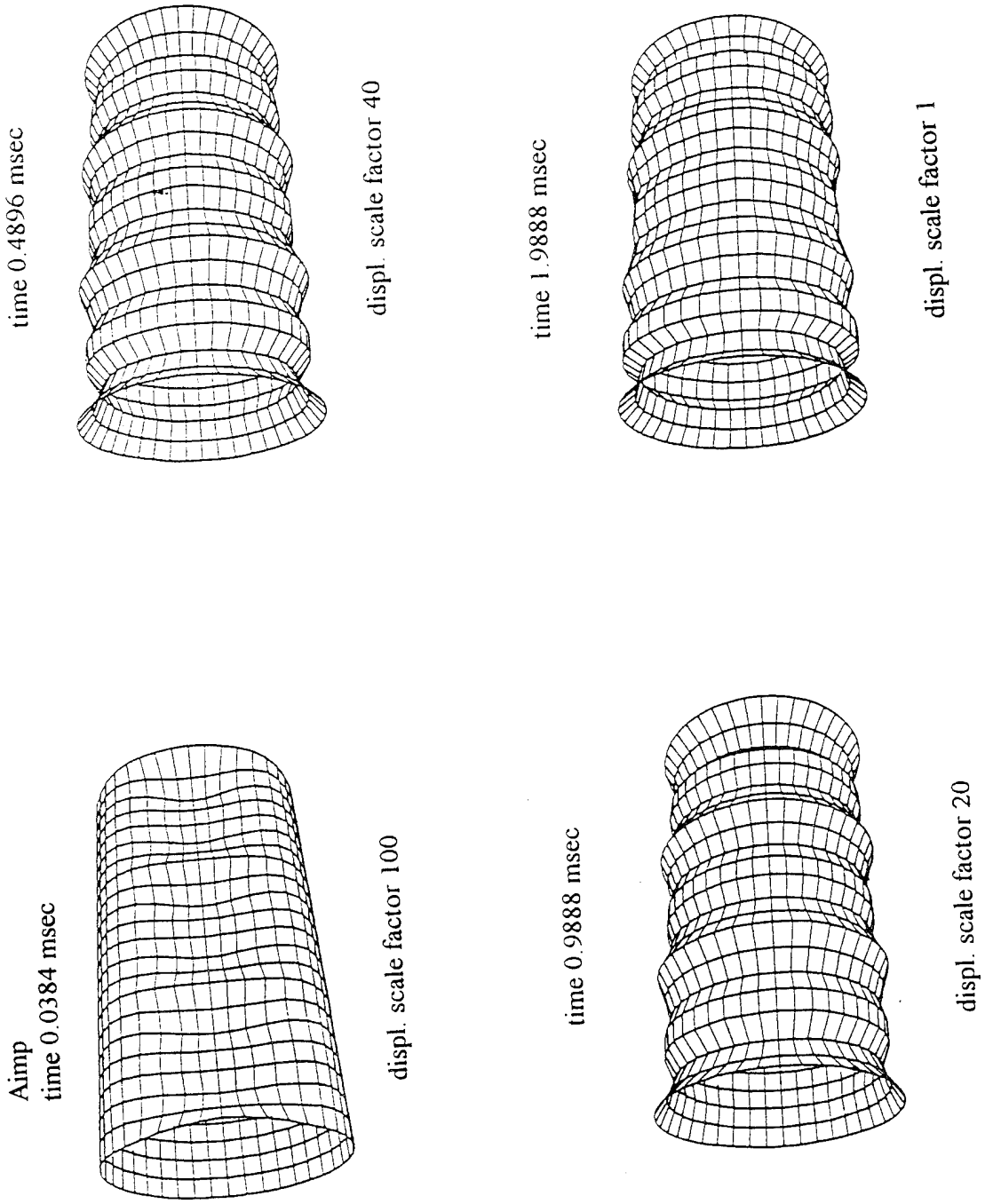

Figure 17. Axial Imperfections: Longitudinal Deformation plots for 0.0384, 0.4896, 0.9888, 1.9888 msec

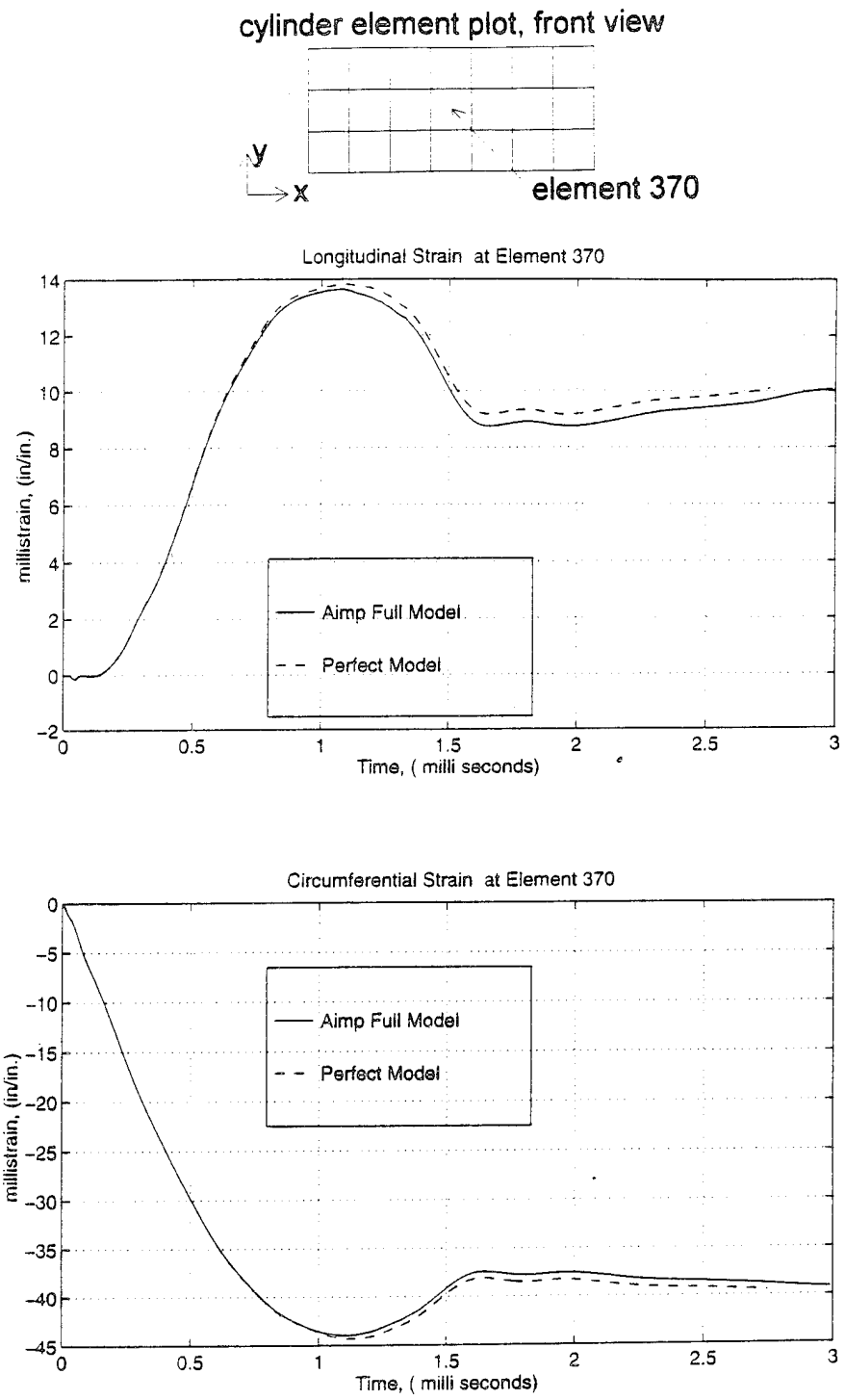

Figure 18. Axial Imperfections: Circumferential and Longitudinal Strain at front of Cylinder Midpoint Centerline

3. Radial and Axial Imperfections (Imp)

The radial and axial imperfection model was the third model to be analyzed. It incorporates the combined radial and axial imperfection into the mesh algorithm. The initial modal imperfections distribution introduced into the cylinder and the resultant three-dimensional mesh plot are provided in Figure 19. The top plot shows the axial view of the modal imperfection scaled by a factor of 50. There is essentially no distinguishable effect by the axial modal imperfection ripples in this plot. The bottom of the figure shows the mesh plot scaled by a factor of 25. The plots are a superposition of the radial peaks or oscillations and the axial ripples. The initial modal imperfection clearly shows the distinguishable twin peak symmetric with the shock axis.

Deformation analysis was conducted using axial and longitudinal deformation plots, von Mises stress contour and effective plastic strain plots. Axial and hoop strain time histories are provided for selected points of interest.

The axial deformation plot, Figure 20 shows a time progression from 0.0384, 0.4896, 0.9881, and 1.9888 msec. These plots have a appearance of the Radial imperfections with the exception of the magnitude. They have the same periodic crumpling with peaks around the circumference of the cylinder. These peaks form relatively sharp points beyond 1 to 2 msec. The final deformation pattern also has the similar appearance to the original modal imperfection. Figure 21 shows the longitudinal deformation plots. They also have similar appearances to the Rimp. It has the similar appearance of a dishing effect between the stiffeners with a greater magnitude of deformation than for the Rimp case.

A comparison of the maximum von Mises stresses between Imp and Rimp shows negligible difference for radial and axial imperfection within the first msec after impact. The difference between Imp and model Perfect is a little greater than 4 percent. This data is provided in Table 2 in Appendix D.

A comparison of the effective plastic strains between Imp and Rimp also shows only a slightly greater difference of 0.2 percent for radial imperfection within the first msec. after impact. This data is provided in Table 3 in Appendix D.

The circumferential and longitudinal strain time histories at the front midpoint

centerline, element 370 are compared to the perfect model in Figure 22. The hoop and axial strains are greater for the radial and axial imperfection case than for the perfect case in both plots. The effective plastic strain at the front centerline right end and backside centerline are shown in Figure 23. In both cases the Imp model has greater plastic strain.

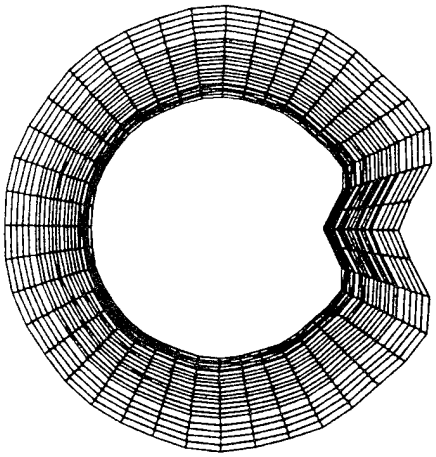

(a) Initial Modal Imperfection distribution, axial view, scaled up 50X

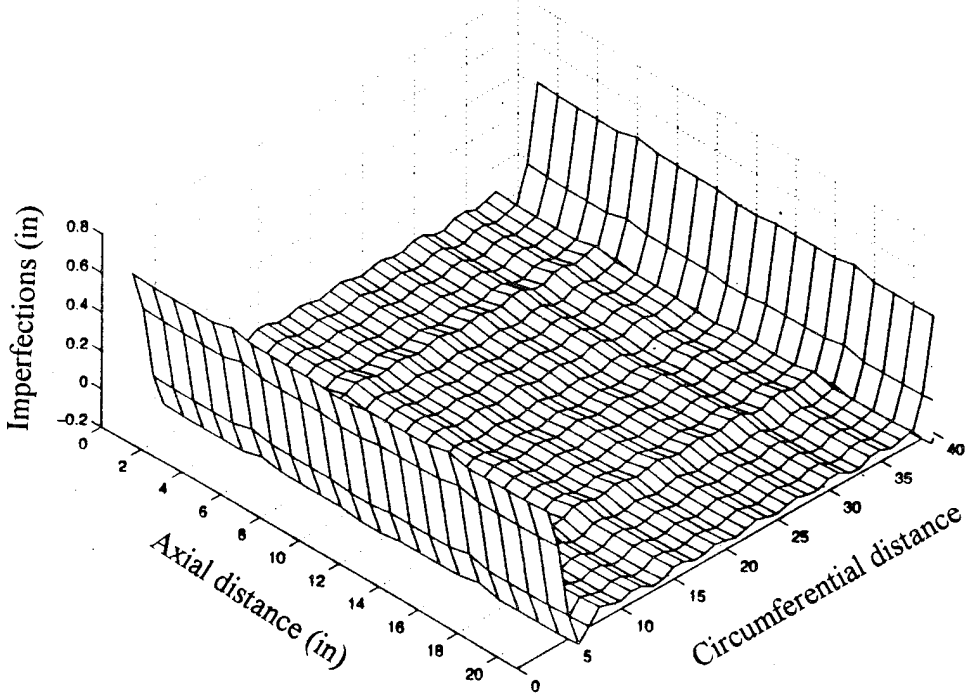

(b) Three Dimensional Mesh Plot of Cylindrical Surface, scaled up 25X

Figure 19. Radial and Axial Imperfection Distribution (Imp): (a) Initial Modal Imperfection distribution, axial view (b) Three-Dimensional Mesh Plot of Cylindrical Surface

Figure 20. Radial and Axial Imperfections: Axial Deformation plots for 0.0384, 0.4896, 0.9888, and 1.9888 msec

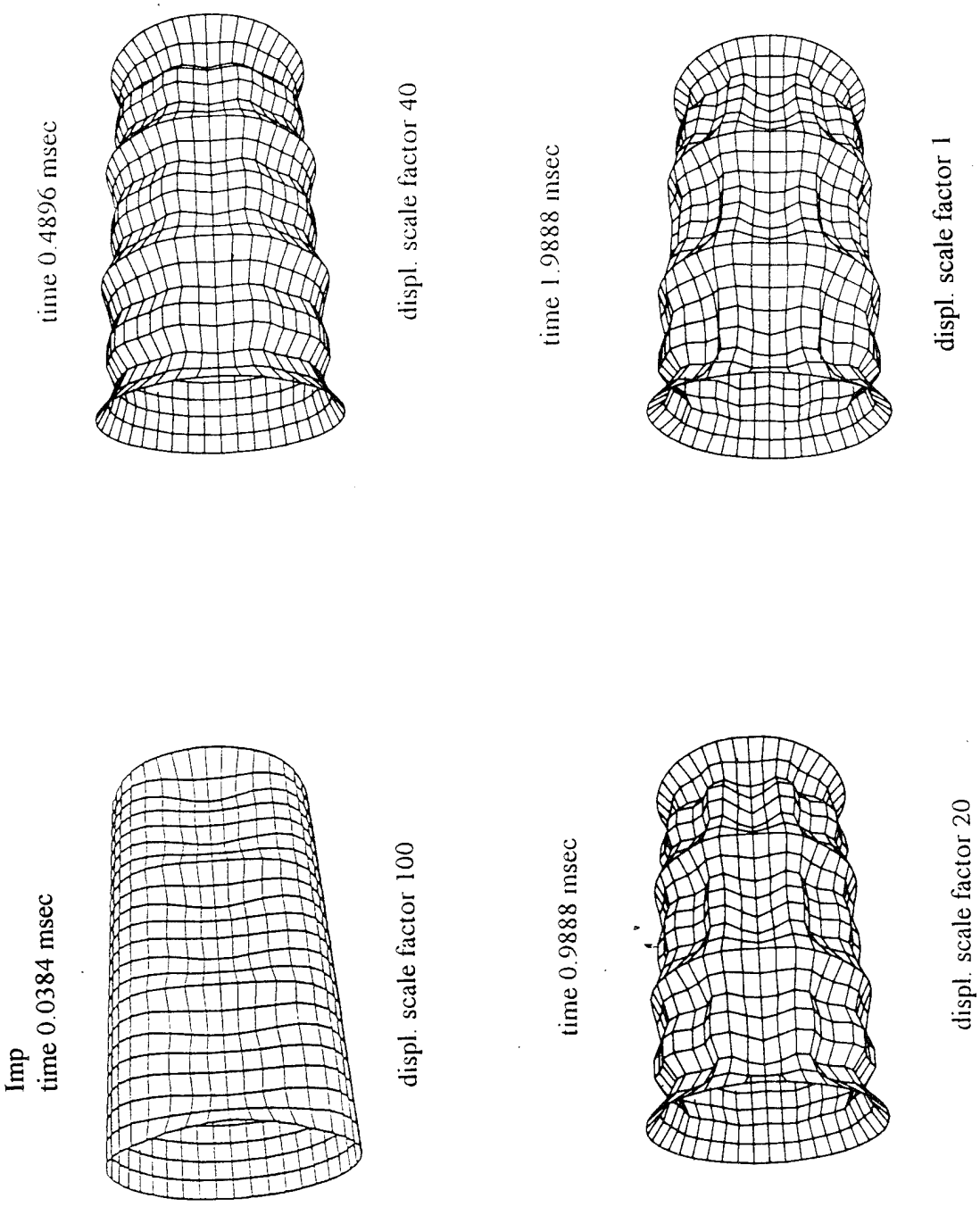

Figure 21. Radial and Axial Imperfections: Longitudinal Deformation plots for 0.0384, 0.4896, 0.9888, and 1.9888 msec

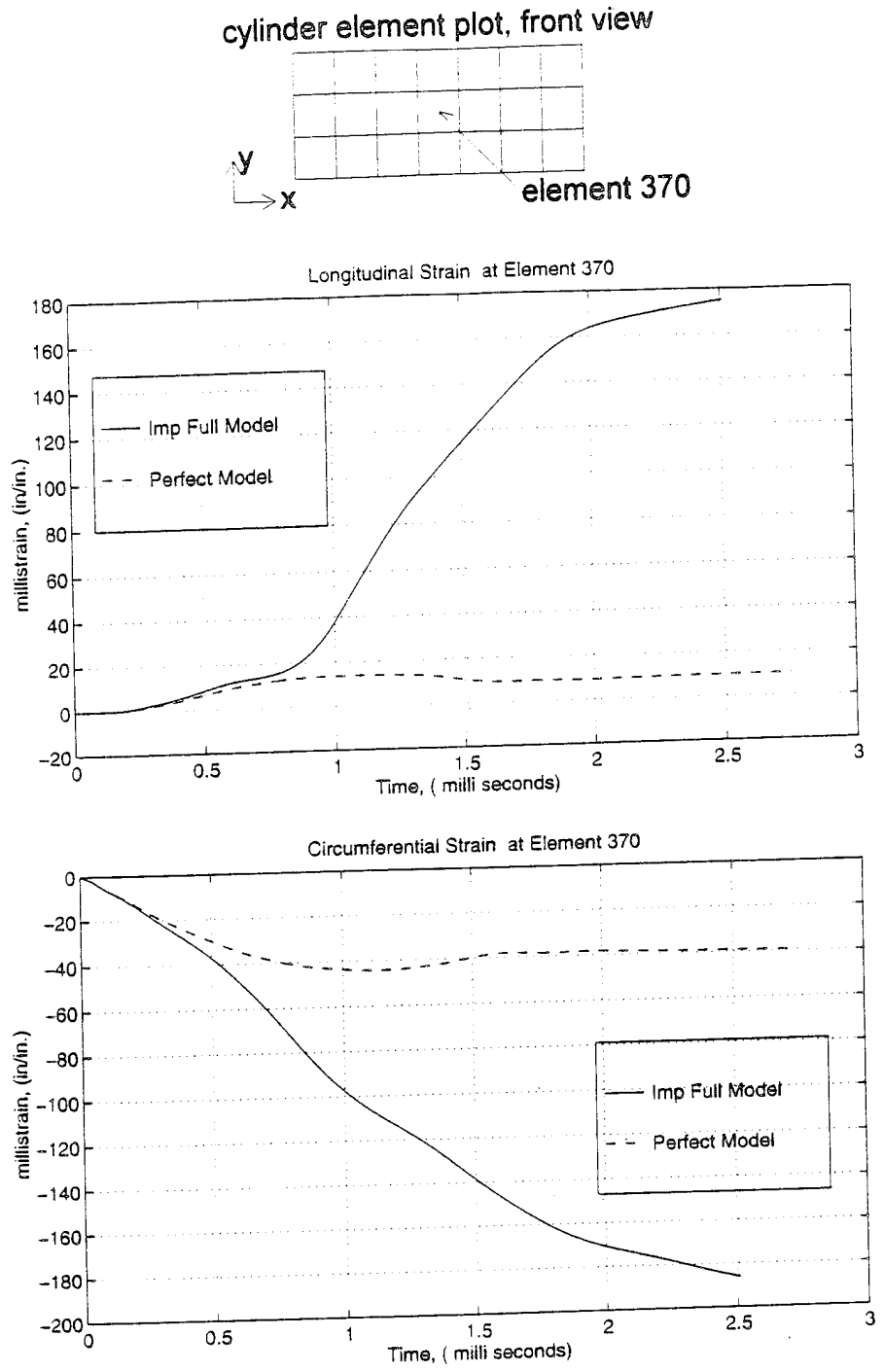

Figure 22. Radial and Axial Imperfections: Circumferential and Longitudinal Strain at front of Cylinder Midpoint Centerline

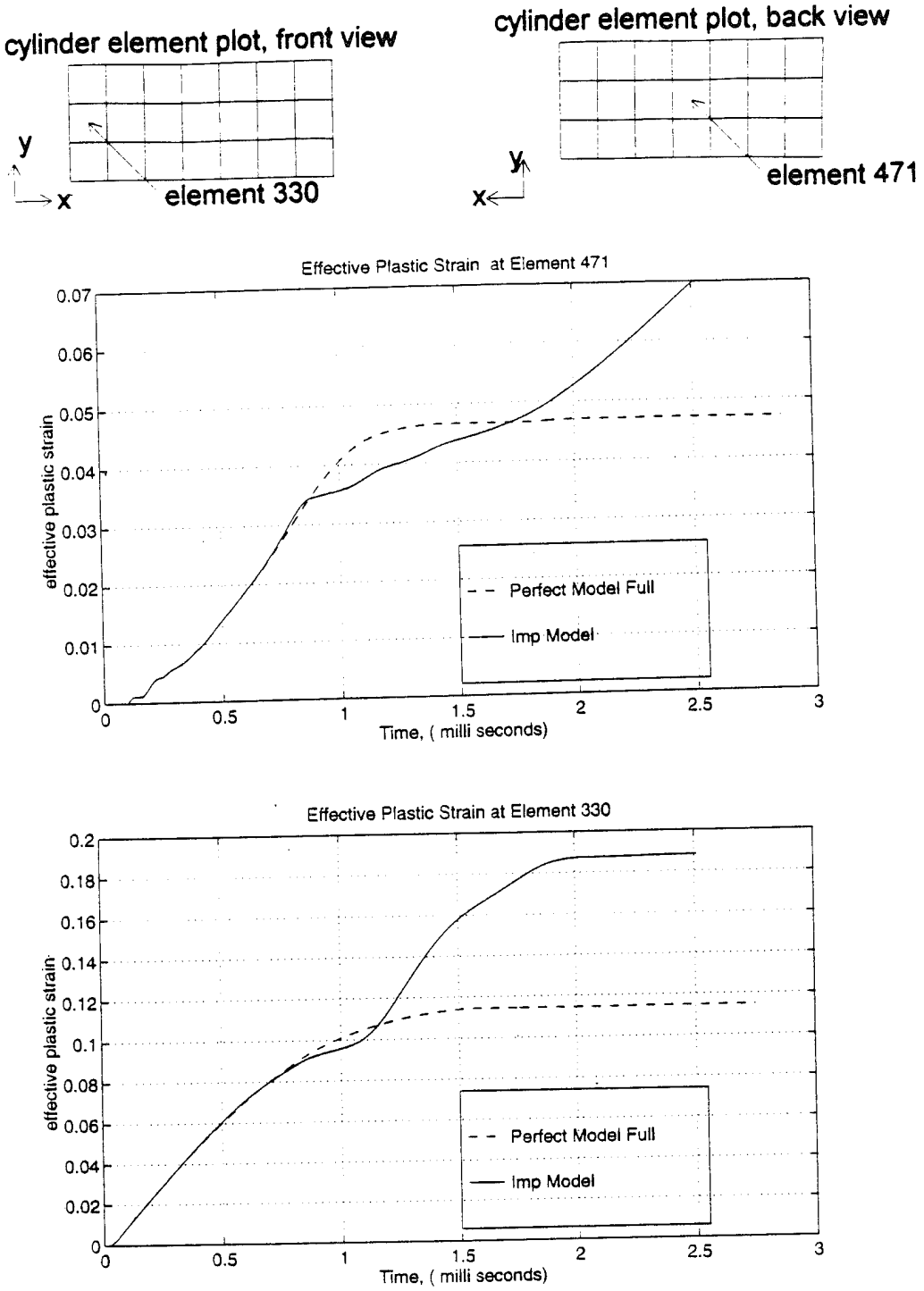

Figure 23. Radial and Axial Imperfections: Effective Plastic Strain at backside of Cylinder Midpoint and front of Cylinder at right end

4. Radial Imperfections with Random Phase Shift (Rimpp)

The radial imperfection with random phase shift was the fourth model to be analyzed. This model has radial and random phase shift combined modal imperfection introduced into the mesh algorithm. The random phase shift assumption is reasonable for cylinders without welded seams. The initial modal imperfections distribution introduced into the cylinder and the resultant three-dimensional mesh plot are provided in Figure 24. The top plot is the axial view of the cylinder with a the modal imperfection scaled by a factor of 50. The random nature of the oscillations is visibly different from the periodic nature of the non-random case. The bottom plot shows the three-dimensional mesh plot with its modal amplitude scaled by a factor of 50. The oscillations are not periodic as in the non-random case.

Deformation analysis was conducted using axial and longitudinal deformation plots, von Mises stress contour and effective plastic strain plots. Axial and hoop strain time histories are provided for selected points of interest.

The axial deformation plot, Figure 25 shows a time progression from 0.0384, 0.4896, 0.9881, and 1.9888 msec. The general deformation appearance is different from the non-random models, for example the dominant twin peaks. There appears to be an increase in the periodic crumpling with peaks around the circumference of the cylinder as compared to the non-random Rimp. This deformation is also progressing in relation to the initial modal imperfection. The longitudinal deformation plot in Figure 26 shows the deformation as the shock induced pulse progresses through the cylinder. There is an greater appearance of a single ridge dishing effect on the front between the stiffeners than for the other cases.

The maximum von Mises stresses as compared to model Perfect and Rimp are within 1.1 and 1.5 percent respectively after the first msec. The tabulated data is provided in Table 2 in Appendix D.

The effective plastic strain contour plot is similar in appearance to the model perfect but are about 12 percent greater within the first msec after impact. The data is provided in Table 3 in Appendix D.

The circumferential and longitudinal strain time histories at the front of the cylinder midpoint centerline are provided in Figure 27. These plots show a significant difference in magnitude after one msec than compared to the perfect model.

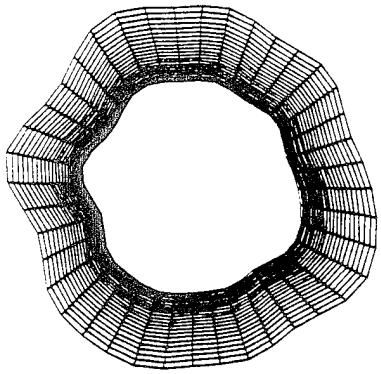

(a) Initial Modal Imperfection distribution, axial view, scaled up 50X

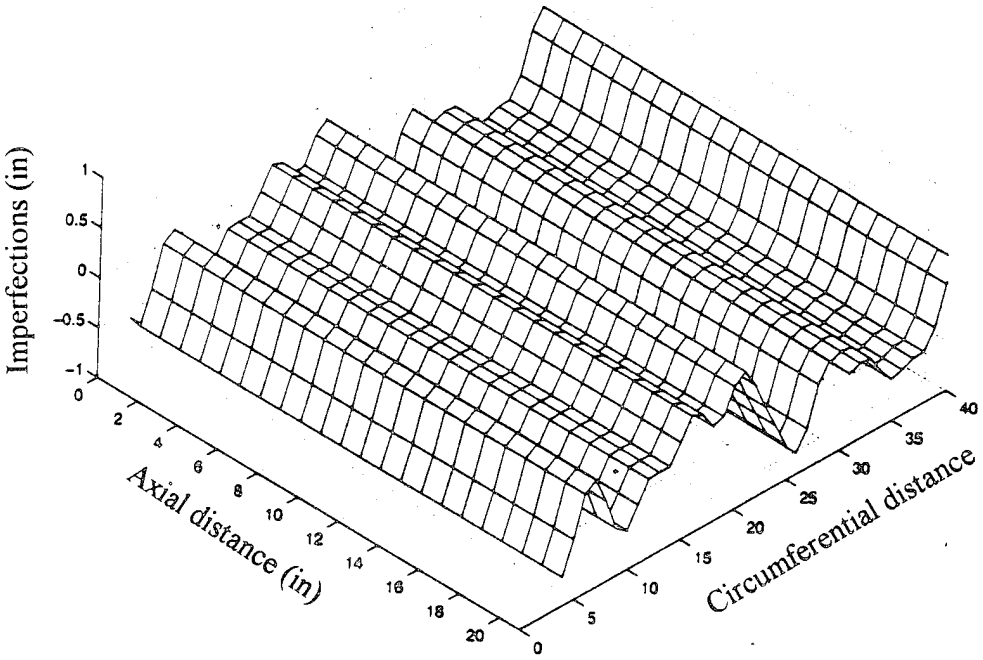

(b) Three Dimensional Mesh Plot of Cylindrical Surface, scaled up 50X

Figure 24. Radial Imperfections with Random Phase Shift (Rimpp): (a) Initial Modal Imperfection Distribution, axial view (b) Three Dimensional Mesh Plot of Cylindrical Surface

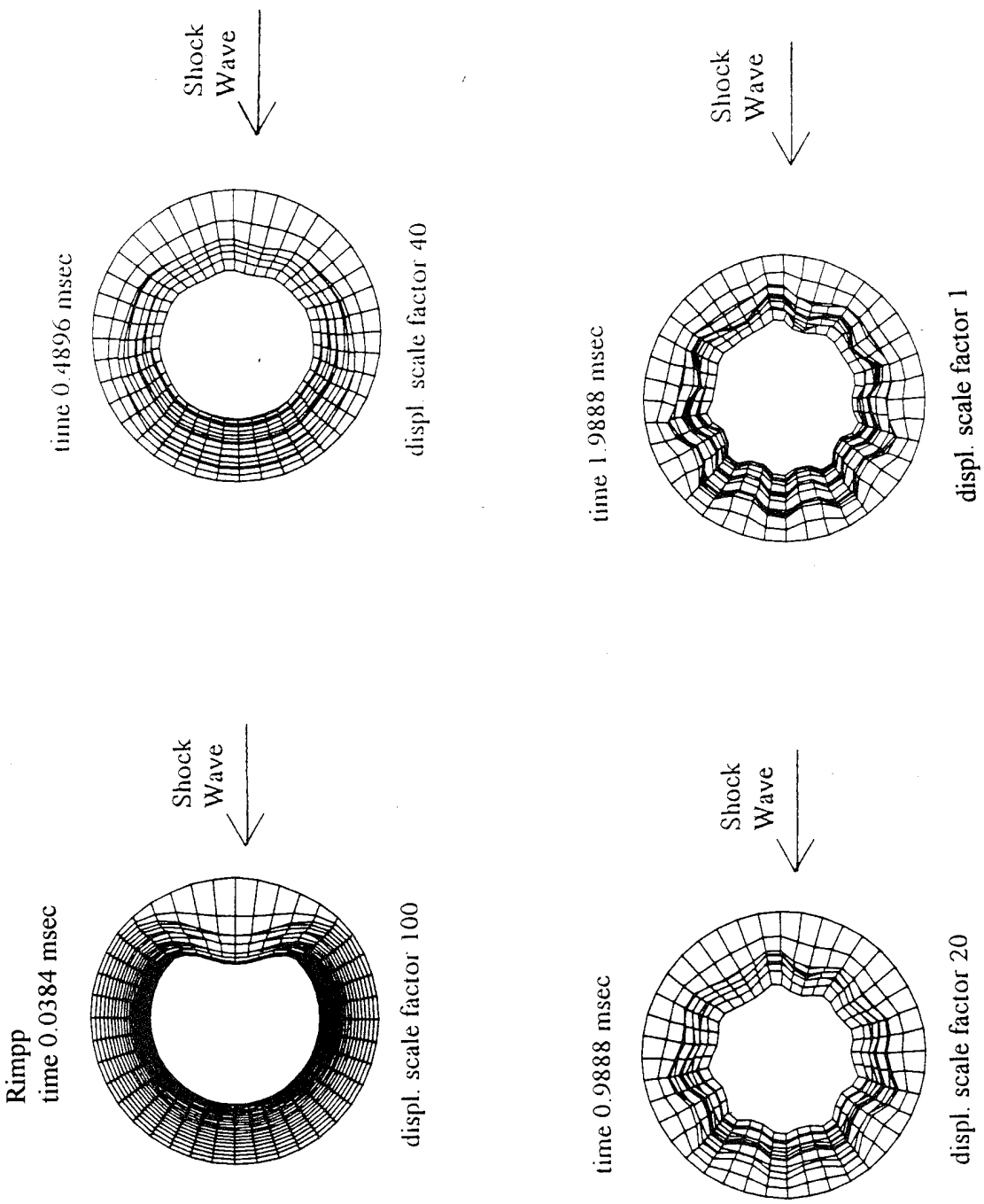

Figure 25. Radial Imperfections with Random Phase Shift: Axial Deformation plots for 0.0384, 0.4896, 0.9888, and 1.9888 msec

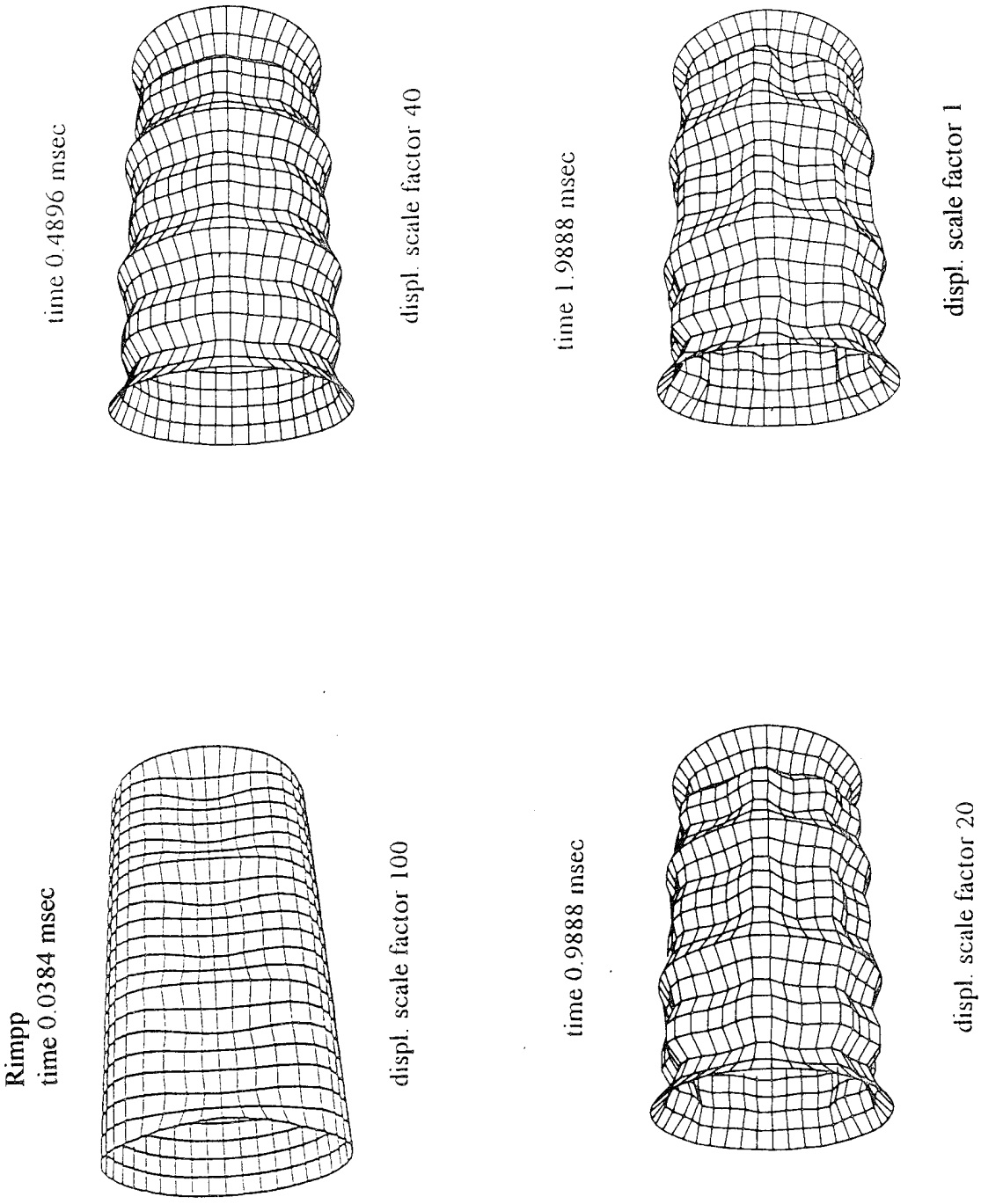

Figure 26. Radial Imperfections with Random Phase Shift: Longitudinal Deformation plots for 0.0384, 0.4896, 0.9888, and 1.9888 msec

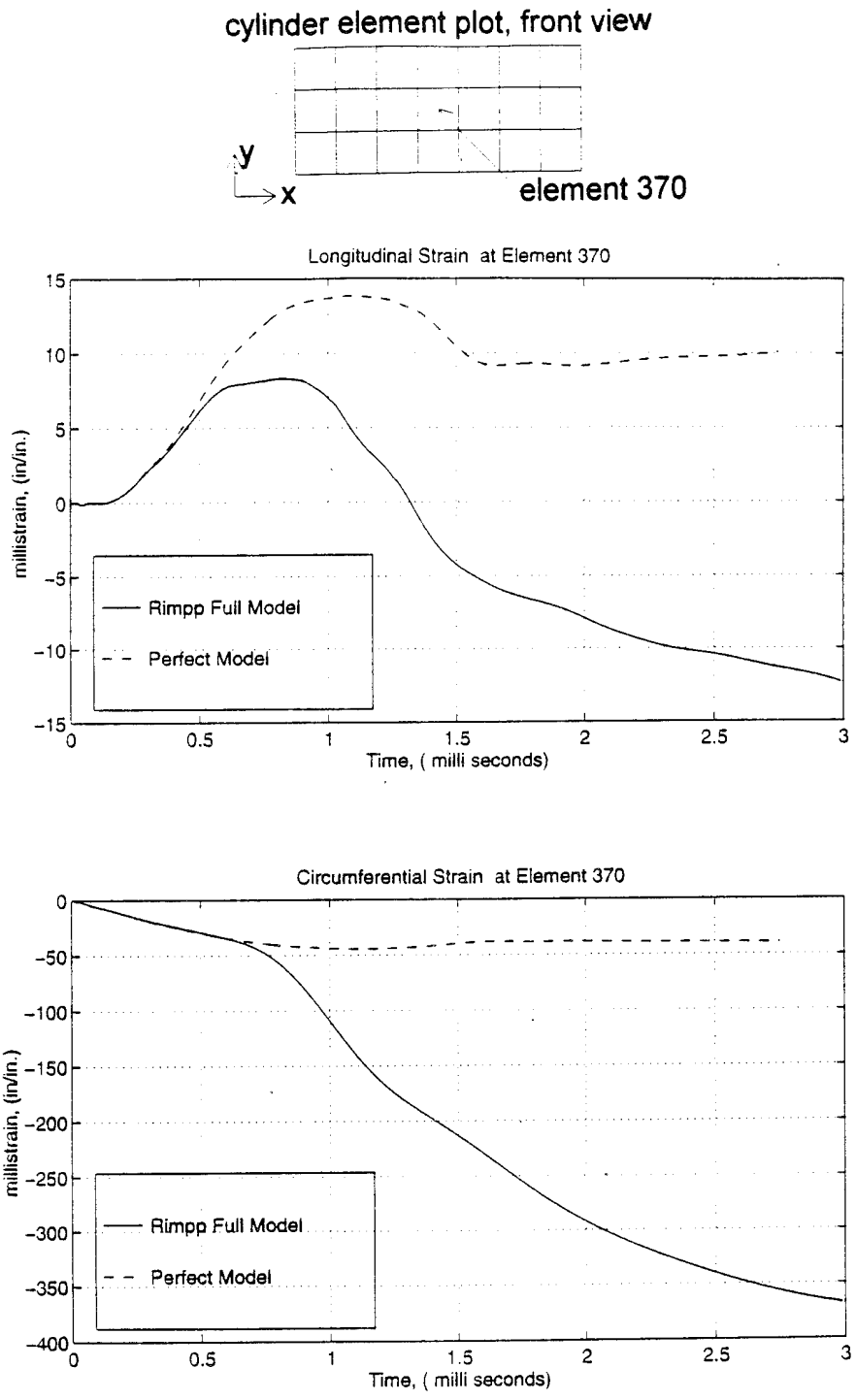

Figure 27. Radial Imperfections with Random Phase Shift: Circumferential and Longitudinal Strain for front of Cylinder Midpoint Centerline.

5. Axial Imperfections with Random Phase Shift (Aimpp)

The axial imperfection with random phase shift was the fifth model to be analyzed. This model has the axial and random phase shift combined modal imperfection introduced into the mesh algorithm. The initial modal imperfections distribution introduced into the cylinder have a smooth oscillatory appearance to that of Aimp. The resultant three-dimensional mesh plot and longitudinal plot are provided in Figure 28. The top longitudinal plot is scaled by a factor of 100 and has a smoother oscillation along the axial direction. The bottom mesh plot which is scaled by a factor of 25 clearly exhibits this smoother oscillatory appearance of the initial modal imperfection.

Deformation analysis was conducted using axial and longitudinal deformation plots, von Mises stress contour and effective plastic strain plots. Axial and hoop strain time histories are provided for selected points of interest.

The axial deformation plot, Figure 29 shows a time progression from 0.0384, 0.4896, 0.9881, and 1.9888 msec. There appears slight periodic crumpling with a couple of peaks around the circumference of the cylinder similar to the model perfect case. This deformation is also progressing in relation to the initial modal imperfection. The longitudinal deformation plot in Figure 30 shows the deformation as the shock induced pulse progresses through the cylinder. It also has the general appearance of the model perfect case.

The maximum von Mises stresses and effective plastic strain contour plots have essentially negligible difference to those of the perfect model. Both the maximum von Mises stress and effective plastic strain data are provided in Tables 2 and 3 in Appendix D.

The circumferential and longitudinal strain time histories at the front of the cylinder midpoint centerline are shown in Figure 31 versus the perfect model. The two graphs clearly show the similarity or negligible difference between the two models.

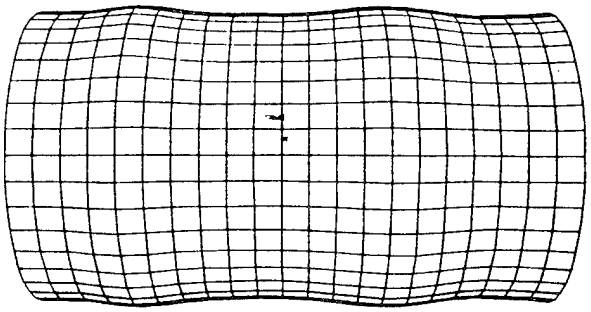

(a) Initial Modal Impefection distribution, longitudinal view, scaled up 100X

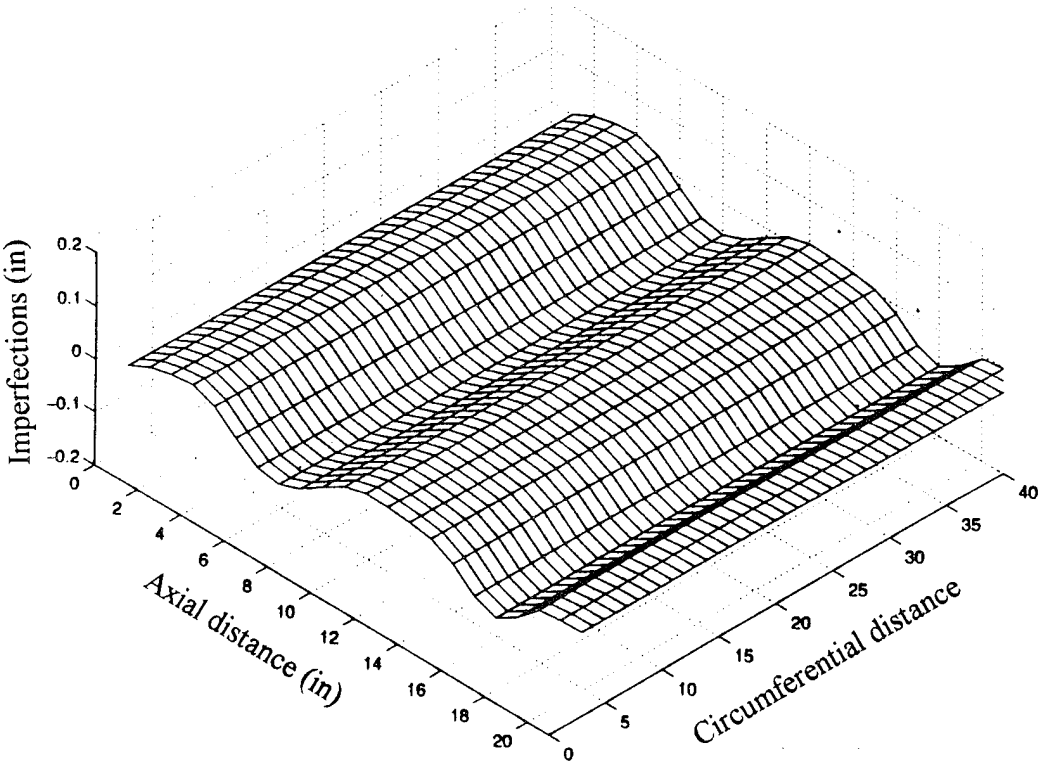

(b) Three Dimensional Mesh Plot of Cylindrical Surface, scaled up 25X

Figure 28. Axial Imperfections with Random Phase Shift (Aimpp): (a) Initial Modal Imperfection Distribution, long view (b) Three Dimensional Mesh of Cylindrical Surface

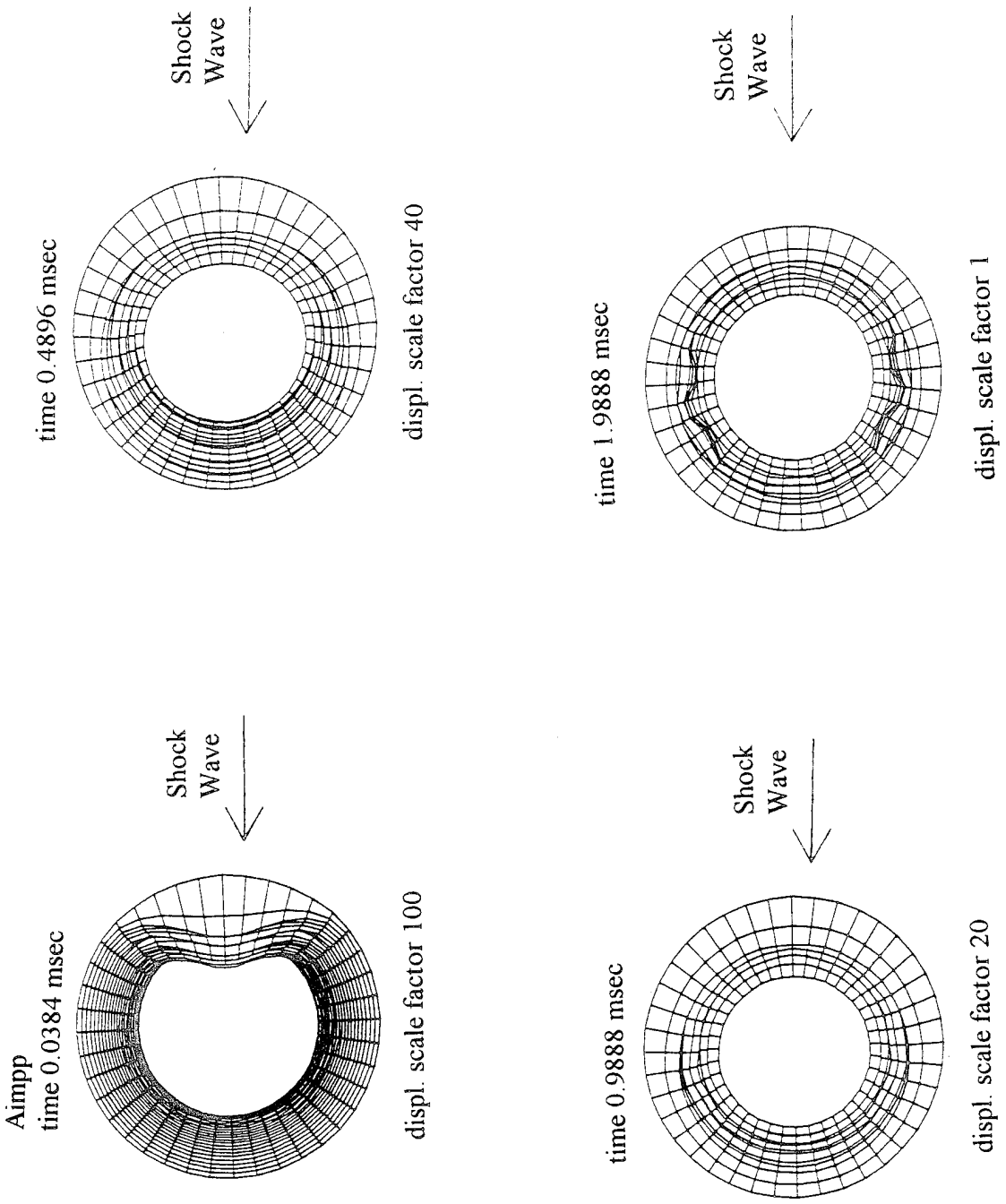

Figure 29. Axial Imperfections with Random Phase Shift: Axial Deformation plots for 0.0384, 0.4896, 0.9888, and 1.9888 msec.

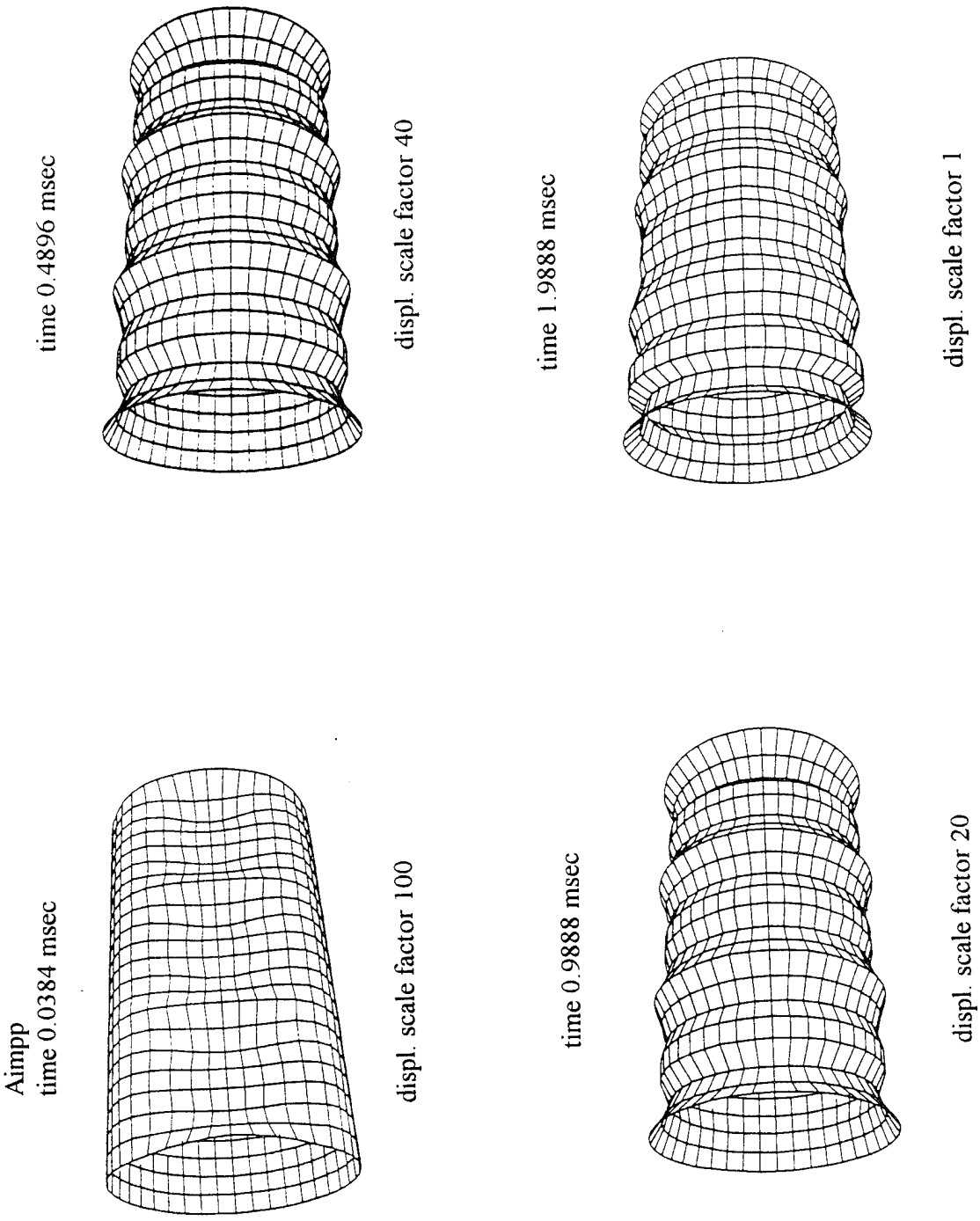

Figure 30. Axial Imperfections with Random Phase Shift: Longitudinal Deformationplots for 0.0384, 0.4896, 0.9888, and 1.9888 msec.

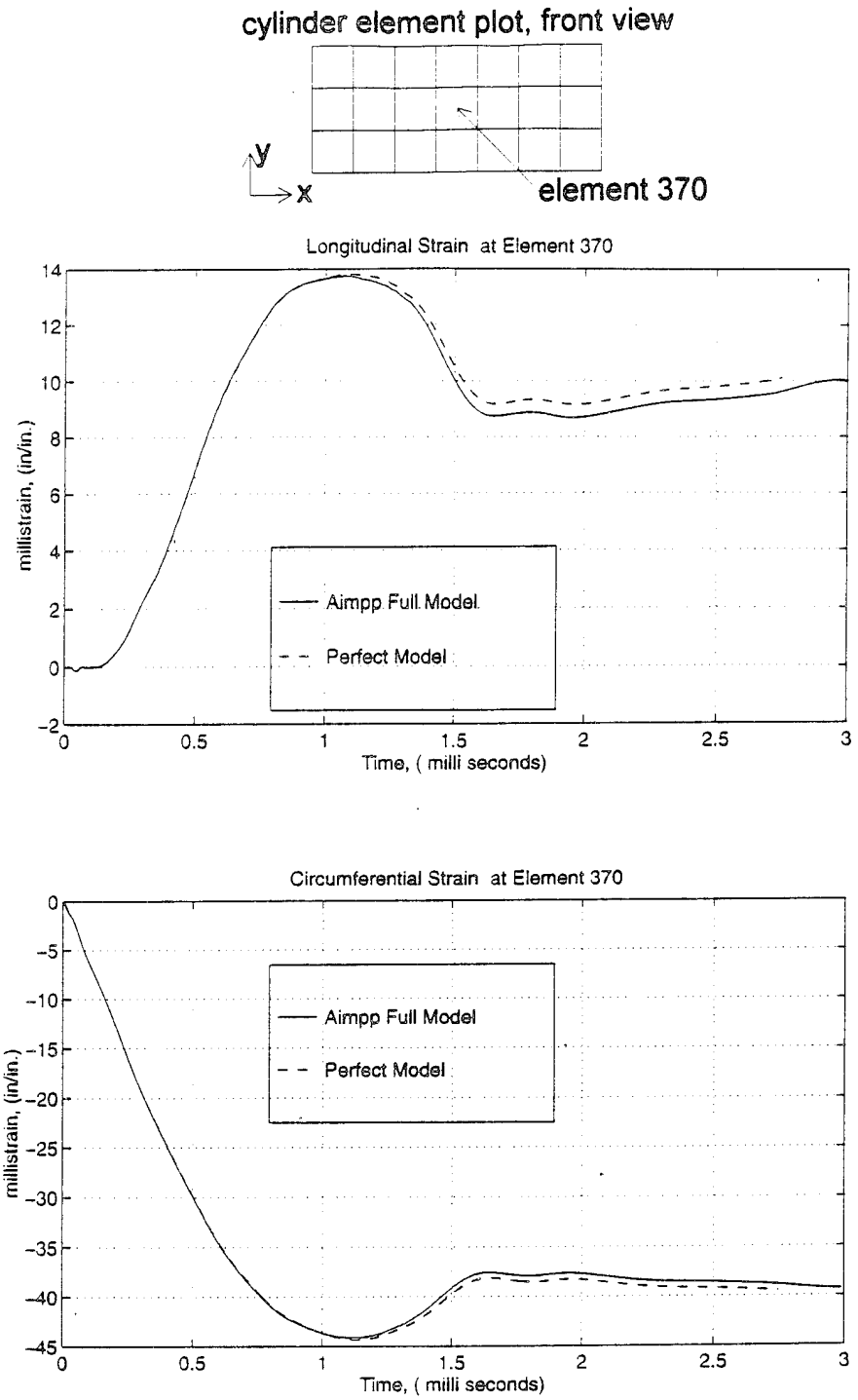

Figure 31. Axial Imperfections with Random Phase Shift: Cirumferential and Longitudinal Strain at front of Cylinder Midpoint Centerline

6. Radial and Axial Imperfections with Random Phase Shift (Impp)

The sixth modal imperfection to be analyzed was the radial and axial imperfection with random phase shift. This model has these combined modal imperfections introduced into the mesh algorithm. The initial modal imperfection distribution introduced into the cylinder and the resultant three-dimensional mesh plot are provided in Figure 32. The top plot show the superposition of both modal imperfections scaled by a factor 50. The bottom mesh plot is scaled by a factor of 50 and clearly shows the superposition of the random radial oscillations and the smooth axial oscillatory motion.

Deformation analysis was conducted using axial and longitudinal deformation plots, von Mises stress contour and effective plastic strain plots. Axial and hoop strain time histories are provided for selected points of interest.

The axial deformation plot in Figure 33 shows a time progression from 0.0384, 0.4896, 0.9881, and 1.9888 msec. There appears an increase in the periodic crumpling with peaks around the circumference of the cylinder. This deformation is also progressing in relation to the initial modal imperfection. The longitudinal deformation plot in Figure 34 shows the deformation as the shock induced pulse progresses thru the cylinder. There is an greater appearance of a single ridge dishing effect between the stiffeners than for the Rimpp case.

A comparison of the maximum von Mises stresses between Impp and Rimpp shows negligible difference for radial and axial imperfection with random phase shift within the first msec after impact. A comparison between Impp and Imp shows a slightly greater than a 1.5 percent difference. These values are provided in Table 2 in Appendix D.

The effective plastic strain contour plot has the typical appearance to the model Perfect. A comparison between Impp and model Perfect show about 15 percent greater difference. In contrast the difference between Impp and Imp are only slightly greater than 1.5 percent difference. These values are provided in Table 3 of Appendix D.

The circumferential and longitudinal strain time histories at the front of the cylinder midpoint centerline, element 370 are compared to the perfect model in Figure 35. The hoop strain is greater for the Impp case than for the perfect case. The axial strain is slightly less

than the perfect model. This could be contributed to the random phase shift assumption that was used in determining the initial modal imperfection. The effective plastic strain at the front centerline right end and backside centerline are shown in Figure 36. In both cases the Impp' model has greater plastic strain as compared to the Rimpp case.

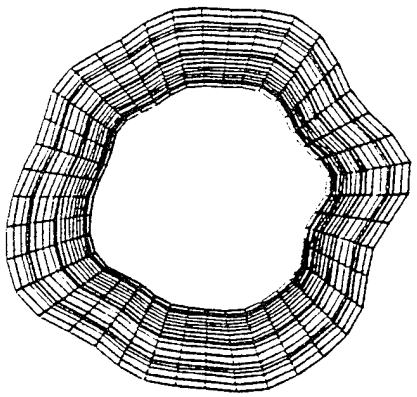

(a) Initial Modal Imperfection distribution, axial view, scaled up 50X

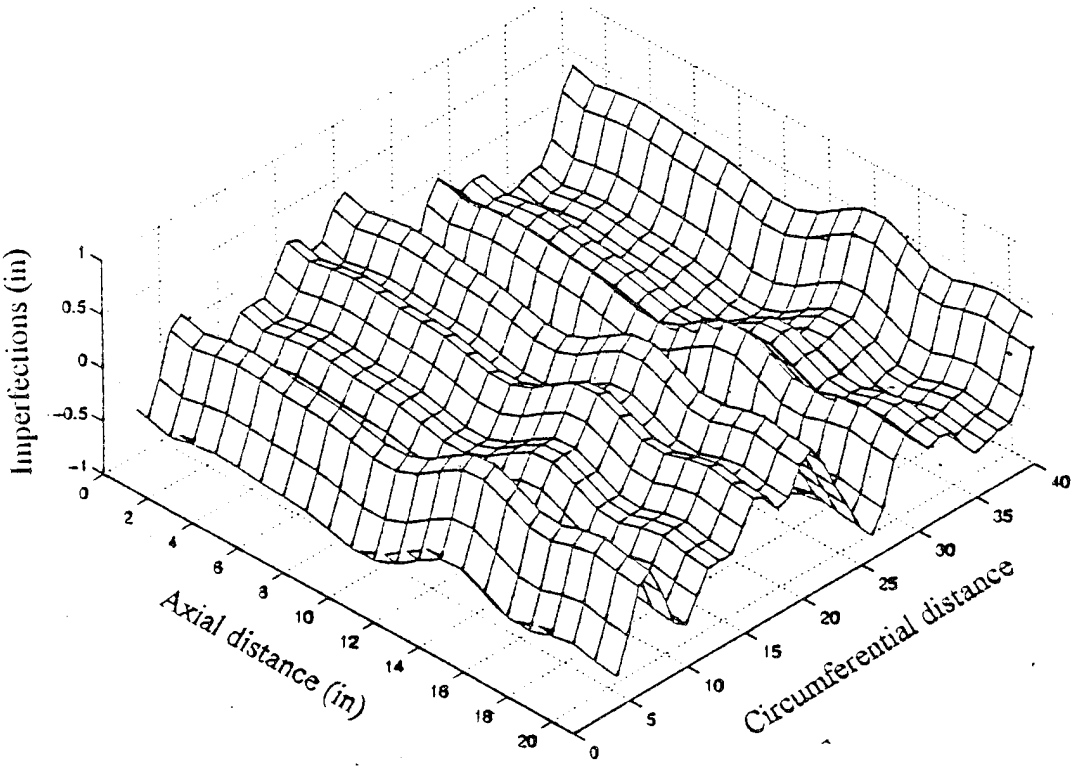

(b) Three Dimensional Mesh Plot of Cylindrical Surface, scaled up 50X

Figure 32. Radial and Axial Imperfections with Random Phase Shift (Impp): (a) Initial Modal Imperfection Distribution, axial view (b) Three Dimensional Mesh Plot of Cylindrical Surface

Figure 33. Radial and Axial Imperfections with Random Phase Shift: Axial Deformation plots for 0.0384, 0.4896, 0.9888, and 1.9888 msec.

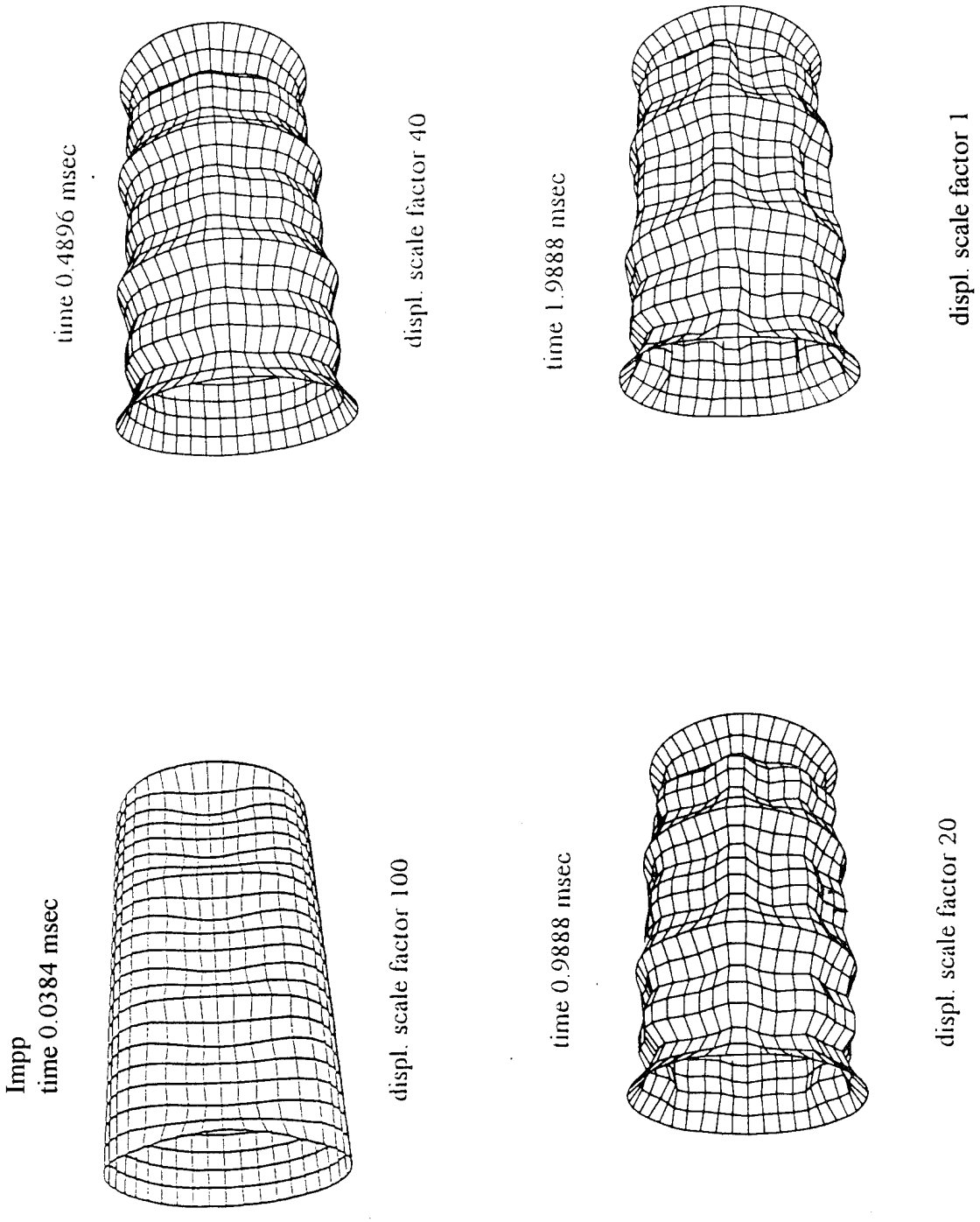

Figure 34. Radial and Axial Imperfections with Random Phase Shift: Longitudinal Deformation plots for 0.0384, 0.4896, 0.9888, and 1.9888 msec.

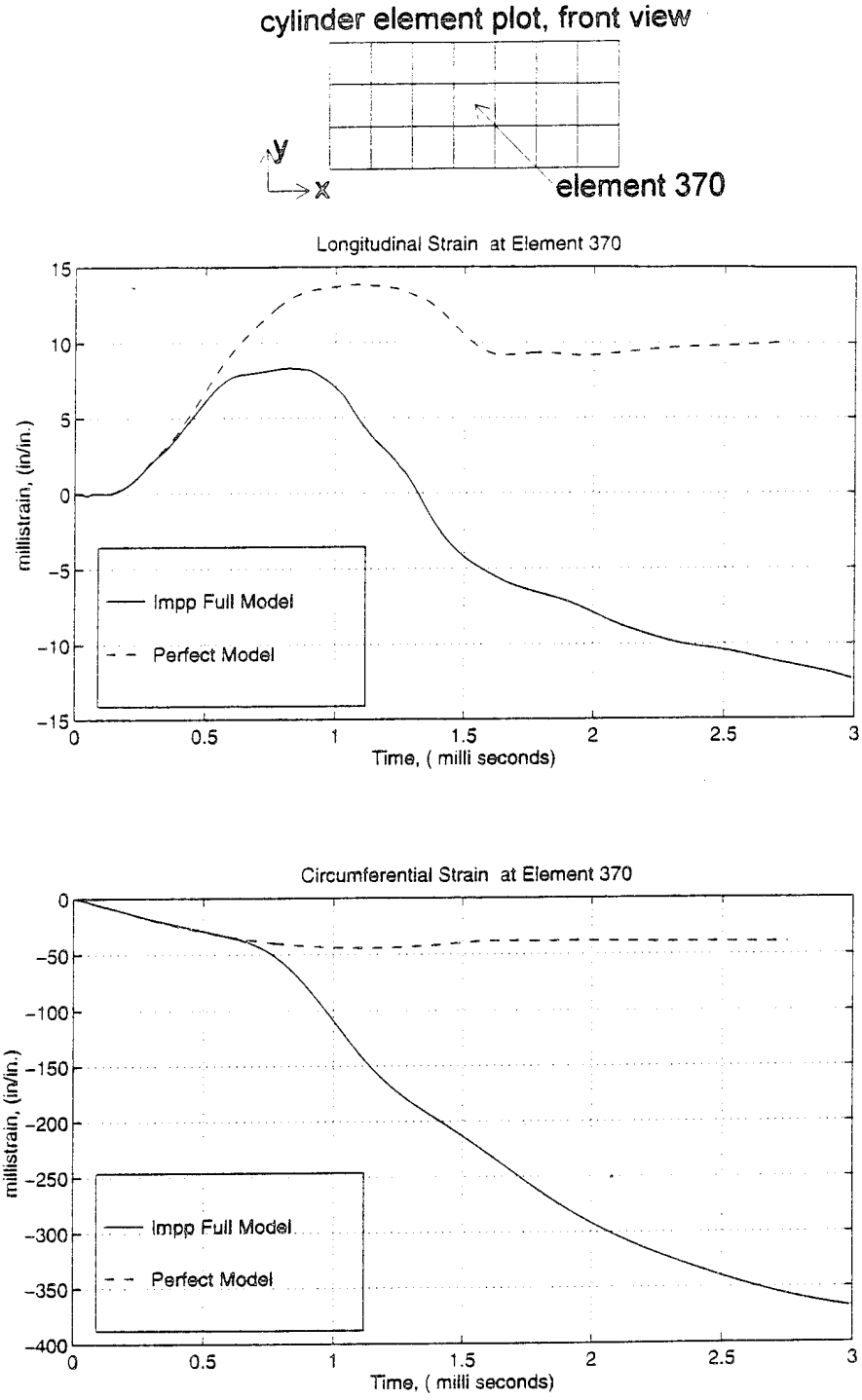

Figure 35. Radial and Axial Imperfections with Random Phase Shift: Circumferential and Longitudinal Strain for the front of Cylinder Midpoint Centerline

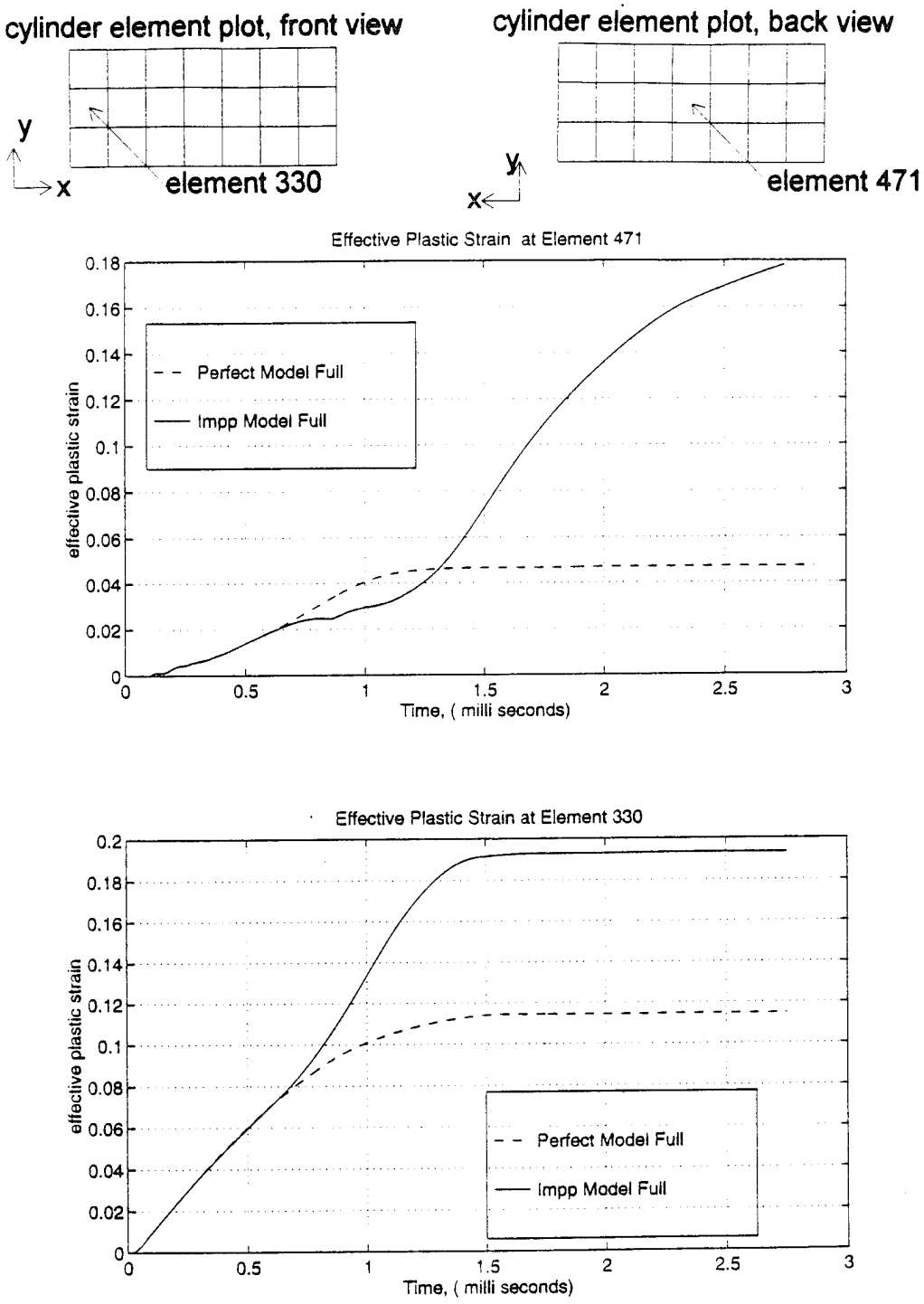

Figure 36. Radial and Axial Imperfections with Random Phase Shift: Plastic Strain for Cylinder backside Centerline and front of Cylinder right end.

7. Material Imperfections

The material imperfection was the seventh model to be analyzed. This model used only the material imperfection introduced into the mesh algorithm. This incorporates a random plus or minus 2.5 or 5 percent difference in the elastic modulus. There is no initial modal imperfection distribution plot as in the other imperfection cases.

Deformation analysis was conducted using axial and longitudinal deformation plots, von Mises stress contour and effective plastic strain plots. Axial and hoop strain time histories are provided for selected points of interest.

The axial deformation plots are not provided for the time progression from 0.0384, 0.4896, 0.9881, and 1.9888 msec because of their similarity in appearance of the plots to those of the perfect model. The longitudinal deformation plots are also not provided but have that distinctive pinching around the stiffeners and the general smooth accordion appearance of the perfect model.

The effective plastic strain contour plots are essentially identical to the model perfect. Maximum von Mises stresses and effective plastic strain data are similar to the third digit. The tabulated data is provided in Tables 2 and 3 in Appendix D.

It can be concluded that the effect of variations in elastic modulus are negligible in this analysis since the underwater explosion pressure pulse creates stresses that exceed the materials elastic limit within 0.5 msec after impact.

8. Material, Radial and Axial Imperfections with Random Phase Shift (Mtlimpp)

The eighth and final model to be analyze was the material, radial and axial imperfection with random phase shift. This model has the combined material, radial and axial imperfection with random phase shift modal imperfection introduced into the mesh algorithm. The initial modal imperfections distribution introduced into the cylinder is similar to the radial and axial imperfection with random phase shift (Impp) case. The mesh plot is not provided but would be similar to the Impp case.

Deformation analysis was conducted using axial and longitudinal deformation plots,

von Mises stress contour and effective plastic strain plots. Axial and hoop strain time histories are provided for selected points of interest.

The axial deformation plot in Figure 37 shows a time progression from 0.0384, 0.4896, 0.9881, and 1.9888 msec. They have the similar periodic crumpling with sharp peaks around the circumference of the cylinder that is distinguishable from the Impp. This deformation is also progressing in relation to the initial modal imperfection. The longitudinal deformation plot in Figure 38 for the same times show the deformation as the shock induced pulse progresses through the cylinder. It also has the appearance of the single ridge dishing effect between the stiffeners as the Impp case.

The maximum von Mises stresses and effective plastic strains are essentially the same as in the Impp and hence the difference is negligible. Tabulated data is provided in Tables 2 and 3 in the Appendix D.

The circumferential and longitudinal strain time histories at the front of the cylinder midpoint centerline are similar to the Impp case and will not be provided.

Figure 37. Material, Radial, and Axial Imperfections with Random Phase Shift: Axial Deformation plots for 0.0384, 0.4896, 0.9888, and 1.9888 msec.

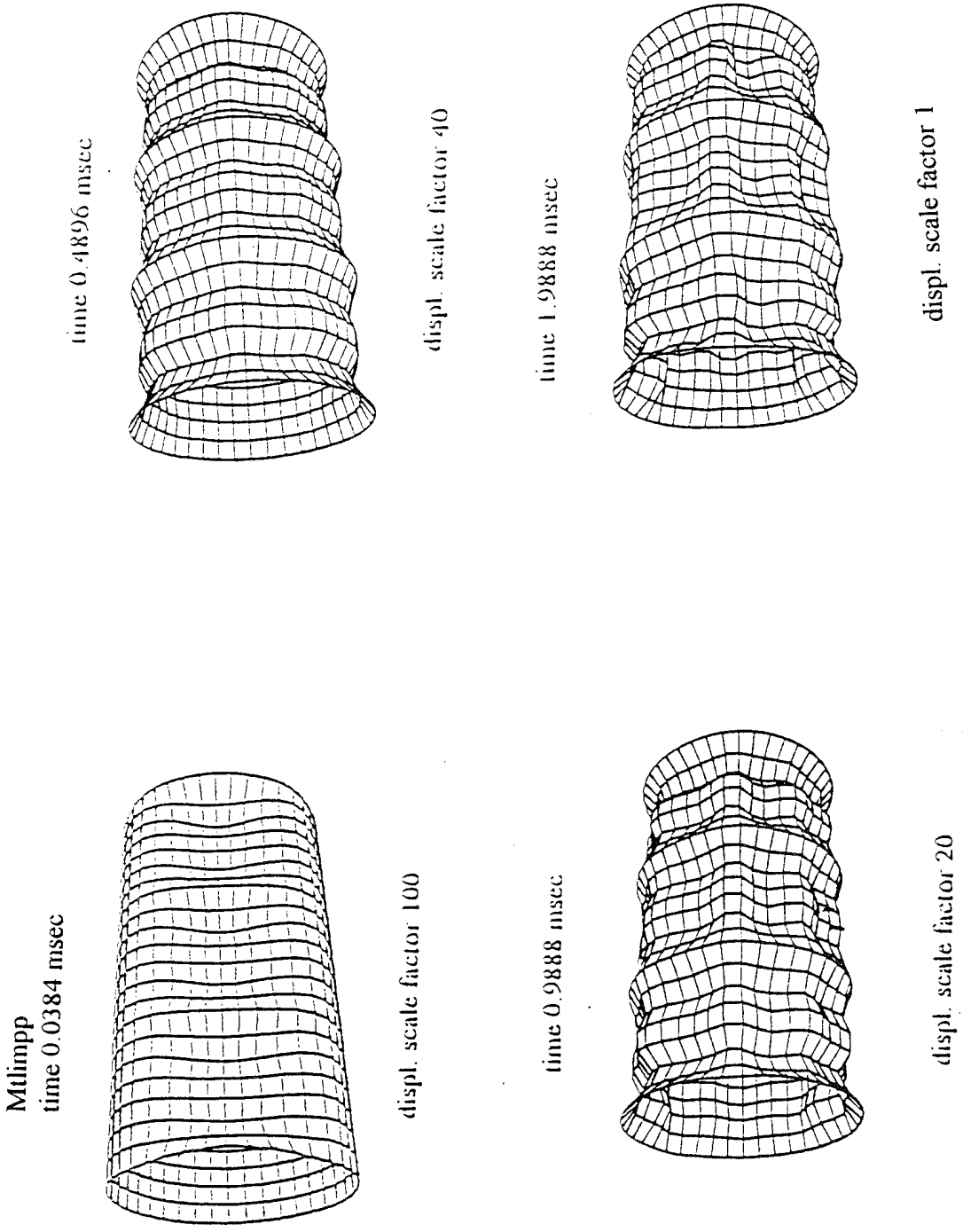

Figure 38. Material, Radial, and Axial Imperfections with Random Phase Shift: Longitudinal Deformation plots for 0.0384, 0.4896, 0.9888, and 1.9888 msec.

C. SUMMARY OF RESULTS

The results of comparing the various modal imperfection distributions clearly shows the dominating effect of the radial imperfection in both the with phase and without random phase shift cases. Figure 39 compares the four major longitudinal deformation plots for the Perfect , Radial and Axial Imperfection (Imp), Radial Imperfection with random phase shift (Rimpp), and Radial and Axial Imperfection with random phase shift (Impp). These cases were chosen to show the variety of deformation patterns achieved. This figure clearly shows the different modal distribution between the perfect and imperfection with random phase and no phase shift cases. The Axial imperfection with and without phase were neglected due to negligible visual difference to the model Perfect.

The perfect model has its distinguishing pinching and overall accordion appearance. This is in sharp contrast to the Imp case which shows the pronounced frontside twin ridge dishing effect between the stiffeners. The Radial Imperfection with random phase shift (Rimpp) has a noticeably different single ridge dishing from the Radial and Axial Imperfection (Imp) case. As noted before this is resultant of the introduction of the initial imperfection distribution. The final deformation plot, Radial and Axial Imperfection with random phase shift (Impp) is provided to show the slight to negligible difference that the axial imperfection contributed to crumpling or buckling.

Figure 40 compares the four major axial deformation plots for the same cases as above. The model Perfect axial deformation plots shows only two small indentations on the top and bottom of the cylinder. This is also in sharp contrast to the Radial and Axial Imperfection (Imp) appearance of periodic crumpling with ten peaks around the circumference of the cylinder. The difference between Radial Imperfection with random phase shift (Rimpp) and Radial and Axial Imperfection with random phase shift (Impp) show no significant change in the amplitude of deformation but does show the distinguishable single peak along the shock axis. It is theorized that the summation of the modal imperfection causes the magnitude of these peaks and valleys.

The results for the material imperfection of five percent change of elastic modulus had little to negligible effect on the deformation or dynamic response.

Figure 39. Comparisions of Longitudinal Deformation Plots for Perfect, Radial and Axial Imperfections(Imp),Radial Imperfections with Random Phase Shift (Rimpp) ,and Radial and Axial Imperfections with Random Phase Shift (Impp)

Figure 40. Comparison of Axial Deformation Plots for Perfect, Radial and Axial Imperfections (Imp) ,Radial Imperfections with Random Phase Shift (Rimpp) and Radial and Axial Imperfections with Random Phase Shift(Impp)

D. PARAMETRIC STUDY OF AXIAL IMPERFECTIONS

In the initial axial imperfection modal distribution the modal amplitude was assumed to be 1/4 of that of the radial imperfection. The axial imperfection case used the similar cosine series as the radial imperfection but as a function of axial distance and multiplied by the axial modal amplitude. The Axial Imperfections (Aimp) and Axial Imperfections with random phase shift (Aimpp) models as determined by deformation plots and dynamic responses provided negligible effect. This section will perform a parametric study using four different axial modal amplitudes. The four are 1/4, 1/2, 3/4 and 1.0 of the radial modal amplitudes. These results were then compared to the model Perfect and an optimized axial modal amplitude was selected to be integrated into the combined modal imperfection distribution.

The axial modal amplitude for each case was implemented into the mesh algorithm in the same procedure as for the other models. Deformation and dynamic response was conducted in the same manner with von Mises stress contour plots, effective plastic strain plots and axial and longitudinal deformation plots. Data for von Mises maximum stresses and maximum effective plastic strains are provided in Tables 4 and 5 in Appendix D.

The deformation plots provided no new or interesting visual differences. They will not be provided due to the similarity of model Perfect, Aimp and Aimpp cases.

The comparison of the maximum von Mises stresses for the four axial modal amplitudes and model perfect shows negligible, 0.3 percent difference after the first msec.

The comparison of the effective plastic strain for the same models shows a 1.3 percent difference for the 1/4 and 3/4 models and a 1.6 percent difference for the 1/2 and 1 models. Figure 41 is the circumferential an longitudinal strain time histories at the front of the cylinder midpoint centerline. This clearly shows the significant difference of the first axial modal amplitude. The optimum choice was selected as the 1/2 axial modal amplitude. This was selected because it has a greater effective plastic strain than the 1/4 and 3/4 cases but not as great as the effect of the 1.0 or fourth modal amplitude. The final modal amplitude of 1.0 would affect the dynamic response on the order of the radial imperfections and this was determined to be unreasonable.

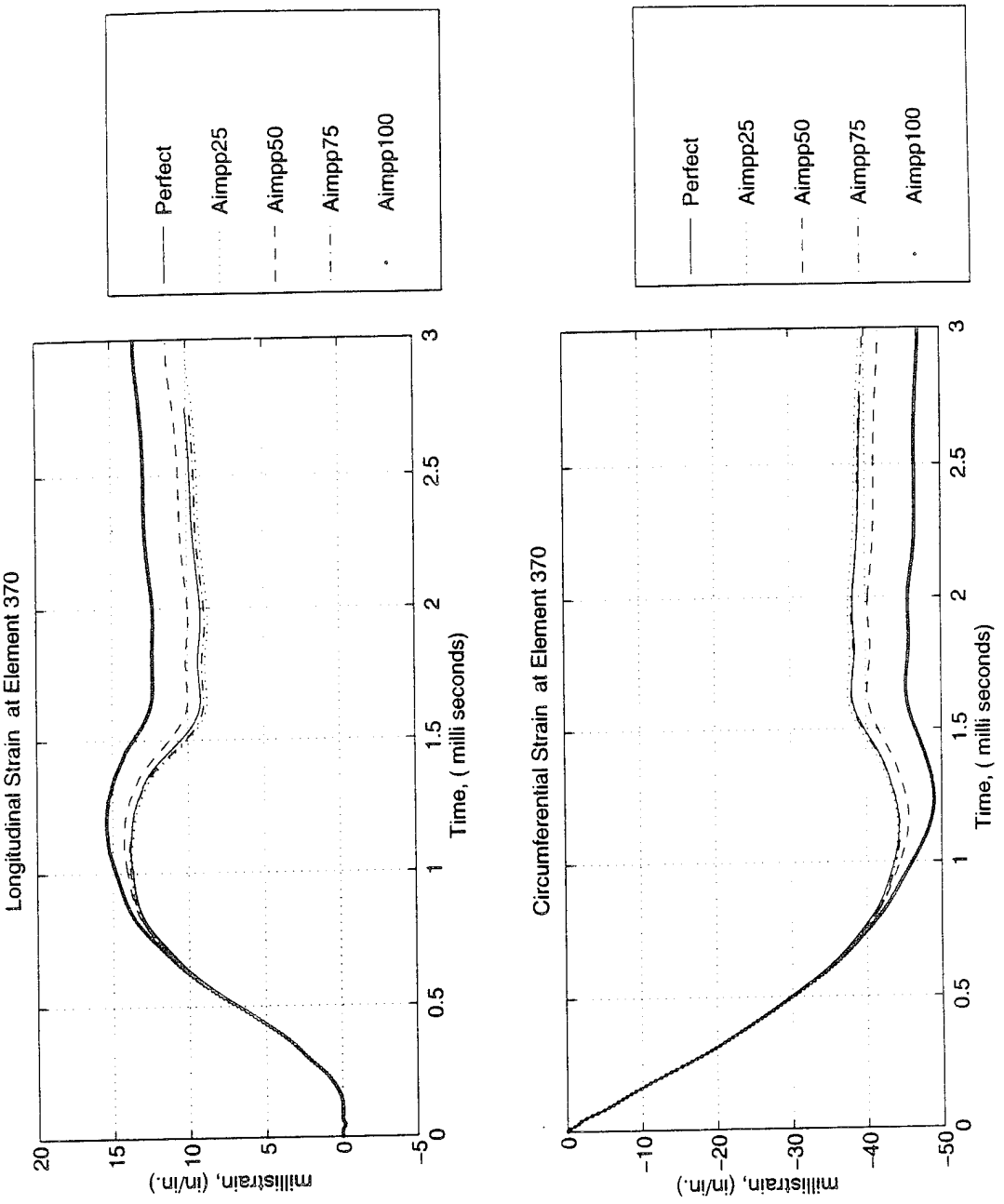

Figure 41. Axial Modal amplitude: Circumferential and Longitudinal Strain for Cylinder front Midpoint Centerline for 1/4, 1/2, 3/4 , 1, and Model Perfect.

E. MATERIAL PROPERTY IMPERFECTION ANALYSIS

In the analysis of the material property imperfection the elastic modulus was initially investigated. These results concluded that a variation of elastic modulus had negligible effect on the deformation response. This is due to the fact that the material's elastic limit was exceeded shortly after impact and the dynamic response was mostly in the plastic region. There are other material property imperfections that should affect the nonlinear dynamic response like variation in yield strength and tangential hardening modulus. This section analyzed independently the effects of variations on material density, yield strength, and tangential hardening on the deformation and dynamic response. The optimized material properties were then used with the optimized axial modal amplitude in the combined modal imperfection distribution that will be compared to experimental data.

As in the material imperfection model, a fortran program was used to modify these two parameters by 5 percent of their average values. These values of the modified material properties were implemented into the mesh generator algorithm as in the preceding models and the resulting deformation and dynamic response was analyzed.

1. Variation of Material Density

The variation of material density was the first case to be analyzed in the material property imperfection analysis. It used the standard 5 percent variation in density as described above.

Deformation and dynamic response analysis was conducted in the same manner as previous models with von Mises contour plots, effective plastic strain plots and axial and longitudinal deformation plots.

The comparison of the variation of material density shows a similar appearance in both axial and longitudinal plots at 1.9888 msec to that of the elastic modulus case. The only major difference in the axial plot of Figure 42, is that the density plot has an extra peak along the axis of impact. In the longitudinal plot of Figure 43 this is observed as slight dishing between the two major stiffeners.

The maximum von Mises and effective plastic strains for the variation of material

density provided reasonable values in both cases. The difference between material density and model Perfect is within 0.5 percent after the first msec. The effective plastic strain comparison between material density and model Perfect is within 2.2 percent after the first msec. Data for von Mises maximum stresses and maximum effective plastic strains are provided in Tables 4 and 5 in Appendix D.

2. Variation of Material Yield Strength

The variation in material yield strength was the second case to be analyzed. In this case two separate 5 and 2.5 percent difference models were analyzed.

Deformation and dynamic response analysis was conducted in the same manner with von Mises contour plots, effective plastic strain plots and axial and longitudinal deformation plots.

The axial deformation plot in Figure 42 at 1.988 msec shows the comparison of the variation of yield strength for the 5.0 percent case. This plot clearly shows a similar peak in front as with the density case but also shows a distinctive formation of multiple peaks surrounding the backside of the cylinder. The longitudinal plot is provided in Figure 43 at 1.988 msec. It shows the similar slight dishing between the two major stiffeners in the front as seen with the density case. The longitudinal plot does not clearly show the backside of the cylinder which would have multiple dishes due to various peaks surrounding the backside.

The comparison of the maximum von Mises stresses and effective plastic strains for the 5 percent different yield strength case proved to be on the order of the 1/2 axial modal amplitude case. In the maximum von Mises stresses this was on order of 2 percent greater than model Perfect within the first msec. The maximum effective plastic strain were also within 2 percent of the model Perfect within the first msec. The second 2.5 percent case was investigated and provided maximum von Mises stresses and effective plastic strains with almost negligible difference between model Perfect. Data for the maximum von Mises stresses and maximum effective plastic strains are provided in Tables 4 and 5 in Appendix D.

3. Variation in Material Tangential Hardening Modulus

The variation of material tangential hardening modulus was the final case to be analyzed in the material property imperfection analysis. In this case there were two separate 5 and 7.5 percent difference tangential hardening modulus cases analyzed.

Deformation and dynamic response analysis was conducted in the same manner as previous models with von Mises contour plots, effective plastic strain plots and axial and longitudinal deformation plots.

The final axial deformation plot in Figure 42 shows the comparison of the 5.0 percent variation of tangential hardening modulus. This plot clearly shows the similarity in appearance to the elastic modulus case at 1.9888 msec after impact. In the longitudinal plot of Figure 43, it has that distinctive pinching around the stiffeners and the general smooth accordion appearance of the perfect model.

The comparison of the maximum von Mises stresses and effective plastic strains for the 5 percent tangential hardening proved to be less sensitive than the yield strength case. There was negligible difference compared to model Perfect until the stresses reached their yield strength. Even after reaching yield strength this parameter had a minimum effect on the maximum stresses or plastic strains. This affected the dynamic response within 1.5 percent of model Perfect within the first msec. A 7.5 percent different of tangential hardening case was analyzed. It provided no more than 1/4 percent greater values than the 5 percent case. Data for von Mises maximum stresses and maximum effective plastic strains are provided in Tables 4 and 5 in Appendix D.

Figure 42. Comparison of Axial Deformation plots at 1.988 msec: Material Elastic Modulus, Material Density, Material Yield Strength, and Material Tangential Hardening.

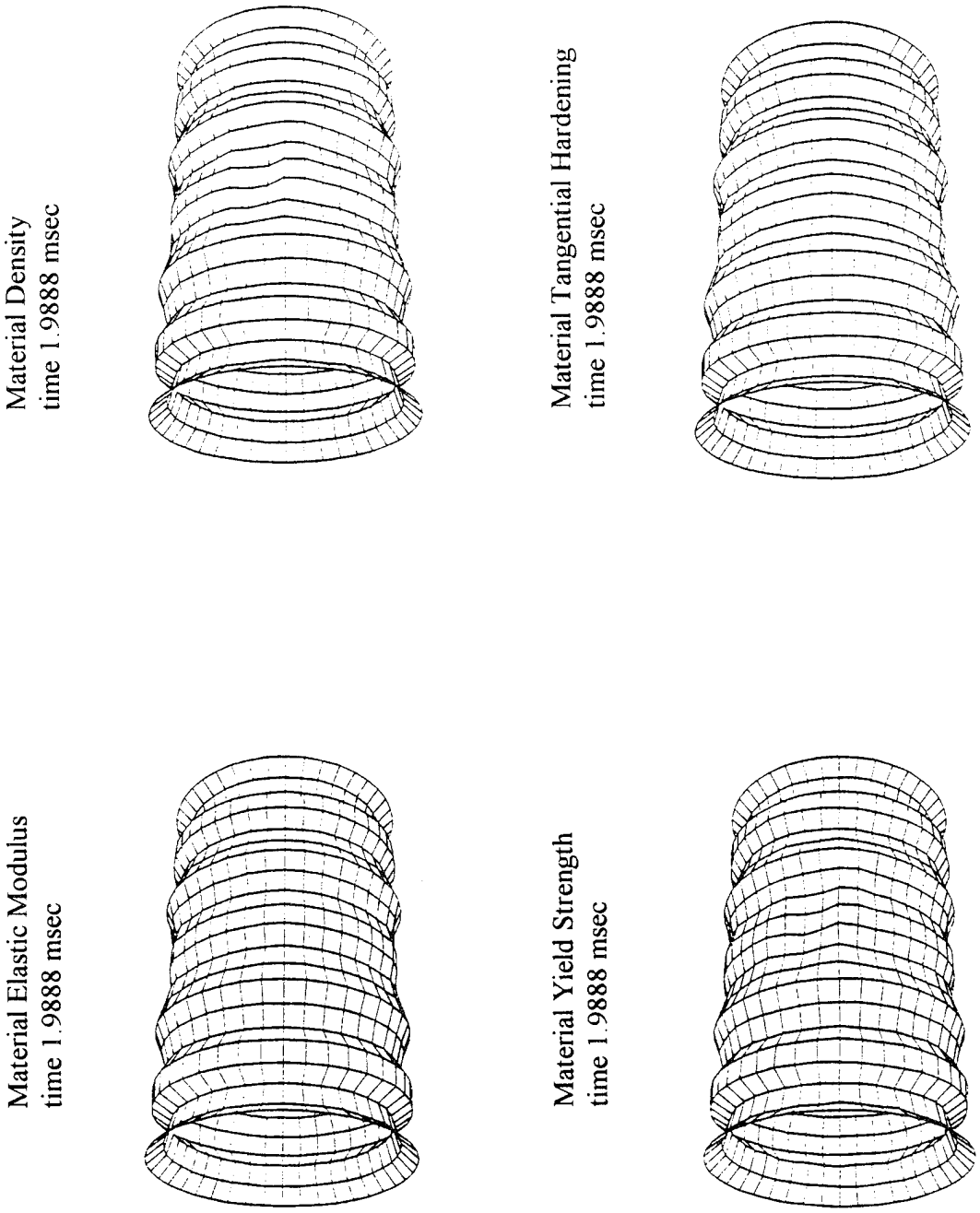

Figure 43. Comparison of Longitudinal Deformation plots at 1.988 msec: Material Elastic Modulus, Material Density, Material Yield Strength, and Material Tangential Hardening

IV. NUMERICAL AND EXPERIMENTAL RESULTS

A. UNDERWATER EXPLOSION TEST

An underwater explosion test was conducted at Dynamic Testing Incorporated (DTI), in Rustburg, Virginia in August 1991 in support of UNDEX research by Nelson (1992). The test facility is located in a quarry where the water depth is approximately 130 feet. This water depth reduces the possibility of bottom reflection affecting the test data.

A compressive shock was produced by a 60 pound charge of HBX-1 with a 15 foot standoff distance. The test depth for both the charge and cylinder was 10 feet. The peak pressure generated by the charge was 4163 psi. The calculated peak pressure pulse using the exponential equation was 4807 psi.

B. PHYSICAL CYLINDRICAL SHELL MODEL

The test specimen was an instrumented aluminum cylinder. Its shell was constructed of 6061-T6 aluminum with a 12 inch diameter, 42 inch length, and 1/4 inch thickness. The stiffeners were of the same aluminum material with a 1/4 inch thick. The material properties were elastic modulus 10,800 ksi, Poisson's ratio 0.33, and yield strength 40.0 ksi. The end plate material was 1.0 inch aluminum. The aluminum was treated as a kinematic/isotropic elastic plastic with no strain rate sensitivity.

A total of 18 strain gages were attached as shown in Figure 44 for the side-on underwater explosion test. These gages were positioned to measure both axial and circumferential strains. Locations of strain gages were based on pre-test calculations to determine critical deformation zones.

C. NELSON'S USA/DYNA3D MODEL

The following is the original three-dimensional ring stiffened finite cylindrical model used by Nelson(1992). A 1/2 symmetric cylindrical model 42 inches in length, 12 inches in diameter with a single stiffener placed at the midpoint. The shell and stiffener material is modeled as 6061-T6 aluminum, an kinematic/isotropic elastic-plastic material with an elastic

modulus of 10800 ksi, a Poisson's ratio of 0.33, and a yield stress of 40 ksi with a shell thickness of 1/4 inches. The endplate material is 1 inch aluminum.

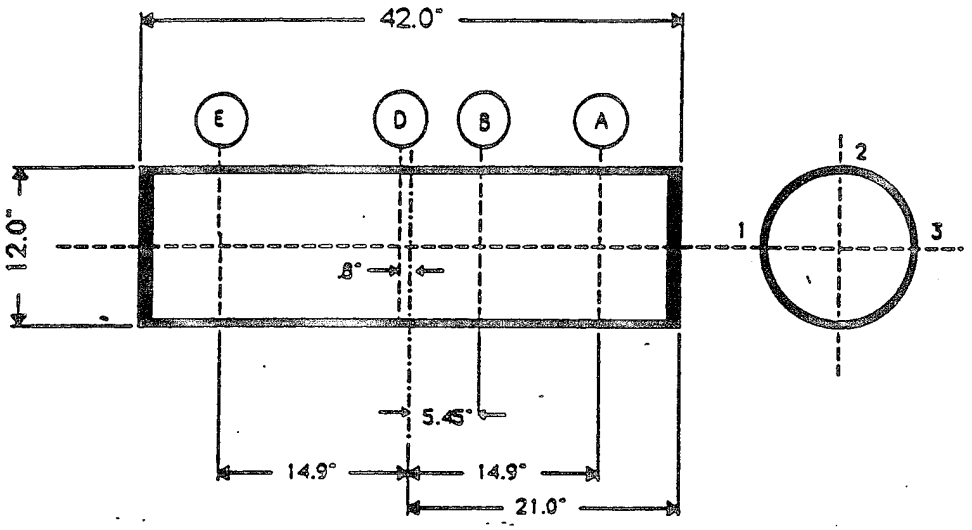

A1A: Axial strain at gage location A and radial position 1.
A1C: Hoop strain at gage location A and radial position 1.
A2A: Axial strain at gage location A and radial position 2.
A2C: Hoop strain at gage location A and radial position 2.
B1A: Axial strain at gage location B and radial position 1.
B1C: Hoop strain at gage location B and radial position 1.
B2A: Axial strain at gage location B and radial position 2.
B2C: Hoop strain at gage location B and radial position 2.
B3A: Axial strain at gage location B and radial position 3.
B3C: Hoop strain at gage location B and radial position 3.
D2A: Axial strain at gage location D and radial position 2.
D2C: Hoop strain at gage location D and radial position 2.
D3A: Axial strain at gage location D and radial position 3.
D3C: Hoop strain at gage location D and radial position 3.
E1A: Axial strain at gage location E and radial position 1.
E1C: Hoop strain at gage location E and radial position 1.
E2A: Axial strain at gage location E and radial position 2.
E2C: Hoop strain at gage location E and radial position 2.

Figure 44. Instrumentation Locations for Nelson's Model.

1. Nelson's Perfect Model Half

Nelson's model had to be alter to reproduce the similar deformation response of the actual cylinder. A 0.86 reduction to the nominal thickness was used for elements in the top of the model. This resulted in the deformation pattern as shown in Figure 45.

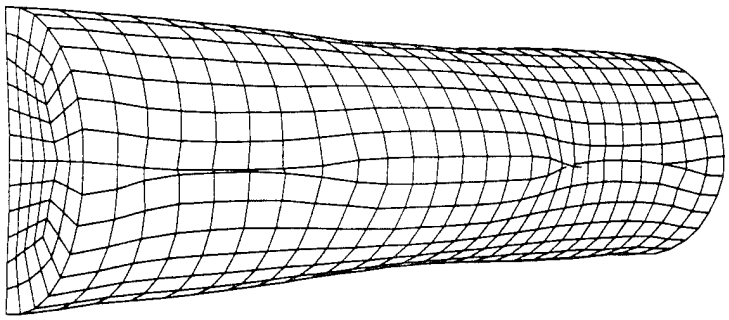

Figure 45. Nelson's 1/2 Model Deformation plot, view of top of cylinder for 1.48 msec.

D. NELSON'S IMPERFECT MODEL

Nelson's Modal Imperfection Model incorporated the optimized combined material, radial and axial imperfections into the mesh algorithm. Both imperfection cases with and without random phase shift were evaluated. Both models uses the combined material imperfection distribution that consists of the superposition of the 5 percent elastic modulus, 5 percent density variation, 5 percent yield strength, and 5 percent tangential hardening. The axial imperfection used in this distribution is the 1/2 axial modal amplitude. The initial modal imperfections distribution introduced into the Nelson half model are only the even mode

shapes. The even mode shapes of the first ten modal imperfections is a limitation due to the geometry of the half model.

1. Nelson's Material, Radial and Axial Imperfections with Random Phase Shift (Nelmtlimpp)

Deformation analysis was conducted using longitudinal deformation plots as used with the prior analysis. Hoop and axial strains were analyzed for strategic locations around the front and top of the cylindrical surface. From Figure 44 the locations that were analyzed were points B1, A2, and D2. Of the 18 strain gages placed on the test specimen half failed on impact of the pressure pulse. Several other strain gages provided useful data only between 0.25 to one msec.

Axial and hoop strain time histories are provided for points B1A and B1C which are located 5.45 inches to the right from centerline. The longitudinal deformation plot is provided for time 1.4796 msec. The original Ntlmtlimpp provided a deformation response of severe crumpling and buckling in the back, symmetric with either side of centerline and the dishing effects in the four end corners of the front side. Unfortunately as shown in, Figure 46 the actual deformation occurs at the top. Nelson (1992) reasoned this occurrence as possibly some inadvertent stress concentrations placed in the top of the cylinder during fabrication, storage or handling. A second analysis was conducted with a 90 degree shift in modal imperfections to adjust for these known stress concentrations. The deformations provided in Figures 47 and 48 show an excellent similarity to the actual deformation. The deformations are located in the correct geometric positions and with approximately the proper amplitudes.

The axial and hoop strain time histories at the B1A and B1C for experimental, numerical and perfect cases are provided in Figure 49. This plot clearly shows the that the numerical hoop strain closely predicts that of the experimental hoop strain during the critical first 3 msec after detonation. The longitudinal strain shows the numerical predication is not as close as the hoop strain but still reasonable for the first 3 msec. Hoop and axial strain gage information from A2 and D2 provided incomplete data for the 3 msec and will not be

provided. The data was in close agreement with the hoop strain until wire rupture at 1/2 msec. The longitudinal strain provided good to average data correlation with numerical results.

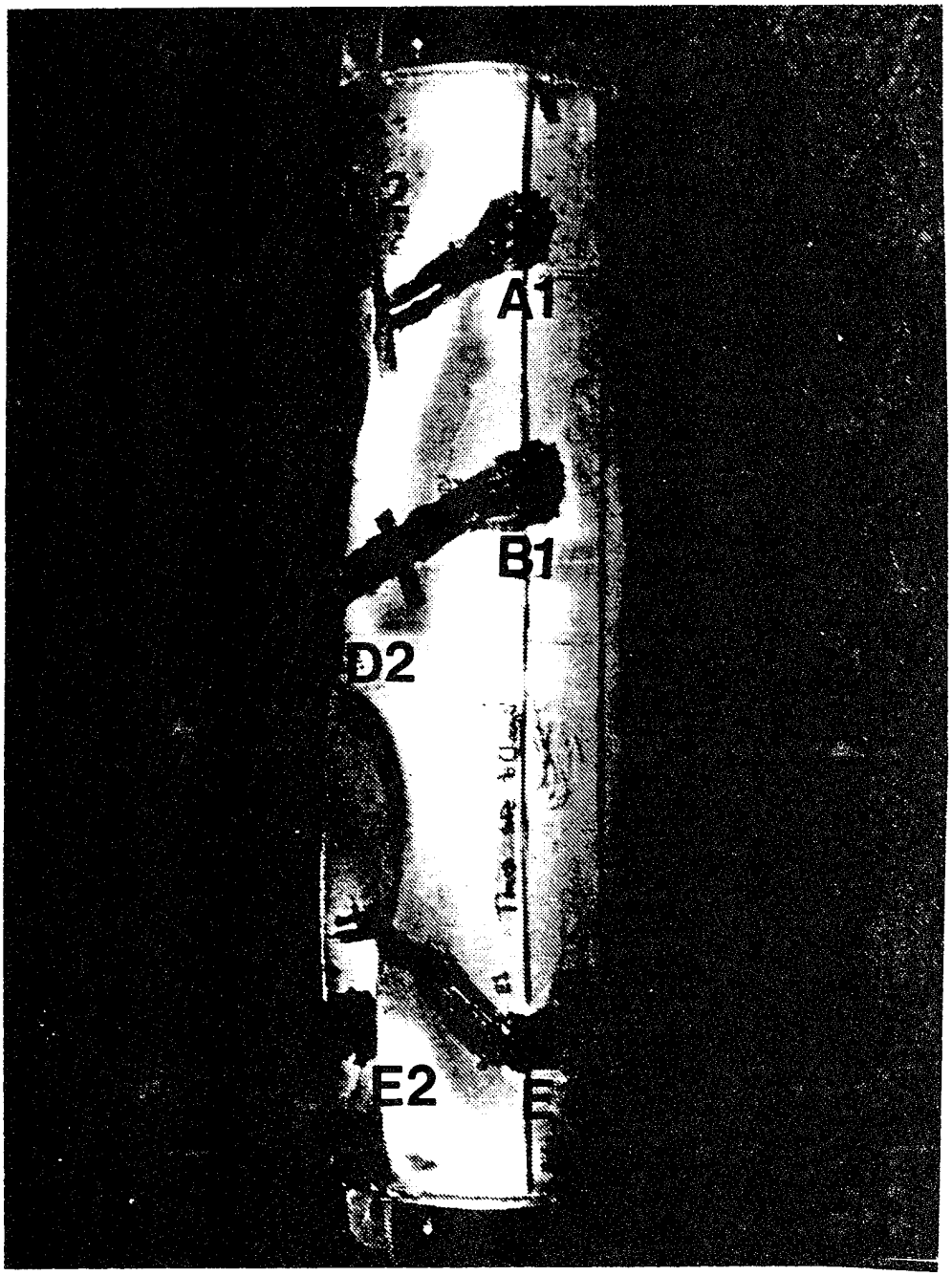

Figure 46. Damage Cylinder Subjected to Side-on Attack (Charge Location to Right of Cylinder.

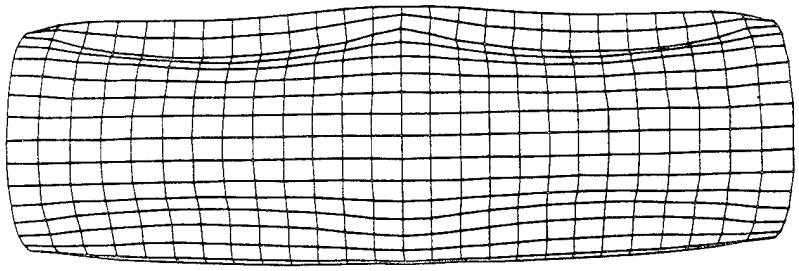

(a) front view

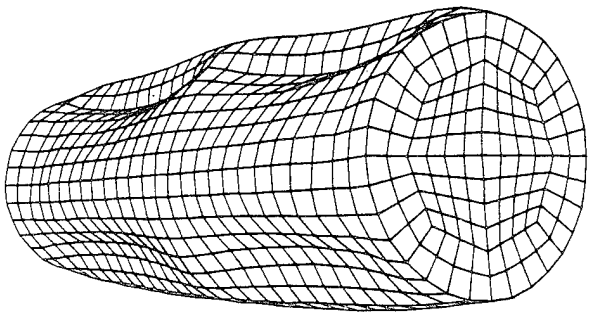

(b) backside view

Figure 47. Nelson's Material, Radial, and Axial Imperfection with Random Phase Shift: (a) Deformation plot with charge axis directly in front (b) Deformation plot looking at backside

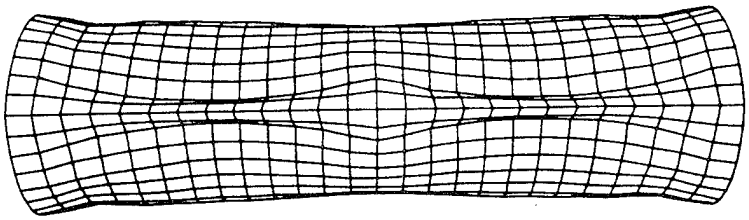

(a) top view

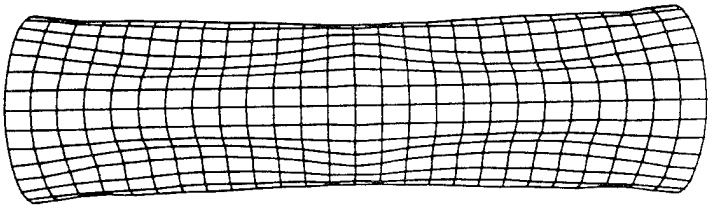

(b) bottom view

Figure 48. Nelson's Material, Radial, and Axial Imperfection with Random Phase Shift: (a) Deformation plot from top of cylinder (b) Deformation plot from bottom of cylinder

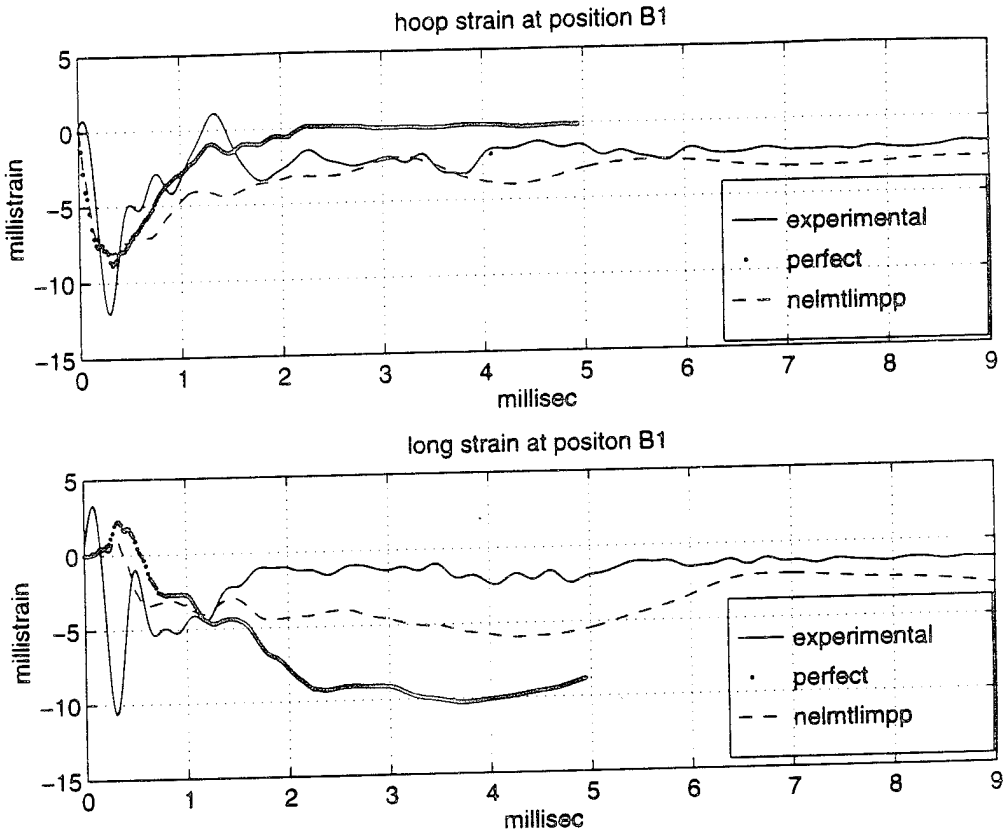

Figure 49. Nelson's Material, Radial, and Axial Imperfections with Random Phase Shift: Circumferential and Longitudinal Strain plots at B1A and B1C.

2. Nelson's Material, Radial and Axial Imperfections (Nelmtlimp)

Deformation analysis was conducted using longitudinal deformation plots as used with the prior analysis. Hoop and axial strains were analyzed for the same strategic locations around the front and top of the cylindrical surface as for the Nelmtlimpp case.

Axial and hoop strain time histories are provided for points B1A and B1C which are located 5.45 inches to the right from centerline. The longitudinal deformation plot is provided for time 1.4796 msec. The deformation plots provided in Figure 50, show even a more exact similarity to the actual deformation.

The axial and hoop strain time histories at the B1A and B1C for experimental, numerical, and perfect are provided in Figure 51. This plot clearly shows the that the numerical hoop strain generally predicts that of the experimental hoop strain during the critical first 9 msec after detonation. This plot clearly shows the Nelmtlimp case provides better correlation than that of the perfect case. The longitudinal strain shows the numerical predication is not as close as the hoop strain but still reasonable for the first 9 msec. Despite data correlations of strain histories of experimental to numerical Nelson reasoned that the post-processor strain time histories can be misleading because the plot continues generating data points even after an element has reached failure strain criteria.

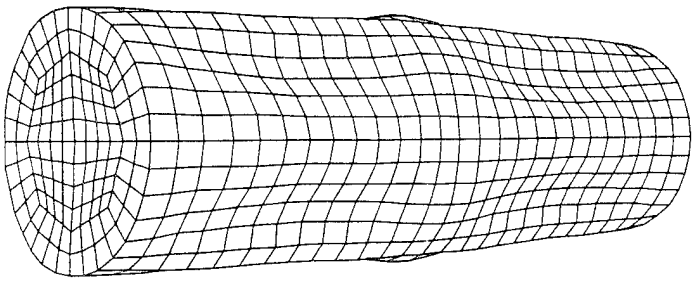

(a) front view

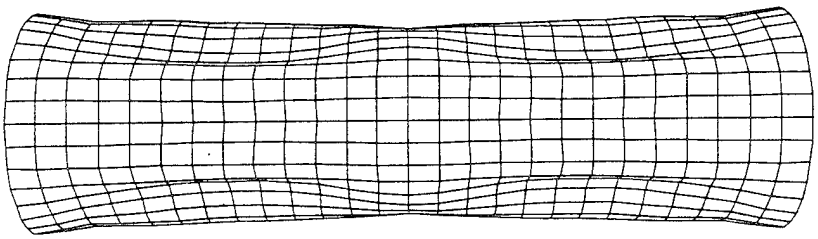

(b) top view

Figure 50. Nelson's Material, Radial, and Axial Imperfections: (a) Deformation plot with charge axis directly in front (b) Deformation plot from top of cylinder.

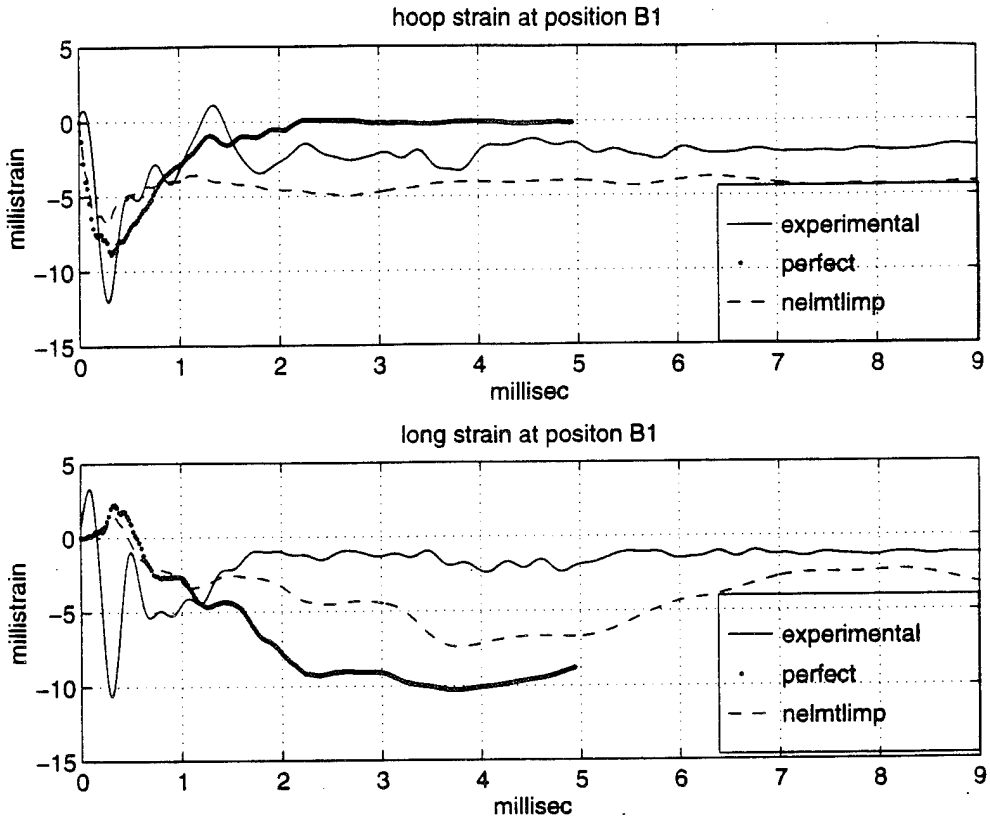

Figure 51. Nelson's Material, Radial, and Axial Imperfections: Circumferential and Longitudinal Strain plots at B1A and B1C.

V. DEFORMATION ANALYSIS ON MULTIPLE STIFFENED CYLINDRICAL SHELLS

The analysis of cylindrical shells in the prior USA/DYNA3D models has been in the area of finite cylindrical shell with stiffeners. The number of stiffeners used were either one centerline by Nelson's half model and two equally spaced by Hooker's half model. In both cases the models were 12 inch diameter cylinder 42 inches long made of mild steel with HY-80 or 100 endplates. The question arises if a larger model with multiple stiffeners subjected to an underwater explosion will behave with similar responses.

A. PHYSICAL MODEL

The ONR cylinder is a 1/12 scale reproduction of a submarine hull developed by the Naval Surface Warfare Center with the purpose of collecting experimental data on deformation and dynamic responses. The ONR cylinder has a diameter of 33.625 inches ,length of 253.125 inches and a shell thickness of 0.1875 inches. There are six evenly spaced deep frame stiffeners that are 2 inches thick and 4.125 inches wide. There are also 40 shallow frame stiffeners equally spaced that are 0.25 inches thick and 1.25 inches wide. The shell, endplates, and deep frames are made of mild steel while the deep frames are constructed of HTS steel.

B. ONR MODEL

The ONR model was developed in the same manner as earlier models. Its notable exception is that it is a three-dimensional multiple stiffened finite cylindrical shell half model as shown in Figure 52. It uses 2064 nodes and 1080 wet elements with the same kinematic/isotropic elastic plastic mild steel parameters that was used before. It was subjected to an underwater explosion of HBX-1 270 pound charge at a standoff distance of 15 feet that produced a peak pressure pulse of 8530 psi.

The two different cases that were analyzed were the perfect model and combined imperfection model with random phase shift. The optimized combined modal imperfection

distribution was integrated into the finite element mesh algorithm in the same manner as in previous models.

The deformation analysis was also conducted with axial and longitudinal deformation plots, von Mises contour and effective plastic strain plots.

The longitudinal deformation plot, Figure 53 shown for the shock induced pulse at time 1.9875 msec for both perfect and imperfect models with a displacement scale factor of two. This figure shows the pronounced buckling or pinching around the major stiffeners in each model due to the added stiffness provided by the deep frame stiffeners. There is also distinguishable ripples between the extent of crumpling of the minor or shallow stiffeners in both cases. The noticeable difference between the two models is the more pronounced dishing between the stiffeners in the combine imperfection model as compared to the perfect model smoother appearance.

A comparison of the maximum von Mises stresses between ONR perfect and combine imperfect shows a 1.1 percent greater difference within the first msec. A similar comparison between the two models show a 5.3 percent greater difference after three msec after impact.

The effective plastic strain contour plot has the typical similar appearance to the model perfect. A comparison of the effective plastic strains between the two cases shows a 19 percent greater difference within the first msec after impact.

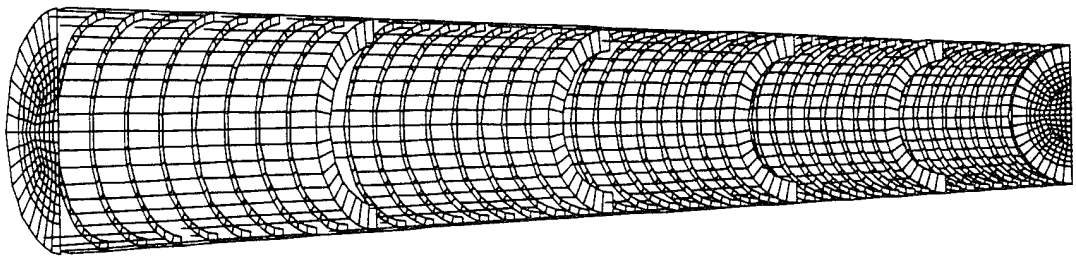

Three Dimensional Multiple Stiffened Cylindrical Shell 1/2 Model

Figure 52. Model ONR

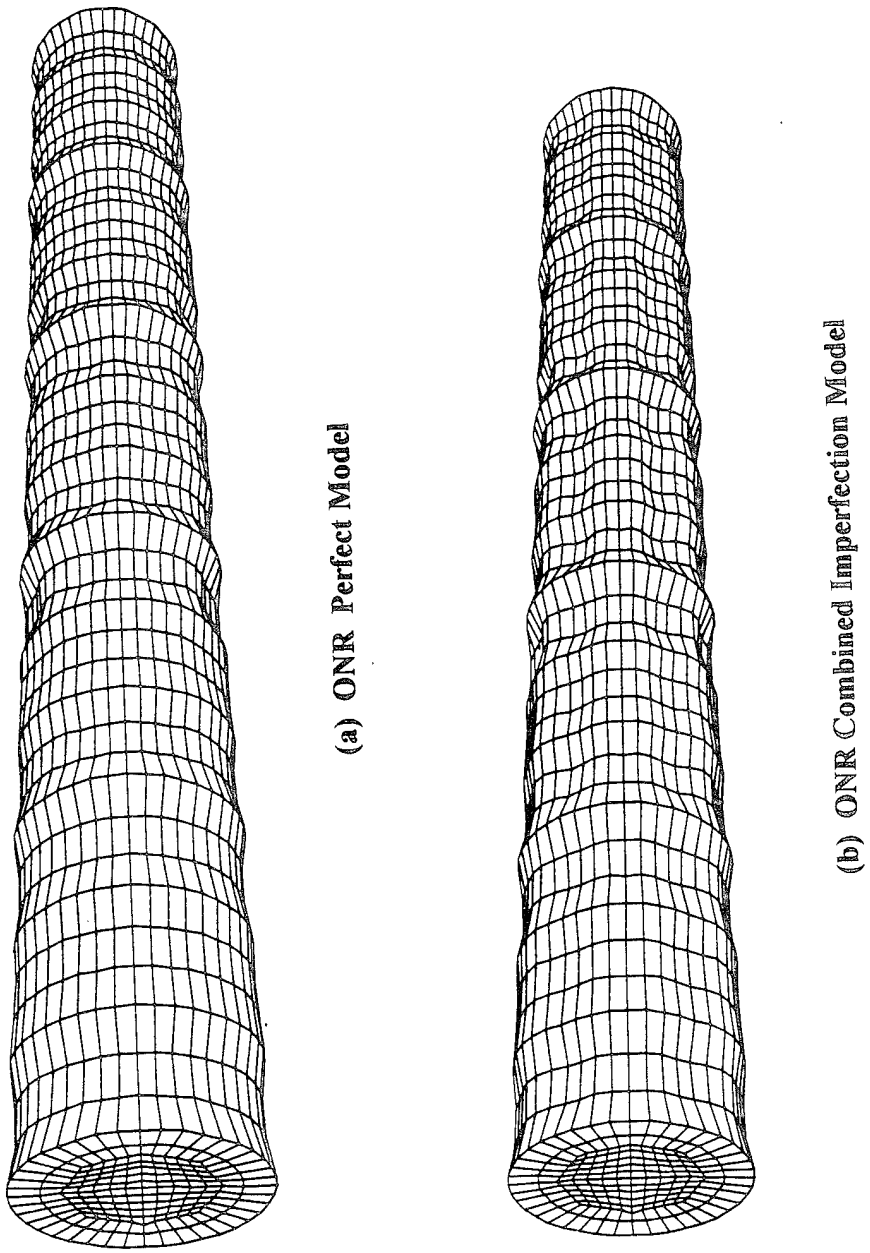

Figure 53. Model ONR Perfect versus Combine Imperfect: Longitudinal Deformation plot at 1.9875: (a) Perfect ONR model (b) ONR Combined Imperfections

VI. CONCLUSIONS AND RECOMMENDATIONS

Predicting the dynamic and deformation response of a cylindrical shell subjected to an underwater explosion has a great many complex variables. Initial geometric and material imperfections are part of those complex variables that make numerical analysis of complicated cylindrical structural systems difficult to simulate. Introducing an initial modal imperfections into the numerical analysis significantly reduces the effects of these imperfections on the cylindrical model. As shown by the comparisons of the numerical to experimental data of the Nelson's model this has greatly increased the ability to numerically predict deformations and dynamic responses.

A. IMPERFECTION SENSITIVITY ANALYSIS

The geometric, radial and axial modal imperfections were analyzed independently as well as combined for random and non-random phase shift cases. The analysis of the eight modal imperfection cases used the following set of data: hoop and axial strains , axial and longitudinal deformation plots, maximum von Mises stresses, and the effective plastic strains. After comparing the individual modal imperfection data to the perfect model it was determined that the radial imperfections dominated the dynamic response of cylindrical shells to within two percent. These results would concur with prior theoretical research that neglecting the axial imperfections due to the slight variations in the axial directions would not influence the results to within engineering accuracy.

The material imperfections that were introduced into the mesh algorithm were also analyzed. The same above procedure was used to compare the material imperfection versus the perfect model. The results were very similar to those of the perfect model. The elastic modulus and variation in density probably can not be increase past the 5 percent that was used in this analysis due the homogeneous/isotropic nature of the material. This research has established that the material imperfection affected the dynamic response less than 1/2 percent. The variation in elastic modulus may be more significant in the dynamic response in the elastic region. The variation of yield strength was determined to be slightly sensitive in the plastic

region to the magnitude of dynamic response and probably is only capable of 1 to 2 percent difference. The tangential hardening modulus is a property that only slightly affects the dynamic response in the plastic region and is limited to about 1 to 2 percent.

B. RECOMMENDATIONS

The significance of using the proper initial modal imperfection can not be overemphasized. This is important because the deformation or actual damage will follow this progression though to ultimate failure. Kirkpatrick (1989) specifically stated that the output of the dynamic and deformation response is only as accurate as the actual initial imperfection distribution. This means a knowledge of fabrication or machine process would at least provide a rough estimate at an initial imperfection distribution.

The following recommendations are made for further study:

1. Investigate the ability to implement material and geometric imperfections in other USA/DYNA3D elements like beam or brick elements and analyze the differences between those of the shell elements.
2. Fabricate a cylindrical shell and perform an imperfection sensitivity analysis. Compare actual three-dimensional mesh of cylinder to the combined imperfection distribution. Perform UNDEX test and compare numerical to experimental UNDEX data.
3. Perform combined imperfection analysis with a full model using greater number than 1500 wet elements. This would reduce the mesh size and use a summation of the first 50 even and odd modal shapes could be analyzed.

In conclusion there is a significant effect by geometric and material imperfections on the dynamic and deformation response of cylindrical shells subjected to underwater explosions. These initial geometric and material imperfections provide a far more realistic representation of the physical system of the cylindrical shell and will provide a more accurate prediction of damage and deformation of structures due to shock induced vibrations.

APPENDIX A

INGRID INPUT FILES

The following input files consist of ingrid which creates the geometric model for DYNA3D, flumas, augmat, and timint. The flumas, augmat and timint files provide input for the USA program.

```
model.full
dn3d vec term 0.003 plti 10.0e-6 prti 1000

mat 1 type 3 e 2.9e+7 pr 0.3 ro 7.356e-4
      etan 5.1e+4 sigy 3.2e+4 shell quad 5 thick 0.060 endmat

      c  material 1 is the shell surface and is made of mild steel
      c  kinematic/isotropic elastic/plastic material 0.060 inch thick

mat 2 type 3 e 2.9e+7 pr 0.3 ro 7.356e-4
      etan 5.02e+4 sigy 1.08e+5 shell quad 5 thick 0.25 endmat

      c  material 2 is the cylinder end plate and is made of HY-100
      c  material 1 is the shell surface and is made of mild st
      c  kinematic/isotropic elastic/plastic material 0.25 inch thick


mat 3 type 3 e 2.9e+7 pr 0.3 ro 7.356e-4
      etan 5.1e+4 sigy 3.2e+4 shell quad 5 thick 0.12 endmat

      c  material 3 is the shell stiffeners and is made of mild steel
      c  kinematic/isotropic elastic/plastic material 0.120 inch thick

lcd 1 2  0.0  0.0     1.0  0.0                    c  load curve definitions
lcd 2 2  0.0  1.6e-6  1.0  1.6e-6


start                                            c  construct shell surface
-1  6  -11 ;
 1 22 ;
-1  6  -11 ;
-1  0  1
 0.0  21.0
-1  0  1
 a 1 0 1 3 0 3  2  6.0
 pri -1 -3 ; ; -1 -3; 1 -1.0  0.0 0.0 0.0        c  pressure load for part
 mate 1                                          c  shell in made of material 1
end
                                                 c  surface definitions
sd 1 cyli  0 0 0 0 1 0 6.0                       c  outer shell radius
sd 2 cyli  0 0 0 0 1 0 [6.0*3/5]
```

```
start                                                    c  construct endplates
 1 5 10 15 19 ;
-1 ;
 1 5 10 15 19 ;
-1 -1 0 1 1
 0.0
-1 -1 0 1 1
 pri ; -1 ; ; 1  -1.0  0.0 0.0 0.0                       c  pressure load for part
 di 1 2 0 4 5 ; ; 1 2 0 4 5                              c  delete corners for circle
 sfvi -2 -4; ; -2 -4; sd 2                               c  form vertex filler for inter
 sfi -1 -5; ; -1 -5 ; sd 1                               c  form circular outer shape
 mate 2                                                  c  endplate in made of material
end

start
 1 5 10 15 19 ;
-1 ;


 1 5 10 15 19 ;
-1 -1 0 1 1
 21.0
-1 -1 0 1 1
 pri ; -1 ; ; 1  -1.0  0.0 0.0 0.0
 di 1 2 0 4 5 ; ; 1 2 0 4 5
 sfvi -2 -4; ; -2 -4; sd 2
 sfi -1 -5; ; -1 -5 ; sd 1
 mate 2
end

start                                                    c. construct stiffeners
 1 2 7 12 13 ;
-1 ;
 1 2 7 12 13 ;
-1 -1 0 1 1
 7.0
-1 -1 0 1 1
 di 1 2 0 4 5 ; ; 1 2 0 4 5                              c  delete corners for circle for
 a 1 0 1 5 0 5  2  6.0
 a 2 0 2 4 0 4  2  5.0
 d 2 0 2 4 0 4
 mate 3                                                  c  construct stiffener from
end                                                      c  material 3

start
 1 2 7 12 13 ;
-1 ;
 1 2 7 12 13 ;
-1 -1 0 1 1
 14.0
-1 -1 0 1 1
 di 1 2 0 4 5 ; ; 1 2 0 4 5
 a 1 0 1 5 0 5  2  6.0
 a 2 0 2 4 0 4  2  5.0
 d 2 0 2 4 0 4
 mate 3
end

end
```

```
FLUMAS DATA FOR MODEL FULL
sim.flu sim.geo dyna.pre sim.daa  $  FLUNAM  GEONAM  GRDNAM  DAANAM
T T F T                          $  PRTGMT  PRTTRN  PRTAMF  CALCAM
T F F F                          $  EIGMAF  TWODIM  HAFMOD  QUAMOD
F F T T                          $  PCHCDS  NASTAM  STOMAS  STOINV
F F F F                          $  FRWTFL  FRWTGE  FRWTGR  FRESUR
F T F F                          $  RENUMB  STOGMT  ROTGEO  ROTQUA
F F F F                          $  PRTCOE  STRMAS  SPHERE  ROTSYM
F F F F                          $  OCTMOD  CAVFLU  FRWTFV  INTCAV
DYNA                             $  MAINKY
0 1442  0  1360                  $  NSTRC   NSTRF   NGEN    NGENF
0 0 0                            $  NBRA    NCYL    NCAV
9.356E-05  57600.0               $  RHO     CEE
5                                $  NVEC
6                                $  NSRDI
6.0  0.0  1    105  1            $  RAD1    RAD2    JBEG    JEND    JINC
0.0  6.0  106  210  1
6.0  0.0  211  315  1
0.0  6.0  316  630  1
6.0  0.0  631  840  1
0.0  0.0  841 1360  1
0                                $  NSORDER
```

```
AUGMAT DATA FOR MODEL.FULL
dyna.pre sim.flu sim.geo sim.pre
F  F  F  F
F  F  F  T
F  F  F  T
F  F  F  F
F
DYNA
0.50
1442  4326  3  3
1
0   1   1360   1
```

```
$   STRNAM   FLUNAM   GEONAM   PRENAM
$   FRWTGE   FRWTST   FRWTFL   PLNWAV
$   FLUSKY   DAAFRM   SYMCON   DOFTAB
$   PRTGMT   PRTTRN   PRTSTF   PRTAUG
$   MODTRN   STRLCL   INTWAT   CFADYN
$   LUMPFM
$   MAINKY
$   DAA2
$   NSTR     NSFR     NFRE     NFTR
$   NSETLC
$   NDICOS   JSTART   JSTOP    JINC
```

```
r=d3dump
TIME INTEGRATION DATA FOR MODEL FULL
sim.pre sim.pos
sim.rst
F  F  F
T  F  F  F
F  T  F  F
1
0.0
0.0   10.5   186.0
0.0   10.5   6.0
101
1.0
12.2E-06
1
60.0   15.0   10.0
1  0
0.0   1.6E-06
5000   5000
0  0  0  0
F  F
F
```

```
$   PRENAM   POSNAM
$   RESNAM
$   BUBPUL   REFSEC   FLUMEN
$   EXPWAV   SPLINE   VARLIN   PACKET
$   HYPERB   EXPLOS   DOUBDC   VELIMP
$   NCHARG
$   HYDPRE
$   XC    YC    ZC
$   SX    SY    SZ
$   JPHIST
$   PNORM
$   DTHIST
$   CHGTYP
$   WEIGHT   SLANT   CHGDEP
$   NTINT    NCHGAL
$   STRTIM   DELTIM
$   NSAVER   NRESET
$   LOCBEG   LOGRES   LOCWRT   NSTART
$   FORWRT   STBDA2
$   DISPLA
```

APPENDIX B

FORTRAN PROGRAM FOR MODIFYING INGRIDO FILES FOR GEOMETRIC IMPERFECTIONS

The following fortran programs modify the ingrido input file and allow the implementing of radial and axial imperfections into the mesh generator algorithm.

```
************************************************************************
*       This program modifies the nodes of a file called               *
*       ingrido.old, which is the original input file for              *
*       USA/DYNA3D.  This program writes the output to                 *
*       impp.raw file that then can be imported back into              *
*       the ingrido file for modification.  The program uses           *
*       separate random number generation for both radial and          *
*       axial phase shift.                                             *
************************************************************************
*       VARIABLE LIST:                                                 *
*                                                                      *
*       a1    - weighting factor for each modal imperfection           *
*       beta  - angle from reference axis to axial postion of          *
*               node                                                   *
*       da    - change in axial position due to modal                  *
*               imperfection                                           *
*       dr    - change in radial postion due to modal                  *
*               imperfection                                           *
*       h     - thickness of shell                                     *
*       nodes- node number                                             *
*       m     - number of nodes                                        *
*       r     - radial position of node                                *
*       phi   - phase shift for each  radial modal imperfection        *
*       si    - phase shift for each axial modal imperfection          *
*       theta- angle from reference axis to radial position            *
*               of node                                                *
*       x     - global x coordinate of node                            *
*       y     - global y coordinate of node                            *
*       z     - global z coordinate of node                            *
************************************************************************

      Program Imperfection
      double precision a1,a2,a3,a4,a5,a6,a7,a8,a9,a10
      double precision dr1,dr2,dr3,dr4,dr5,dr6,dr7,dr8
      double precision dr9,dr10,da1,da2,da3,da4,da5,da6
      double precision da7,da8,da9,da10,h,pi,xx,yy,theta
      double precision si(10),phi(10),xnew,znew,beta
      double precision b1,b2,x,y,z,del,dr,da(22),ynum
      integer idum, i, nodes,n

************************************************************************
*       OPEN INPUT AND OUTPUT FILES                                    *
************************************************************************

      open(10, file='ingrido.old')
      open(15, file='impp.raw')
      h = 0.06
      pi = 3.141592653589793
```

```
*************************************************************************
*       INPUT NUMBER OF NODES TO  BE MODIFIED                           *
*       AND WEIGHTING COEFFICIENTS OF THE FIRST TEN MODE SHAPES         *
*************************************************************************

      nodes = 880
      do 20  i=1,42
             read(10,*)
 20   continue

      a1 = 0.05*h
      a2 = 0.05*h
      a3 = 0.05*h
      a4 = 0.05*h
      a5 = 0.05*h
      a6 = 0.05*h
      a7 = 2*h/49
      a8 = 2*h/64
      a9 = 2*h/81
      a10 = 2*h/100

*************************************************************************
*       CALL SUBROUTINES TO GENERATE RANDOM NUMBERS FOR                 *
*       CALCULATING  RANDOM PHASE SHIFT ANGLES                          *
*************************************************************************

      do 30 i=1,10
            idum = i
            xx = ran2(idum)
            yy = ran3(idum)
            phi(i) = xx
            si(i) = yy
30    continue

*************************************************************************
*       DO LOOP TO READ INPUT DATA                                      *
*************************************************************************

      do 100 i=1,nodes
            read(10,*) n,b1,x,y,z,b2

*************************************************************************
*       CALCUATE RADIUS OF NODE POSITION                                *
*       THEN CALCULATE THE ANGLE FROM THE REFERENCE AXIS TO THE         *
*       NODE POINTS; beta and theta                                     *
*************************************************************************

            r= dsqrt(x*x + z*z)
            beta = (pi*y)/21

              if (dabs(x) .lt. 0.001) then

               if (z .gt. 0.0) then
                  theta= 0.0
               else
                  theta= pi
               endif
            else

               theta= datan(x/z)
               if (z .lt. 0.0) then
                   theta= theta + pi
               endif
            endif
```

```
*****************************************************************
*       MODIFY THE NODE POSITIONS USING THE FIRST TEN MODE      *
*       SHAPES  IN BOTH RADIAL AND AXIAL DIRECTIONS             *
*****************************************************************

              dr1 = a1 * dcos(theta + 2.0*pi*phi(1))
              dr2 = a2 * dcos(2.0 * theta + 2.0*pi*phi(2))
              dr3 = a3 * dcos(3.0 * theta + 2.0*pi*phi(3))
              dr4 = a4 * dcos(4.0 * theta + 2.0*pi*phi(4))
              dr5 = a5 * dcos(5.0 * theta + 2.0*pi*phi(5))
              dr6 = a6 * dcos(6.0 * theta + 2.0*pi*phi(6))
              dr7 = a7 * dcos(7.0 * theta + 2.0*pi*phi(7))
              dr8 = a8 * dcos(8.0 * theta + 2.0*pi*phi(8))
              dr9 = a9 * dcos(9.0 * theta + 2.0*pi*phi(9))
              dr10 = a10 * dcos(10.0 * theta + 2.0*pi*phi(10))

              da1 = 0.25 * a1 * dcos(beta + 2.0*pi*si(1))
              da2 = 0.25 * a2 * dcos(2.0 * beta + 2.0*pi*si(2))
              da3 = 0.25 * a3 * dcos(3.0 * beta + 2.0*pi*si(3))
              da4 = 0.25 * a4 * dcos(4.0 * beta + 2.0*pi*si(4))
              da5 = 0.25 * a5 * dcos(5.0 * beta + 2.0*pi*si(5))
              da6 = 0.25 * a6 * dcos(6.0 * beta + 2.0*pi*si(6))
              da7 = 0.25 * a7 * dcos(7.0 * beta + 2.0*pi*si(7))
              da8 = 0.25 * a8 * dcos(8.0 * beta + 2.0*pi*si(8))
              da9 = 0.25 * a9 * dcos(9.0 * beta + 2.0*pi*si(9))
              da10 = 0.25 * a10 * dcos(10.0 * beta + 2.0*pi*si(10))

              dr = dr1+dr2+dr3+dr4+dr5+dr6+dr7+dr8+dr9+dr10

              da(i) = da1+da2+da3+da4+da5+da6+da7+da8+da9+da10

              del = dr + da(i)

*****************************************************************
*       CALCULATE THE CARTESIAN COORDINATES OF THE NODES        *
*****************************************************************

              xnew  = x - del * dsin(theta)
              znew = z - del  * dcos(theta)
              x = xnew
              z = znew

*****************************************************************
*       WRITE DATA TO TEMPORARY DATA FILE IMPP.RAW              *
*****************************************************************

              write(15,99) n,b1,x,y,z,b2
 99           format(i8,f5.0,3e20.13,f5.0)
 100       continue

*****************************************************************
*       CLOSE INPUT AND OUTPUT FILES                            *
*****************************************************************

            close(10)
            close(15)
            stop
            end

*****************************************************************
*       SUBROUTINE FOR RANDOM NUMBER GENERATION                 *
*****************************************************************
```

APPENDIX C

FORTRAN PROGRAM FOR MODIFYING INGRIDO FILES FOR MATERIAL IMPERFECTIONS

The following fortran programs modify the ingrido input file and allow the implementing of material imperfections into the mesh generator algorithm.

```
*****************************************************************
*       This program modifies the elements of a file called     *
*       ingrido.mtl, which has been modified for just the       *
*       element cards for DYNA3D input file.  This program      *
*       randomly provides ten values that will  be used to      *
*       modify the material properties at that element.  The    *
*       output in written into mimp.raw that then can be        *
*       imported back into the ingrido file for modification.   *
*****************************************************************
*       VARIABLE LIST:                                          *
*                                                               *
*       mtl    - material type for a particular element         *
*       n1     -  node numbers associated with a element        *
*       nel    - element number                                 *
*       num    - number of data records to be read in from      *
*                from ingrido.mtl                               *
*       wetel - number wet elements                             *
*                                                               *
*****************************************************************

      Program Material Imperfections
      real xx,yy
      integer i,idum,mtl,n1,n2,n3,n4,nel
      dimension a, b, c, d

*****************************************************************
*       OPEN INPUT AND OUTPUT FILES                             *
*****************************************************************

      open(10, file='ingrido.mtl')
      open(15, file='mimp.raw')
      h = 0.06
      pi = 3.141592653589793

*****************************************************************
*       INPUT NUMBER OF WET ELEMENTS TO  BE MODIFIED            *
*****************************************************************

      wetel= 840
      num= 2*wetel

*****************************************************************
*       CALL SUBROUTINES TO GENERATE RANDOM NUMBERS FOR         *
*       CALCULATING  RANDOM MATERIAL TYPE FOR ELEMENTS          *
*****************************************************************
```

```
      idum=1
      yy = ran2(idum)

      do 100  i=1,num,2
              read(10,*) nel, mtl, n1, n2, n3, n4
              read(10,*) a, b, c, d
              idum= i
              xx= ran3(idum)
              mtl= 10*xx
              mtl= int(mtl)
              if (mtl .lt. 1) mtl= 1
              if (mtl .eq. 2) mtl= 11
              if (mtl .eq. 3) mtl= 12



*****************************************************************
*       WRITE DATA TO TEMPORARY DATA FILE MIMP.RAW              *
*****************************************************************

              write(15,300) nel, mtl, n1, n2, n3, n4
              write(15,400) a, b, c, d

100     continue


300     format(1x,3x,i4,3x,i2,4x,i4,4x,i4,4x,i4,4x,i4)
400     format(1x,E9.3,1x,E9.3,1x,E9.3,1x,E9.3)

*****************************************************************
*       CLOSE INPUT AND OUTPUT FILES                            *
*****************************************************************

        close(10)
        close(15)
        close(20)
        stop
        end

*****************************************************************
*       SUBROUTINE FOR RANDOM NUMBER GENERATION                 *
*****************************************************************
```

APPENDIX D

Table of Data

Model	time (msec)				
	0.0384	0.4896	0.9888	1.9888	2.9888
Perfect	32.07	35.18	37.88	40.66	41.38
Rimp	32.08	35.26	37.76	40.90	43.67
Aimp	32.07	35.18	37.86	40.67	41.37
Imp	32.08	35.26	37.75	40.88	43.11
Rimpp	32.07	35.39	38.31	46.63	40.24
Aimpp	32.07	35.18	37.98	40.74	41.41
Impp	32.08	35.39	38.34	46.69	42.22
Mtl	32.08	35.18	37.88	40.66	41.39
Mtlimpp	32.08	35.40	38.34	46.71	42.19

Table 2. Maximum Von Mises Stresses for Modal Imperfections in (ksi).

Model	time (msec)				
	0.2448	0.4896	0.9888	1.9888	2.9888
Perfect	.0307	.0652	.1171	.1761	.1894
Rimp	.0307	.0647	.1330	.2659	.2971
Aimp	.0307	.0652	.1168	.1754	.1889
Imp	.0307	.0647	.1327	.2656	.2967
Rimpp	.0314	.0676	.1344	.3406	.3627
Aimpp	.0307	.0652	.1187	.1773	.1907
Impp	.0314	.0677	.1348	.3404	.3619
Mtl	.0307	.0652	.1171	.1766	.1900
Mtlimpp	.0314	.0677	.1349	.3412	.3630

Table 3. Maximum Effective Plastic Strain (in/in).

Model	time (msec)				
	0.0384	0.4896	0.9888	1.9888	2.9888
Aimpp1/4	32.07	35.18	37.98	40.72	41.41
Aimpp1/2	32.07	35.18	37.99	40.74	41.43
Aimpp3/4	32.07	35.18	37.97	40.72	41.41
Aimpp1/1	32.07	35.19	38.00	40.81	41.43
Mtldensity	32.08	35.19	37.96	40.73	41.42
Mtlyield2.5	32.46	35.54	38.19	40.92	41.62
Mtlyield5.0	32.86	35.89	38.69	41.52	41.94
Mtltang5.0	32.08	35.24	37.99	40.78	41.48

Table 4. Maximum Von Mises Stresses for Axial and Material Imperfections in (ksi).

Model	time (msec)				
	0.0384	0.4896	0.9888	1.9888	2.9888
Aimpp1/4	.0307	.0652	.1187	.1773	.1907
Aimpp1/2	.0307	.0654	.1190	.1755	.1889
Aimpp3/4	.0307	.0653	.1187	.1756	.1886
Aimpp1/1	.0307	.0654	.1191	.1766	.1896
Mtldensity	.0307	.0653	.1171	.1766	.1900
Mtlyield2.5	.0311	.0656	.1185	.1791	.1934
Mtlyield5.0	.0319	.0668	.1199	.1819	.1990
Mtltang5.0	.0306	.0652	.1176	.1773	.1908

Table 5. Maximum Effective Plastic Strain for Axial and Material Imperfections in (in/in).

LIST OF REFERENCES

Arbocz, J., (1982). "The Imperfection Data Bank, A Means to Obtain Realistic Buckling Loads." In Buckling of Shells, Proc. of a State-of-the-Art Colloquium, New York, N.Y.

Brush, D.O., and Almroth, BO., (1975). Buckling of Bars, Plates, and Shells. McGraw Hill Publishers.

DeRuntz, J.A. Jr., (1989). The Underwater Shock Analysis Code and its Applications, Paper presented at the 60th Shock and Vibration Symposium, Virginia Beach, VA.

Fox, P.K. (1992). Nonlinear Dynamic Response of Cylindrical Shells Subjected to Underwater Side-on Explosions. Master's Thesis , Naval Postgraduate School, Monterey, CA, 1992.

Hallquist, J.O., and Stillman, D.W. (1990). "VEC/DYNA3D users manual (Nonlinear Dynamic Analysis of Structures in Three Dimensions)." Livermore Software Technology Corporation Report 1018.

Hallquist, J.O., and Stillman, D.W. (1985). LS-INGRID: A Three-Dimensional Mesh Generator for modeling non linear systems. Livermore Software Technology Corporation Report UCID-20506.

Hallquist, J.O., and Stillman, D.W. (1990). LS-TAURUS: An Interactive Post-processor for the Programs LS-DYNA3D, LS-NIKE3D, AND TOPAZ-3D.. Livermore Software Technology Corporation Report 1009, April 1990.

Hooker, D.T. (1993) Effect of Initial Imperfections on the Response of Cylinders to Underwater Explosion. Engineers Thesis, Naval Postgraduate School, Monterey, CA, 1993.

Kirkpatrick, S.W., and Holmes, B.S. (1989). "Effect of Initial Imperfections on Dynamic Buckling of Shells." Journal of Engineering Mechanics, v.115 pp. 1075-1093.

Lindberg, H.E., and Florence, A.L., (1987) Dynamic Pulse Buckling. Martinus Nijhoff Publishers, Dordrecht, the Netherlands.

Nelson, K.W. (1992) Dynamic Response and Failure Analysis of Aluminum Cylinders Subjected to Underwater Explosion. Master's Thesis, Naval Postgraduate School, Monterey, CA, 1992.

Shin, Y.S. , and Geers, T.L., (1991) Response of Marine Structures to Underwater Explosions, short course notes.

INITIAL DISTRIBUTION LIST

		No. of Copies
1.	Defense Technical Information Center Cameron Station Alexandria, VA 22304-6145	2
2.	Library, Code 052 Naval Postgraduate School Monterey, CA 93943-5101	2
3.	Professor Young S. Shin, Code ME/Sg Department of Mechanical Engineering Naval Postgraduate School Monterey, CA 93943-5002	2
4.	Professor Young W. Kwon, Code ME/Kw Department of Mechanical Engineering Naval Postgraduate School Monterey, CA 93943-5002	1
5.	Department Chairman, Code ME Department of Mechanical Engineering Naval Postgraduate School Monterey, CA 93943-5002	1
6.	Naval Engineering Curricular Office (Code 34) Naval Postgraduate School Monterey, CA 93943-5002	1
7.	Dr. Kent Goering Defense Nuclear Agency 6801 Telegraph Road Alexandria, VA 22310	1
8.	Mr. Douglas Bruder Defense Nuclear Agency 6801 Telegraph Road Alexandria, VA 22310	1

9. LT Robert E. Kaufman, USN 1
139 Star Rim
East Peoria, IL 61611

10. Mr. Michael Riley 1
Naval Surface Warfare Center
UERD
Portsmouth, VA 23709-5000

11. Mr. Mike Talley 1
Naval Surface Warfare Center
UERD
Portsmouth, VA 23709-5000